A NMR STUDY ON ZERO ELECTRIC FIELD GRADIENT NEMATIC LIQUID CRYSTALS

By

Thambirajah Chandrakumar

B. Sc., University of Peradeniya, Sri Lanka, 1984

M. Sc., The University of British Columbia, 1989

A THESIS SUBMITTED IN PARTIAL FULFILLMENT OF

THE REQUIREMENTS FOR THE DEGREE OF

DOCTOR OF PHILOSOPHY

in

THE FACULTY OF GRADUATE STUDIES

DEPARTMENT OF CHEMISTRY

We accept this thesis as conforming

to the required standard

.....

.....

.....

.....

THE UNIVERSITY OF BRITISH COLUMBIA

July 1994

In presenting this thesis in partial fulfilment of the requirements for an advanced degree at the University of British Columbia, I agree that the Library shall make it freely available for reference and study. I further agree that permission for extensive copying of this thesis for scholarly purposes may be granted by the head of my department or by his or her representatives. It is understood that copying or publication of this thesis for financial gain shall not be allowed without my written permission.

Department of Chemistry
The University of British Columbia
2075 Wesbrook Place
Vancouver, Canada
V6T 1W5

Date: 26th Aug. 94

Abstract

The role of intermolecular forces in describing the orientational nature of liquid crystals is not well understood. Previous studies using dideuterium as a solute in liquid crystals have demonstrated the importance for orientation of the interaction between the solute molecular quadrupole moment and the average electric field gradient present in liquid crystals. With the aim of learning about additional orientational mechanisms, we have studied the orientation of solutes in special mixtures of liquid crystals, where the contribution from the environment to the average electric field gradient at the ^{2}H nucleus of dideuterium is negligibly small. In order to understand the role of short-range forces in such special mixtures, orientational studies have been undertaken in the mixtures 55 wt% ZLI-1132(1132)/N-(-4-ethoxybenzylidene)-4'-butylaniline (EBBA), 56.5 wt% 1132/EBBA and 70 wt% 4-n-pentyl-4'-cyanobiphenyl (5CB)/EBBA.

As a starting point, the C_{2V} and D_{2h} symmetry solutes meta dichlorobenzene, ortho dichlorobenzene, para dichlorobenzene, ortho dicyanobenzene, furan, tetrathiofulvalene and fluorobenzene have been studied in the special mixtures 56.5 wt% 1132/EBBA at 323K and 70 wt% 5CB/EBBA at 316K, using proton NMR. The measured electric field gradient for these two mixtures has been found to be zero. The order parameters obtained from an analysis of the NMR spectra indicate that the solutes experience a similar anisotropic potential in both mixtures. The results are interpreted in terms of a model for the short-range anisotropic potentials experienced by the solutes.

To further explore the investigation of the short-range forces in zero electric field gradient mixtures, the temperature dependence of the solutes meta dichlorobenzene, ortho dichlorobenzene, 1,3-bromochlorobenzene, benzene and 2-butyne has been studied

in the special mixtures 55 wt% 1132/EBBA and 70 wt% 5CB/EBBA, using proton NMR. These solutes vary from each other in symmetry and shape. The aim was to see how the different shaped solutes experience the short-range forces in the liquid crystal mixtures. The results indicate that the solutes experience a similar anisotropic potential in both mixtures. The biaxial order parameters measured for the solutes meta dichlorobenzene, ortho dichlorobenzene, and 1,3-bromochlorobenzene have also been analysed to magnify the differences between the mixtures.

To extend our understanding on the intermolecular forces among constituent liquid crystal molecules, a temperature dependence study of the liquid crystal 5CB $-$ d_{19} as solute has been undertaken in the three liquid crystal mixtures: 55 wt% 1132/EBBA, 56.5 wt% 1132/EBBA and 70 wt% 5CB/EBBA, using $^2H - NMR$. The study of 5CB $-$ d_{19} as solute has been used to compare the short-range interactions in these special mixtures. The spectra of 5CB $-$ d_{19} in the two 1132/EBBA mixtures are equivalent, but are different from those in the 5CB/EBBA mixture. The spectra in 55 wt% 1132/EBBA and 70 wt% 5CB/EBBA have been analysed using two different models for the short-range potential, and parameters of the models have been used to compare the potentials in the different mixtures. It has been shown that, for a given spectral splitting of the chain C_1 deuteron, the reduced short-range potential is the same in all three mixtures studied. The spectral differences observed are a consequence of different nematic-isotropic phase transition temperatures combined with the effect of trans-gauche isomerization in the hydrocarbon chain.

Table of Contents

List of Tables

List of Figures

Acknowledgement

I would like to thank my supervisor, Prof. Elliott Burnell, for his direction and encouragement to accomplish this thesis. His positive attitude, patience and excellent teaching ability certainly helped me to complete this thesis. I should also mention about the coffee meetings at "Trekkers" and "Expresso", where we discussed a lot of science in the past few years. Certainly, this kind of friendly, informal interaction is an asset to our research group.

Secondly, I thank my colleagues Dr. Dan Zimmerman, Leon C. Ter beek and James Polson for their useful discussions in the past few years. I should mention particularly James Polson, who as a physicist, helped me to understand the fundamentals of NMR. I also thank my former labmates K.Y. Li and Z. Sun. I also like to thank the people in the electronic shop, NMR lab and mechanical shop.

Finally, I must thank my parents in Jaffna, Sri Lanka. Their constant support over the past few years certainly gave me the strength to complete this thesis. I also thank my brother, T. Vasanthakumar, and my sisters, Gowri, Bavani and Shanthy for their support.

Chapter 1

Introduction

Section 1.1 briefly describes the nature of liquid crystals. Section 1.2 introduces the orientational order in liquid crystals and explains how the orientational order can be measured using NMR (Nuclear Magnetic Resonance) techniques. Section 1.2.3 briefly describes how the orientational order can be related to an orientational potential. Section 1.3 deals with the intermolecular forces. The first part of this section describes a few models which have been successful in explaining the intermolecular potential. The second part gives the background of models used in this thesis. Section 1.4 describes a particular system of liquid crystal mixtures, zero electric field gradient mixtures, where only the short range potential is responsible for the orienting mechanism. Finally, section 1.5 briefly describes an outline of the following chapters of this thesis.

1.1 Liquid crystals

1.1.1 General

Some organic compounds show an intermediate phase when these compounds are heated from the solid phase to the liquid phase. The solid phase starts to turn into a "cloudy liquid", and as the heating continues this "cloudy liquid" disappears and turns into an ordinary liquid. This "cloudy liquid" is known as a liquid crystal, and the phase of "cloudy liquid" is known as a liquid crystalline phase or mesomorphic phase. In 1888, Reinitzer first reported the discovery of liquid crystals [1].

One of the most obvious characterstics of liquid crystals is that they appear cloudy, whereas isotropic liquids appear clear. The appearance of cloudiness stems from the interaction of the light with the liquid crystal medium as light passes through. Light, an electromagnetic wave, propagates in the forward direction as it travels inside a material. Only at boundaries between two different materials can its path be changed.

A uniaxial liquid crystal has two principal refractive indices, $n_{||}$ and $n_{\perp}$. In general, the magnitude of $n_{||}$ is greater than $n_{\perp}$. The axis along $n_{||}$ is known as the director axis, and $\perp$ indicates the direction perpendicular to the director. In reality, there exist several domains in liquid crystals; in each domain the liquid crystal molecules align in a preferred direction. When the light passes through the liquid crystal from one domain to another, the director direction also changes. As a result, the refractive indices also change from one domain to another. Therefore, the original wave can cause a new electromagnetic wave to propagate in a direction other than the forward direction. This produces a scattered wave in liquid crystals. It is this scattered light that makes the liquid crystal appear cloudy. The scattering of visible light by nematics is 10^6 times higher than that of a conventional isotropic liquid.

The liquid crystalline phases can be created either by purely thermal processes (thermotropic liquid crystals) or by the influence of solvents (lyotropic liquid crystals). The thermotropic liquid crystals are classified into three categories: nematic, smectic and cholesteric. In the nematic phase, the liquid crystal molecules prefer to align parallel to each other, making a small angle from one to another. The molecules diffuse rapidly and randomly so that there is no positional ordering in the nematic phase. On the other hand, the smectic phases have layered structures; within layers the molecules tend to lie parallel to each other. Therefore, the smectic phases possess a certain degree of positional order. The cholesteric phase is a special category of the nematic phase, formed by optically active molecules. This thesis deals only with the nematic liquid crystals.

Whenever we use the term liquid crystal in the following text, it always refers to nematic liquid crystals.

The liquid crystalline phase is a fluid phase where the liquid crystal flows and takes the shape of its container. Its cloudiness, however, indicates that the liquid crystal differs from ordinary liquids in some fundamental ways. One of the major differences between liquid crystals and either solids or liquids is illustrated in Figure 1.1. The molecules in solids have positional order as well as orientational order. When the solid turns into a liquid, both the positional order and orientational order are lost because of the fast motion of the molecules. In nematic liquid crystals, however, the positional order is lost because of the diffusion of the molecules, but some orientational order remains. The orientational order in nematic liquid crystals is not as perfect as in solids. The molecules in nematic liquid crystals align in a preferred direction, known as the liquid crystal director.

1.1.2 The Effect of magnetic field

In the presence of a strong magnetic field, such as in Nuclear Magnetic Resonance (NMR) experiments, the liquid crystal director aligns either parallel or perpendicular to the field direction. When a magnetic field is applied to a sample of liquid crystal, the electrons around the nuclei precess under the influence of the magnetic field. This leads to an induced magnetic moment that counteracts the field from which it originates. In aromatic systems, the π-electrons in the benzene ring are delocalised and form a ring current. Consequently, when the applied magnetic field is perpendicular to the plane of the ring, a large counteracting magnetic moment in induced.

The amount of magnetization depends on the strength of the applied field. A quantity magnetic susceptiblity is defined as a ratio between the magnetization and the strength of the magnetic field. The magnetic susceptiblity of a liquid crystal is a tensor property, and it has two independent elements $\chi_{||}$, magnetic susceptiblity when the applied

field is parallel to the director, and $\chi_{\perp}$, magnetic susceptiblity when the applied field is perpendicular to the director.

Some liquid crystals prefer to align parallel with the magnetic field, whereas others prefer to align perpendicular to the magnetic field. Liquid crystal molecules having benzene rings usually align their director axis parallel to the field since when the field is parallel to the plane of the benzene ring the interaction energy is lowered. On the other hand, some liquid crystals do not have benzene rings but do have a CN bond. In these liquid crystals, the presence of CN bond along the long axis will have ring current perpendicular to the long axis [2]. As a result, these liquid crystals prefer to align their long axis perpendicular to the magnetic field.

The coupling between the induced magnetic moment and the applied field is very small. A previous study [3] shows that the coupling energy per molecule is the order of $10^{-5}K$ which is very small compared to the thermal energy, k_BT. For a nematic sample, however, the number of molecules in a nematic domain is the order of 10^{23}. Therefore, the coupling energy is much greater than the thermal energy, k_BT. This implies that the director axis of the nematic sample will be aligned with the applied magnetic field.

This thesis deals only with the liquid crystals where the director aligns parallel to the field direction. Alignment of the director can also take place in the presence of an electric field or at the surface of prepared glass plates [3].

1.1.3 Liquid Crystal Display(LCD)

The alignment of the liquid crystals on the surface of glass plates is widely used in Liquid Crystal Display(LCD) technology, which is a major industrial application of liquid crystals. This section briefly describes how the Liquid Crystal Display works.

Polarization filters are fitted on the outside of two glass plates. The polarization planes of the glass plates are turned at 90^0 to each other. The plates are coated on the

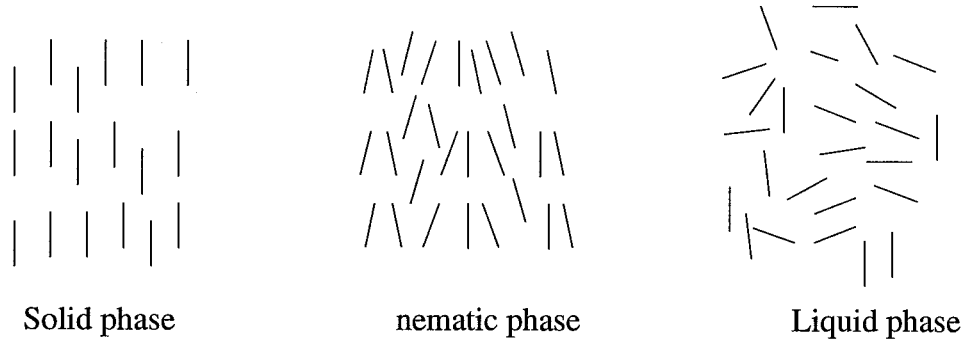

Figure 1.1: Schematic illustration of the solid, liquid crystal and liquid phases. The sticks represent molecules

inside with a transparent,conducting material such as indium tin oxide so that they act as electrodes. The inside glass plate surfaces have a molecule-orienting layer. The liquid crystal material is now placed between the glass plates in such a way that the liquid crystal molecules on the glass plates lie in the direction of the polarization plane. As a result, the director of the nematic liquid crystal is forced to twist through an angle of 90^0. This twist is just like the twist of a chiral nematic liquid crystal, so this produces rotation of the polarization direction as light propagates through the liquid crystal layer. With the correct thickness of the liquid crystal layer and liquid crystal material, the rotation of the polarization direction can be made to follow the twist of the director. The polarization direction of the light is therefore rotated through 90^0 when it strikes the second polarizer at the second glass plate, which is set at 90^0 angle with respect to the first polarizer. Therefore, the light passing through the first polarizer can pass through the second polarizer. There is a reflector, placed behind the second polarizer, which reflects back the light.

If an electric field is applied to both electrodes, the polar liquid crystal molecules line

up parallel to this field, and the director of the liquid crystal molecules are not twisted. Therefore, the light passing through the first polarizer can not get through the second polarizer. Since no light is passed through the second glass plate, no light is reflected back from the reflector. Therefore, the areas with an applied voltage appear dark against those areas without an applied voltage which appear silvery clear. When the electric field is switched off, the elasticity of the molecules makes them return to their helical structure.

The major advantage of LCD technology is the low power consumption which is in the order of 1 $\mu A/cm^2$. Due to the low power consumption of LCD technology, it is possible to link the LCD with modern electronic components. Further, LCDs are light-weight, flat in design and ideal for portable use.

1.2 NMR and Orientational order

There are several techniques used to study the physical properties of nematic liquid crystals, including measurement of magnetic susceptiblity [2], measurement of dielectric constants [2], viscosity measurements and dynamics studies [3]. The orientational order of liquid crystals can be measured using techniques such as Raman scattering [3], Quasi-elastic scattering of X-rays or neuterons [3] and EPR (Electron Paramagnetic Resonance) [3]. NMR has also been a very useful technique to measure the orientational ordering of liquid crystals [4, 5, 6, 7]. NMR has also been used to investigate intermolecular forces among liquid crystal molecules [5, 7]. Further, NMR studies on relaxation phenomena of liquid crystals have been useful in understanding the type of motions in liquid crystals [8, 9, 10, 11, 12]. The first two parts of this section deal with the background theory of Proton NMR ($^1H - NMR$) and Deuteron NMR ($^2H - NMR$). The final part briefly describes the relationship between the orientational order and orientational potential.

1.2.1 $^1H - NMR$

Consider a pair of protons labelled i and j in a molecule in a nematic phase. In a $^1H - NMR$ experiment, an external magnetic field, H_0, is applied along an arbitary direction Z. Each proton spin is coupled to H_0 by the Zeeman interaction, H_Z, which can be written as:

$$H_Z = -\nu_i I_{Zi} - \nu_j I_{Zj} \tag{1.1}$$

where ν_i and ν_j are the resonance frequencies of nuclei i and j. $I_{Z\alpha}$ are the spin operators of these two nuclei along the field direction Z, and α=i, j. The resonance frequencies, ν_α, depend on the chemical shift, $\sigma_{ZZ,\alpha}$ of the nuclei α, the gyromagnetic ratio of the protons, γ_H, and the field strength, H_0

$$\nu_\alpha = \gamma_H H_0(1 - \sigma_{ZZ,\alpha}) \tag{1.2}$$

In addition to the Zeeman interaction, each nucleus experiences a local magnetic field due to the dipolar field created by the other nuclei. The truncated dipolar-dipolar Hamiltonian, H_d, can be written as [13]:

$$H_d = \frac{-\gamma_i\gamma_j h^2}{8\pi^2 r_{ij}^3} < (3\cos^2\theta_{ijZ} - 1) > (3I_{Zi}I_{Zj} - I_i.I_j) \tag{1.3}$$

where γ_i, γ_j are the gyromagnetic ratios of nuclei i and j, r_{ij} is the internuclear distance between nuclei i and j, and θ_{ijZ} is the angle between the interproton vector $\vec{r_{ij}}$ and the external magnetic field direction Z. The angular bracket indicates the statistical average over all possible θ_{ijZ} values. The quantity $\frac{<(3\cos^2\theta_{ijZ}-1>}{2}$ is known as the order parameter, $S^{(ij)}$. In general, the order parameter is non-zero in the nematic phase. As a result, the order parameter is measurable for a pair of protons in the nematic phase. In the isotropic phase, however, this quantity vanishes.

Although the orientation for a pair of protons can be described by a single order parameter, $S^{(ij)}$, the orientation of a molecule, which may have a large number of protons,

in the nematic phase cannot be described by a single order parameter. To describe the orientation of a molecule in a nematic phase, the molecule-fixed axes (x,y,z) are defined, and the order parameters are given by a Saupe ordering matrix S [14]. The matrix elements, $S_{\alpha\beta}$, are given by

$$S_{\alpha\beta} = \frac{1}{2} < (3\cos\theta_{\alpha Z}\cos\theta_{\beta Z} - \delta_{\alpha\beta} >, \tag{1.4}$$

where Z is the direction along the external magnetic field, and α, β = x,y,z, molecule fixed axes. The order matrix is real, symmetric and traceless, and thus it has five independent matrix elements. The number of matrix elements can be reduced, depending on the symmetry of the molecule. In particular, for molecules with C_{3V} or higher symmetry there is only one independent order parameter, and C_{2V} and D_{2h} symmetry molecules have two independent order parameters. The order parameters, $S_{\alpha\beta}$, of the molecule can be obtained from the dipolar splittings of a ^1H-NMR spectrum. The dipolar couplings, D_{ij}, of the molecule are related to its order parameters, $S_{\alpha\beta}$, by the following equation [4]:

$$\begin{aligned} D_{ij} &= \frac{-\gamma_i\gamma_j h}{8\pi^2 r_{ij}^3}[S_{zz}(3\cos^2\theta_{ijz} - 1) + (S_{xx} - S_{yy})(\cos^2\theta_{ijx} - \cos^2\theta_{ijy)}) + \\ &\quad 2S_{xy}(\cos\theta_{ijx}\cos\theta_{ijy}) + 2S_{xz}(\cos\theta_{ijx}\cos\theta_{ijz}) + 2S_{yz}(\cos\theta_{ijy}\cos\theta_{ijz})] \end{aligned} \tag{1.5}$$

Although the ^1H-NMR technique is useful in obtaining the order parameters of a molecule with a few spins, the ^1H-NMR spectrum of a molecule with a large number of spins could be too complicated to analyse. This complexity can be simplified by using ^2H-NMR on partially or fully deuterated molecules.

1.2.2 ^2H-NMR

Deuterium nuclei, which have spin $I = 1$, have electric quadrupole moments. In addition to the Zeeman interaction experienced by deuterium nuclei, the dominant interaction is

that between the nuclear electric quadrupole moment of the ^2H nucleus and the electric field gradient experienced by the nucleus. The Quadrupolar Hamiltonian, H_Q, in the principal axis system (x',y',z') is given by the following [13]:

$$H_Q = \frac{eQ}{6}[V_{z'z'}(3I_{z'}^2 - I^2) + (V_{x'x'} - V_{y'y'})(I_{x'}^2 - I_{y'}^2)] \tag{1.6}$$

where $V_{\alpha\alpha}$ is the electric field gradient tensor component along the principal axis direction α= x', y', z'. eQ is the electric quadrupole moment of the ^2H nucleus and $I_{x'}$, $I_{y'}$, $I_{z'}$ are spin operators of the ^2H nucleus. By defining eq=$V_{z'z'}$ and $\eta = \frac{V_{x'x'} - V_{y'y'}}{V_{z'z'}}$, equation (1.6) can be rewritten as:

$$H_Q = \frac{e^2qQ}{4I(2I-1)}[(3I_{z'}^2 - I^2) + \eta(I_{x'}^2 - I_{y'}^2)] \tag{1.7}$$

Thus, the total Hamiltonian, the Zeeman and Quadrupolar, can be written as:

$$H_T = -\gamma_D h H_0 I_Z + \frac{e^2qQ}{4I(2I-1)}[(3I_{z'}^2 - I^2) + \eta(I_{x'}^2 - I_{y'}^2)] \tag{1.8}$$

where Z is the direction of the external magnetic field. For deuterated molecules, the (x', y', z') axes are defined for each C-D bond. The z' axis is taken to be along the C-D bond axis, and x',y' axes are perpendicular to the C-D bond. Since the spin is quantized along the Z direction, the total Hamiltonian is written in the (X, Y, Z) axis system using a coordinate transformation:

$$H_T = -\gamma_D h H_0 I_Z + \frac{e^2qQ}{4I(2I-1)}[(3I_Z^2 - I^2)][(3\cos^2\theta - 1) + \eta\sin^2\theta\cos 2\alpha] \tag{1.9}$$

where θ is the angle between the C-D bond and the external magnetic field, H_0, direction, and α is the azimuthal polar angle.

In ^2H-NMR experiments, the external magnetic field is of the order of 10^4 gauss; therefore, the quadrupolar Hamiltonian, H_Q, can be treated as a perturbation to the Zeeman Hamiltonian, H_Z. Using first order perturbation theory [13], the energy levels

of the Quadrupolar Hamiltonian are given by:

$$E_m = \frac{e^2qQ}{8I(2I-1)}[(3m^2 - I(I+1)][(3\cos^2\theta - 1) + \eta \sin^2\theta \cos 2\alpha] \tag{1.10}$$

where m is the spin quantum number of the Zeeman Hamiltonian. The energy level splittings due to Zeeman and Quadrupolar interactions are shown in Figure 1.2.

For C-D bonds in methyl groups and methylene groups, the electric field gradient tensor component along the C-D bond is axially symmetric, resulting in $V_{x'x'} = V_{y'y'}$. Thus, the quadrupolar splitting, $\Delta\nu_Q$, is given by

$$\Delta\nu_Q = \frac{3e^2qQ}{4h} < (3\cos^2\theta - 1) > \tag{1.11}$$

where $\frac{<(3\cos^2\theta-1)>}{2}$ is the order parameter, S_{CD}, of the C-D bond. For C-D bonds in rings, the expression for $\Delta\nu_Q$ can be obtained using equation (1.10).

For powder samples, θ takes values ranging from 0^0 to 360^0, and this leads to a powder pattern spectrum [15]. In liquid crystals, however, the S_{CD} is averaged over all motions to take an absolute value between 0 and 1. Therefore, the $^2H - NMR$ spectrum of a deuterium nucleus in liquid crystals consists of a pair of lines separated by $\frac{3e^2qQ}{2h}S_{CD}$. Note that $\frac{<(3\cos^2\theta-1)>}{2}$ is averaged to zero in isotropic liquids because of the rapid tumbling motion of molecules.

1.2.3 The Orientational Distribution Function

The orientation of molecules in a nematic phase can be specified by a singlet distribution function, $f(\Omega)$, where Ω denotes the Eulerian angles. The $f(\Omega)$ can be related to the orientational potential, $U(\Omega)$, by

$$f(\Omega) = \frac{exp(-U(\Omega)/kT)}{Z} \tag{1.12}$$

where $Z = \int exp(-U(\Omega)/kT)d\Omega$. $U(\Omega)$ is the mean field potential experienced by a single molecule, and this potential is responsible for the molecules orienting in a preferred

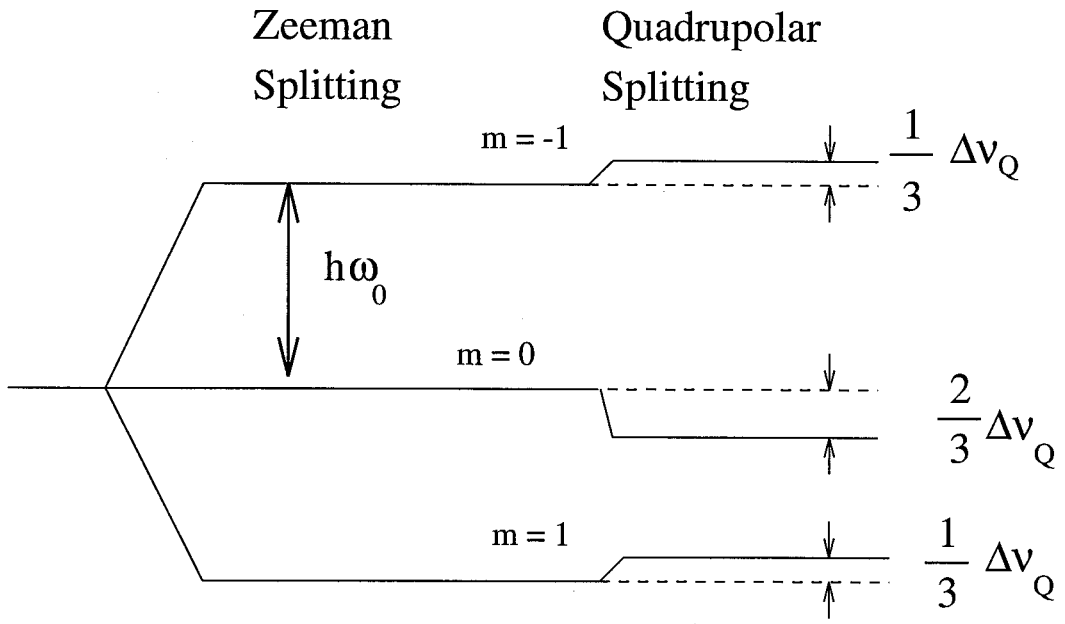

Figure 1.2: Energy level diagram showing the effects of the Zeeman and Quadrupolar interactions on the nuclear states for a spin $I = 1$ nucleus.

direction. Any measurable property, A_{av}, can be given as a statistical summation of a single molecular property, A_Ω, by

$$A_{av} = \int_\Omega f_\Omega A_\Omega d\Omega \tag{1.13}$$

Therefore, the molecular order parameter, $S_{\alpha\beta}$, can be related to the orientational potential, $U(\Omega)$, by following equation (see Appendix A for further details):

$$S_{\alpha\beta} = \frac{\int (3\cos\theta_\alpha \cos\theta_\beta - \delta_{\alpha\beta}) exp(-U(\Omega)/kT) d\Omega}{2\int exp(-U(\Omega)/kT) d\Omega} \tag{1.14}$$

The orientational potential, $U(\Omega)$, can be investigated in various ways. In some studies, the orientational order of pure nematics are measured to investigate the potential. In other cases, a probe solute is dissolved in a liquid crystal solvent and the orientational order of the probe solute is investigated in terms of the orientational potential. In this

thesis, probe solutes are dissolved in liquid crystal solvents to investigate the intermolecular forces.

It is assumed that when liquid crystals are used as solvents, the solute concentration is sufficiently dilute that the solute does not perturb the liquid crystal solvent. In other words, the addition of small amount of solute only changes the physical properties of the liquid crystal such as nematic-isotropic transition temperature and order parameter, but it does not change the fundamental nature of the liquid crystal. Further, it shall be shown in this thesis that the forces acting on a small solute by the surrounding liquid crystal molecules are similiar to those acting on a probe liquid crystal molecule by the surrounding liquid crystal molecules.

1.3 Intermolecular Forces

1.3.1 General

The investigation of intermolecular forces has been important in understanding the physical nature of liquid crystals. The anisotropic intermolecular forces are often described by a mean field pseudo potential which is expressed in terms of a long range potential and a short range potential. The long range force is mainly due to interactions such as dispersion forces and electrostatic interactions. The short range force, on the other hand, is a repulsive interaction which is a consequence of overlap of electron clouds between two neighbouring molecules. The first part of this section describes a few theories which have been successful in explaining intermolecular forces. The second part of this section deals with models used in this thesis for the long range forces and the short range forces.

Maier-Saupe model

Maier-Saupe theory [16] was developed to describe a few thermodynamic properties of nematics. In Maier-Saupe theory, it is assumed that the anisotropic long range forces were responsible for the existence of the nematic phase. The theory also assumed that the constituent liquid crystal molecules are rigid and possess cylindrical symmetry.

The anisotropic pair potential between two molecules, U_a, is written as

$$U_a(r_{12}, \theta_{12}) = -u(r_{12}) P_2(\cos\theta_{12}), \tag{1.15}$$

where $P_2(\cos\theta_{12})$ is the second Legendre polynomial, and $u(r_{12})$ is a proportionality constant that depends upon the intermolecular separation. The potential is a function of the intermolecular separation, r_{12}, and the angle between the two molecular symmetry axes, θ_{12}. The mean field approximation is implemented by taking three averages of the pair potential to derive the mean field potential: over all orientations of intermolecular vector r_{12}, over all orientations of molecule 2, and over the intermolecular separation r_{12}. The mean field potential, $U(\theta)$, can be written as:

$$U(\theta) = -\epsilon < P_2(\cos\theta) > P_2(\cos\theta) \tag{1.16}$$

where ϵ is an interaction coefficent, $< P_2(\cos\theta) >$ is the order parameter of the liquid crystal. This potential was used to calculate the order parameter of the nematics as a function of temperature. A prediction of this theory is that a plot of the order parameter vs. reduced temperature falls on a universal curve.

Emsley - Luckhurst model

The Maier-Saupe theory assumed cylindrical symmetry for constituent molecules forming liquid crystals. In reality, the constituent molecules do not have this high symmetry.

Luckhurst *et. al* [17] extended the Maier-Saupe theory for lath-like molecules. The potential of the mean torque, $U(\theta, \psi)$, now contains two terms:

$$U(\theta, \psi) = -[\epsilon_{2,0} d^2_{0,0}(\theta) + \epsilon_{2,2} d^2_{0,2}(\theta) \cos 2\psi] \tag{1.17}$$

where $d^2_{0,0}(\theta) = P_2(\cos\theta)$ and $d^2_{0,2}(\theta) = \sqrt{\frac{3}{8}} \sin^2\theta$. The θ and ψ are polar and azimuthal angles respectively, describing the orientation of the director in the molecule-fixed frame. The first term in equation (1.17) is equivalent to the potential given by equation(1.16) derived for cylindrically symmetric molecules. The second term results from molecular biaxiality.

Samulski's model

Samulski and coworkers [18, 19, 20] in their study of n-alkanes in liquid crystal solvents have incorporated the molecular shape anisotropy into the intermolecular potential. The potential has two terms:

$$U = -W_0 \sum_{i=1}^{N} P_2(\vec{s^i}, \vec{s^i}) - W_1 \sum_{i=1}^{N-1} P_2(\vec{s^i}, \vec{s^{i+1}}) \tag{1.18}$$

The first term corresponds to alignment of the alkyl chain through aligning of individual C-C bonds in an uncorrelated fashion. Each C-C bond was treated as an independent uniaxial particle whose orientational energy is proportional to $< P_2(\cos\theta_i) >$, where θ_i is the angle between the C-C bond and the director axis, Z. The second term corresponds to the alignment of midpoints of a pair of adjacent C-C bonds (chord model). This term reflects how the shape of the molecule contributes to the short range part of the intermolecular potential.

Other models

Gilson *et. al* have studied small solutes dissolved in liquid crystals to investigate the short range potential [21, 22, 23, 24, 25]. The short range potential is modelled as:

$$U(\theta, \phi) = -AS^{(1)}(\cos^2\theta + B\sin^2\theta\cos 2\phi) \tag{1.19}$$

where θ and ϕ are the polar and azimuthal angles , and $S^{(1)}$ is the solvent order parameter. The parameter A is the potential energy difference between the orientations where the long molecular axis is parallel and perpendicular to the nematic director. The parameter product AB is the potential energy difference between the orientations of the two axes, which are perpendicular to the molecular long axis. This model reflects the size and shape of the solute molecule. Further, Ferrarni *et. al* have described a shape model for the short range potential [26].

1.3.2 Burnell's model

In this section I shall describe how the long range and short range interactions are modelled by Burnell's group. The first part deals with the measurement of an average electric field gradient in liquid crystals and with the long range interaction in terms of electrostatic interactions. The second part deals with modelling of the short range potential.

Long range interaction

Although a liquid crystal molecule generally is an uncharged particle, the presence of charge distribution in the liquid crystal molecule induces an electric field, electric field gradient and higher order terms at a point, say P, in space. The average electric field, $\bar{E}$, experienced at the point P is an average over all the electric fields induced by all

the surrounding liquid crystal molecules at the point P. Due to the inversion symmetry and cylindrical symmetry of the nematic phase, it can be shown that the average electric field, $\bar{E}$, vanishes at the point P.

Similarly, the charge distribution present in the liquid crystal molecule induces an electric field gradient at the point P. The average electric field gradient is an average over all surrounding liquid crystal molecules. The average electric field gradient is a tensor property; it has 9 independent matrix elements; and the electric field gradient is a traceless tensor. Further, due to the inversion and cylindrical symmetry of the nematic phase, it can be shown that the off-diagonal matrix elements, $F_{\alpha\beta}$, become zero, where α, β = X,Y,Z, director fixed axes. In addition, the matrix elements F_{XX} and F_{YY} are indistinguishable due to the cylindrical symmetry of the nematic phase. Therefore, the average electric field gradient for a liquid crystal can be described by a single parameter F_{ZZ}.

The measurement of the average electric field gradient present in liquid crystals has been achieved by many researchers. Jokisaari *et. al* have used monoatomic noble gases dissolved in liquid crystals to measure the average electric field gradient [27, 28, 29, 30]. Burnell *et. al* have used D_2 gas dissolved in liquid crystals to measure the average electric field gradient [31, 32, 33]. The average electric field gradient, $\overline{F_{ZZ}}$, experienced by the D_2 gas in liquid crystals can be written as a sum of intramolecular and intermolecular contributions:

$$\overline{F_{ZZ}} = \overline{F_{ZZ}}(intermolecular) - eqS \tag{1.20}$$

where eq is the electric field gradient component along the D-D bond and S is the order parameter of the D-D bond. The $^2H - NMR$ spectrum of D_2 gas in a liquid crystal environment has been used to obtain the quadrupolar coupling, B_{obs}, and the dipolar coupling, D_{DD}. The B_{obs} and D_{DD} are then related to obtain the experimental order

parameter S and F_{ZZ} by the following equations [32]:

$$B_{obs} = -\frac{3eQ_D}{4h}(F_{ZZ}(intermolecular) - eqS) \tag{1.21}$$

$$D_{DD} = \frac{-\gamma_D^2 h}{4\pi^2 r_{ij}^3} S \tag{1.22}$$

where γ_D is the gyromagnetic ratio of the deuterons and Q_D is the electric quadrupole moment of deuterium nucleus.

The presence of an average electric field gradient in liquid crystals suggests that there is a possiblity of an electrostatic interaction between the average electric field gradient and another second rank tensor property of the solute molecule. The mean-field electrostatic potential is described in terms of the average electric field gradient and the electric quadrupole moment of solute molecule, $Q_{\alpha\beta}$, by [34, 35]:

$$U = -\frac{1}{2}Q_{\alpha\beta}\overline{F_{ZZ}} < (\frac{3}{2}\cos\theta_\alpha \cos\theta_\beta - \frac{1}{2}\delta_{\alpha\beta}) > \tag{1.23}$$

where θ_α, θ_β are the angles between the α, β axes of the solute molecule and the nematic director, Z, axis. The term on the right hand side of equation (1.23) is the third term in the multipole expansion of the mean field potential. The first two terms vanish for uncharged solutes in liquid crystals. The higher order terms are neglected.

Using the values of $\overline{F_{ZZ}}$ and Q_D [36] for D_2, the order parameter, S, was recalculated by using a proper quantum calculation [33]. The calculated order parameter agreed very well with the experimental order parameter. Furthermore, the studies of small solutes H_2, HD dissolved in the liquid crystals showed that the calculated order parameter agreed well with the corresponding experimental order parameters. These results show that the electric field gradient - electric quadrupole interaction is sufficient to explain the orientation of small solutes such as D_2, HD and H_2 in liquid crystals. For planar solutes such as benzene derivatives and for linear molecules, however, the electrostatic potential was not sufficient to describe their orientation in liquid crystals. In order to

describe the orientation of these large solutes in liquid crystals, Burnell and coworkers [38] have included a short range potential, in addition to the long range potential, in the intermolecular potential.

Short range potential

This section describes how the short-range potential is modelled in terms of size and shape of the solute molecule. Van der Est *et al.* [38] introduced a model for the short-range interaction, wherein the liquid crystal is considered as an elastic tube aligned parallel to the nematic director axis, Z. The introduction of the solute displaces the wall of the elastic tube in the X-Y direction, but keeps the wall parallel to the Z direction. The displacement caused by the presence of the solute molecule leads to a restoring force, which is proportional to the deformation of the elastic tube in the X-Y direction (Hooke's law). The restoring force, $dF(\Omega)$, is given by [38, 39]

$$dF(\Omega) = -kdC(\Omega), \tag{1.24}$$

where $C(\Omega)$ is the circumference of the deformed tube, and k is the force constant, a property of the liquid crystal. The potential energy associated with the interaction of the solute molecule with the elastic wall is given by [38, 39]:

$$U_{sr}(\Omega) = -\int F(\Omega)dC(\Omega) = \frac{kC^2(\Omega)}{2} \tag{1.25}$$

The order parameters recalculated using equation (1.25) for a collection of small solutes in the 55% 1132/EBBA mixture agreed well with the experimental order parameters [40]. In this calculation, the experimental order parameters were used to obtain the best fit model parameter k. When the fit was done for individual solutes, the parameter k was consistently smaller for larger solutes such as 2,4-hexadiyne, 1CB (1-cyano biphenyl) and 5CB (5-cyano biphenyl) than for smaller solutes. Zimmerman *et al.* then extended the

original short-range potential [38] in two different ways. The first way shall be referred to as CZ model, and the second way shall be referred to as CI model.

(a) CZ model

In the CZ model, the solute is modelled as a cylinder, and the potential energy is effectively the energy required to displace the liquid crystal solvent molecules upon the introduction of the cylinder. The modified short range potential is written as [40]

$$U_{sr}(\Omega) = 1/2k_z C^2(\Omega) + 1/2k_{xy} Z(\Omega)C(\Omega) \tag{1.26}$$

where k_z and k_{xy} are the model parameters, $Z(\Omega)$ is the length of the cylinder and $C(\Omega)$ is proportional to the radius of the cylinder as shown in Figure (1.3). The short-range potential given by equation (1.26) gave a good and consistent fit for large as well as small solutes in the 55% 1132/EBBA mixture [40]. Equation (1.26) can be rewritten in terms of the model parameters k_z and ξ as

$$U_{sr}(\Omega) = 1/2k_z C(\Omega)^2 + 1/2k_z \xi Z(\Omega)C(\Omega) \tag{1.27}$$

where $\xi = k_{xy}/k_z$ is dimensionless. Calculations using equations (1.26) or (1.27) for the short range potential shall be referred to as CZ model calculations in this thesis. In the notation CZ, the 'C' refers to $C(\Omega)$ term in equations (1.26) and (1.27) the 'Z' refers to the term $Z(\Omega)$.

(b) CI model

In an attempt to introduce a better model for the anisotropic short-range interaction between the solute surface and the liquid crystal, Zimmermann *et al.* [41] suggested that the short range potential can be written

$$U_{sr}(\Omega) = 1/2k_s \int C_Z(\Omega)dZ, \tag{1.28}$$

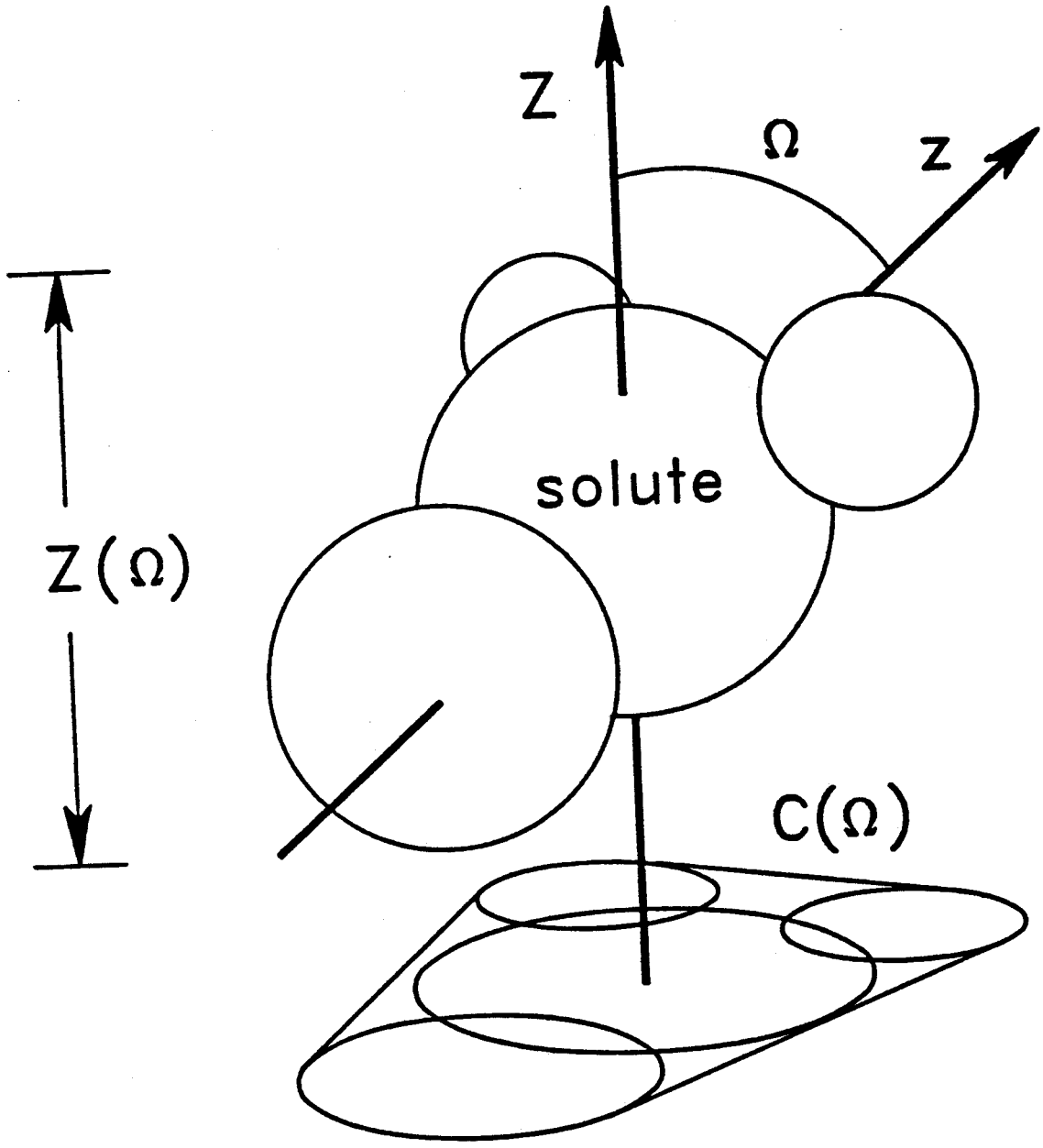

Figure 1.3: The anisotropic potential given by the CZ model, where $Z(\Omega)$ is the projection of the molecule onto the director axis, Z. $C(\Omega)$ is the circumference around the projection onto the (X, Y) plane.

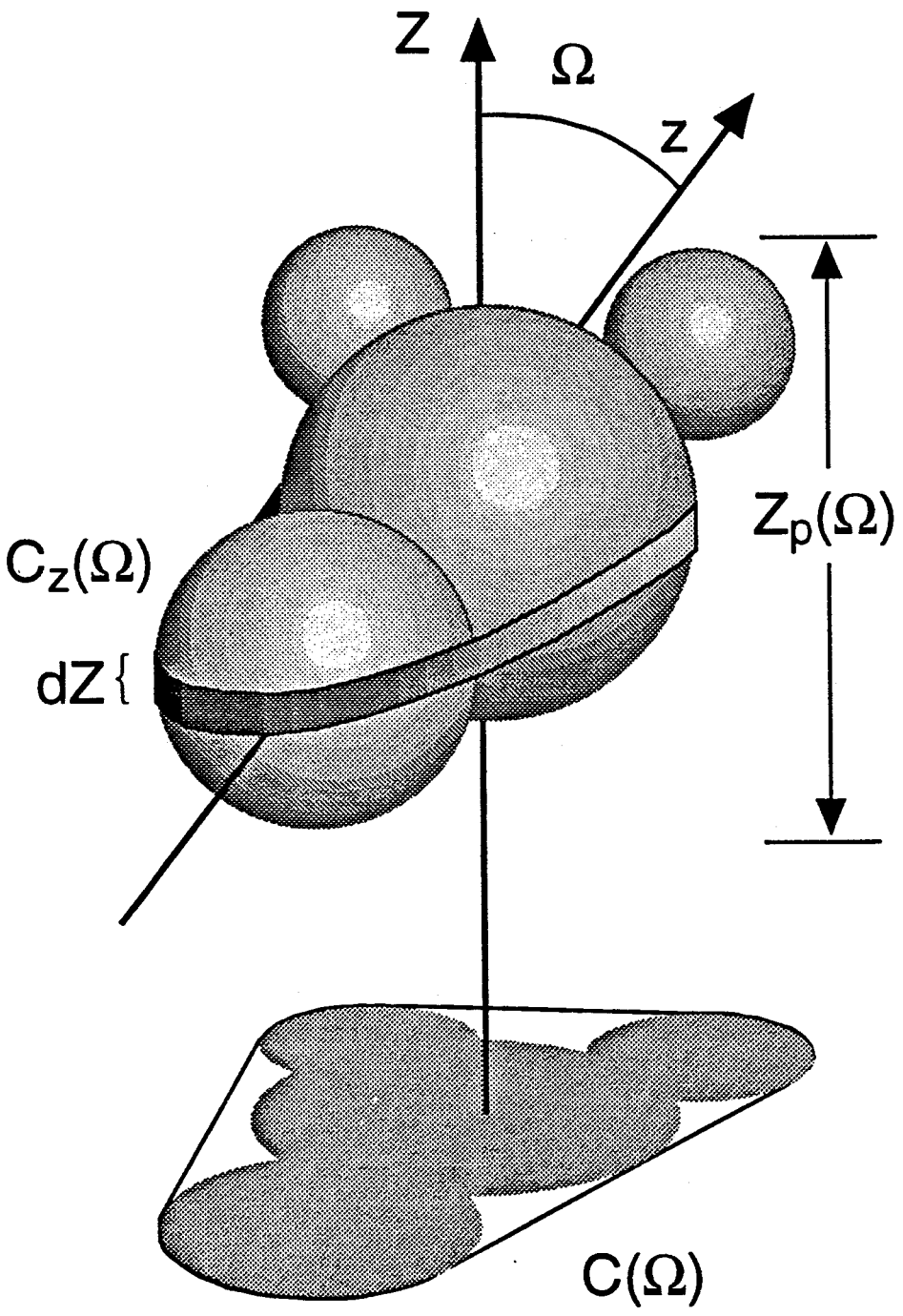

Figure 1.4: The anisotropic potential given by the CI model, where $Z_p(\Omega)$ is the length of the projection of the molecule onto the Z axis. $C_Z(\Omega)$ is the 'minimum' circumference obtained by including only the circles formed by the atoms where they intersect a plane located at Z.

where k_s is the model parameter and $C_Z(\Omega)$ is the circumference of the solute at distance Z. (see figure 1.4) The potential is obtained by adding contributions from the surface elements, where each surface element contributes an amount that depends on its orientation with respect to the director. The short-range potential given by equation (1.28) may be interpreted as an anisotropic surface interaction between the surface of solute molecule and the surrounding liquid crystals.

Combining the solute surface interaction with the liquid crystal medium and the elastic distortion of the liquid crystal (Van der Est's original model), the short range potential is written as:

$$U_{sr}(\Omega) = 1/2kC(\Omega)^2 + 1/2k_s \int C_Z(\Omega)dZ, \tag{1.29}$$

where k and k_s are the model parameters, and $C_Z(\Omega)$ is the circumference of the solute at distance Z (see Fig. 1.4). The first term, as in the case of Van der Est *et al.* [38], accounts for the elastic distortion of the liquid crystal. This model gave the best fit to the experimental order parameters of 46 solutes in 55% 1132/EBBA. Equation (1.29) can be rewritten in terms of the model parameters k and ξ' as

$$U_{sr}(\Omega) = 1/2kC(\Omega)^2 + 1/2k\xi' \int C_Z(\Omega)dZ \tag{1.30}$$

where $\xi' = k/k_s$ is dimensionless. The calculations using equation (1.28) or (1.29) for the short range potential shall be referred to as CI model calculations in this thesis. In the notation CI, the 'C' refers to $C(\Omega)$ term in equations (1.29) and (1.30), and the 'I' refers to the integral term.

1.4 Zero electric field gradient mixtures

This section deals with a system where the long range potential contribution to the intermolecular potential can be eliminated. The long range electrostatic potential depends

on the electric quadrupole moment of solute and the average electric field gradient of the liquid crystal solvent. To remove the long range forces, the system must have either zero electric quadrupole moment of the solute or a zero electric field gradient in the liquid crystal solvent. In reality, it is impossible to find an orienting solute molecule with a vanishing electric quadrupole moment. On the other hand, Burnell and coworkers have shown that a system can be prepared where the average electric field gradient is negligibly small. I shall briefly explain how the system having a zero electric field gradient can be prepared.

The D_2 molecule, as a solute, was used to measure the average electric field gradients of nematic liquid crystal solvents N-(4-ethoxybenzylidene)-4'-n-butylaniline (EBBA) and the mixture Merck ZLI 1132 [31, 33, 32]. The signs of the electric field gradients in these two liquid crystal solvents are opposite, with the sign in 1132 being positive and that in EBBA being negative. A series of liquid crystal mixtures of EBBA and 1132 were studied using D_2 to measure the average electric field gradient [32]. The average electric field gradient was found to be zero for a particular mixture, 55 wt% 1132/EBBA, at 301.4K. Other studies [37] show that the solute methane also experiences an average zero electric field gradient in the mixture 55 wt% 1132/EBBA at 301.4K.

There are several possiblities in preparing zero electric field gradient mixtures. One is to use the same combination of liquid crystals such as 1132 and EBBA, but vary the composition. For example, Barnhoorn *et al.* [42] investigated 56.5 wt% 1132/EBBA using D_2 as a solute and found that the average electric field gradient is zero at 322K. Another possibility is to choose a different pair of liquid crystals which have average electric field gradients of opposite sign. For one of the components, it would be interesting to use the liquid crystal 5CB ((4-n-pentyl)-4'-cyanobiphenyl), a relatively simple nematic liquid crystal that has received a lot of experimental and theoretical attention from the NMR community [43, 44, 45, 46, 47, 48, 49, 50]. D_2 has been used to measure the electric

field gradient in this liquid crystal at various temperatures [50]. The magnitude of the average electric field gradient in 5CB is found to be 30 per cent as large as that observed in EBBA, but of opposite sign. This suggests that the electric field gradient should be zero in a mixture of 5CB and EBBA. A study of D_2 dissolved in the liquid crystal mixture 70 wt% 5CB/EBBA shows that its measured electric field gradient is zero at 316K [42].

These special mixtures 55% 1132/EBBA, 56.5% 1132/EBBA and 70% 5CB/EBBA, in which the measured average electric field gradient is zero, shall be referred to as zero efg mixtures in this thesis. Such mixtures experience a zero electric field gradient at a precise temperature; at other temperatures there exists a small non-zero electric field gradient. However, it will be shown in the following sections that this small electric field gradient does not significantly affect the results. Therefore, throughout this thesis, the term zero efg mixture will be used to include the nematic temperature range of a mixture that exhibits a zero electric field gradient at some temperature within this range.

1.5 Outline of the thesis

One of the aims of this thesis is to compare the intermolecular forces in three different liquid crystal solvents. In order to eliminate the long range contribution to the intermolecular potential, zero efg mixtures are used as liquid crystal solvents in this thesis. Three different zero efg mixtures, 55% 1132/EBBA, 56.5% 1132/EBBA and 70% 5CB/EBBA have been chosen in this study. It is assumed that only short range interactions contribute to the anisotropic potential in the zero efg mixtures. Solutes chosen vary from highly symmetric solutes to a large liquid crystal molecule (5CB-d_{19}).

Chapter 2 briefly explains the experimental techniques used in this thesis. Chapter 3 presents a study of a few solutes with C_{2V} and D_{2h} symmetry using Proton NMR in the zero efg mixtures 70% 5CB/EBBA at 316K and 56.5% 1132/EBBA at 323K. The purpose

is to compare the short range potentials experienced by the solutes with C_{2V} symmetry in these two zero efg mixtures. For these solutes, two independent order parameters S_{zz} and $S_{xx} - S_{yy}$ are measured from the experimental spectrum, and these order parameters are related to the short range potential.

In Chapter 4, two C_3 and higher symmetry molecules, two C_{2V} symmetry molecules, a C_S symmetry molecule and a linear molecule are studied using Proton NMR in the zero efg mixtures 55% 1132/EBBA and 70% 5CB/EBBA as a function of temperature. The purpose is to compare the short range potentials experienced by small solutes of different sizes, ranging from highly symmetric to linear, in the zero efg mixtures.

In Chapters 5 and 6, the molecule 5CB-d_{19} (perdeuterated 5CB) that by itself forms a nematic liquid crystalline phase is studied using ^2H-NMR in the three zero efg mixtures 55% 1132/EBBA, 56.5% 1132/EBBA and 70% 5CB/EBBA as a function of temperature. The purpose here is to compare the short range interactions experienced by a liquid crystal molecule in zero efg mixtures. This particular system is useful to understand the intermolecular forces existing among constituent liquid crystal molecules in the nematic phase. The spectra of 5CB-d_{19} in 55% 1132/EBBA and 70% 5CB/EBBA are analysed using the CZ and CI models. The two-parameter models were chosen for the analysis because they gave a very good fit for larger solute 5CB; as well, the choice of two-parameter models allows us to study the temperature dependence of the ratios of the model parameters, ξ and ξ'.

Chapter 2

Experimental

2.1 Sample Preparation

The liquid crystal ZLI-1132, which is an eutectic mixture of alkylcyclohexylcyanobenzene and alkylcyclohexylcyanobiphenyls, was purchased from Merck and not purified prior to use. The liquid crystal EBBA was synthesized in Amsterdam according to ref. [51]. The liquid crystal 5CB was purchased from Merck and not purified prior to use. Appropriate weights of liquid crystals 1132, EBBA and 5CB were used to prepare the mixtures 55 wt% 1132/EBBA, 56.5 wt% 1132/EBBA, and 70 wt% 5CB/EBBA.

The solutes ortho dichlorobenzene (ODCB) meta dichlorobenzene (MDCB), para dichlorobenzene (PDCB), trichlorobenzene (TCB), furan (FUR), ortho dicyanobenzene (ODCyB), tetrathiofulvalene (TTF), fluorobenzene (FB), 1,3-bromochloro benzene (1,3-BrCl), benzene (BENZ) and 2-butyne (2-BUTY) were all commercially available and were used without further purification. The abbreviations above shall be used throughout this thesis to refer to the appropriate names of the solutes.

For experiments involving the small solutes, the liquid crystal mixtures were placed into 5mm NMR sample tubes, and 1-5 mol% of the solute was dissolved in each liquid crystal mixture. In each sample tube, approximately 0.5 mol% of TCB was also dissolved for scaling purpose. The mixture was heated to the isotropic phase and mixed using a vortex stirrer.

The solute $5CB - d_{19}$ was synthesized at UBC [52] by Prof. Bates. 1-2 wt% of

5CB – d_{19} as solute was dissolved in each of the liquid crystal mixtures, 55 wt% 1132/EBBA, 56.5 wt% 1132/EBBA, and 70 wt% 5CB/EBBA. Each mixture was heated to the isotropic phase and mixed using a vortex stirrer. The sample was subjected to freeze-pump-thaw cycles until no gas evolved from the liquid crystal mixture. The samples were transferred to NMR tubes, and the tubes were flame sealed under vacuum.

2.2 ^1H-NMR experiments

Proton NMR experiments were performed on a Bruker WH-400 spectrometer, with a high resolution probe having a saddle coil, operating at 9.4T. The proton resonance frequency was 400 MHz. For the high resolution probe, the 90^0 pulse length was typically 10-12 microsec. The experiment was a single pulse experiment (90_X - DE- ACQ), where DE is a delay to compensate for receiver deadtime, and ACQ denotes acquisition time of the free induction decay (FID). The value of DE was set automatically by the spectrometer. In single pulse experiments the phases of pulse and receiver were cycled through a four pulse phase cycling scheme X, -X, Y, -Y in order to reduce the effects of pulse and receiver imperfections. Normally 16-32 FID's were collected using a spectral width of 10 KHz. The accumulated FID was Fourier transformed to obtain the spectrum.

In high resolution NMR experiments, the applied magnetic field is along the long axis of NMR sample tube. This permits the sample to be spinned without destroying the orientation of the nematic phase. If spinning is not done, then the magnetic field gradient along the X and Y directions would produce broadened peaks. The spinning rate was 30Hz.

Shimming the magnet is very important to obtain very narrow peaks in high resolution NMR spectroscopy. The shimming can be done either by optimising a lock signal or by optimising the envelope of the FID. Since optimising on the FID was a difficult task in

the nematic phase, a field-frequency lock was used to shim the magnet. Acetone-d_6 was chosen as lock solvent. The lock solvent was filled up to $\frac{2}{3}$ of a capilliary tube, which was mounted coaxially inside the 5mm-NMR sample tube using teflon spacers. The Z and Z^2 magnetic field gradients were shimmed to obtain an optimum lock signal. After shimming, the linewidths of solute peaks in the nematic phase were typically 1-2 Hz for a room temperature spectrum.

Temperature of the experiment was controlled by a Bruker temperature control unit using air flow. The temperature was calibrated against the proton chemical shift difference in an ethylene glycol sample.

2.3 ^2H-NMR experiments

Deuteron NMR experiments were performed on a Bruker CXP-200 NMR spectrometer, with a high power probe having a 1cm-diameter solenoid coil, operating at 4.7T. The deuteron resonance frequency was 30.76 MHz. The 90^0 pulse length was 5μsec. The Quadrupolar echo method (90_X- τ- 90_Y- τ- echo) [53] was used to avoid the effects of receiver deadtime. The delay, τ, was set to 100μsec, and the recycling time was chosen to be 1 sec.

The pulses were cycled through a 4-pulse cycling sequence, (XY, -XY, X-Y, -X-Y), and the resulting echoes were alternatively added and substracted from the computer memory. The quadrupolar echo was digitized by a digital oscilloscope. The FID was collected using a spectral width of 100 KHz. 2048-8096 FID's were accumulated to obtain a good signal to noise ratio, depending on the temperature of the experiment. The accumulated FID was Fourier transformed to obtain the spectrum.

The sample was placed horizontally inside the solenoid coil. The solenoid coil was covered by a cylindrical teflon chamber (4 cm diameter and 3cm height) for insulation.

The temperature of the experiment was controlled by a Bruker temperature control unit. The temperature control unit was equipped with a heating coil and a thermocouple. The thermocouple was placed below the solenoid coil, and the voltage from the thermocouple was compared to a reference voltage corresponding to a "desired temperature" set at the temperature control unit. If the reference voltage was greater than the thermocouple voltage, then a voltage proportional to the difference of two voltages was applied to the heating coil. This heating coil was surrounded by a glass tube such that air can be passed through this flow tube. The heated air was circulated into the sample chamber in order to heat the sample. Once the thermocouple reached the same temperature as the "desired temperature", then a constant current was applied to the heating coil.

The temperature of the sample was measured using another Copper-Constantan thermocouple, which was placed just above the solenoid coil. The end of this thermocouple was connected to a digital volt meter (DVM) to measure the voltage. The voltage measured by the DVM was converted into temperature to an accuracy of $+0.1^0$ C, using a calibrated conversion table.

2.4 Microscopic study

Separate microscope slides were prepared from the pure solvents 55 % 1132/EBBA and 70% 5CB/EBBA, and were studied using a Leitz Laborlux 12POL polarizing microscope equipped with a Mettler FP-2 heating stage by Dr. Mary E. Neubert at Kent state University to determine the phase transitions of these zero efg mixtures. It was found that T_{NI}, the nematic-isotropic transition temperature, of 55 % 1132/EBBA is in the range 341.8K to 342.4K, and that T_{NI} of 70% 5CB/EBBA is in the range 320.6K to 321.4K. It was also found that these two liquid crystal mixtures are in the nematic phase over the temperature range used for the NMR experiments.

Chapter 3

Orientation of C_{2V} and D_{2h} symmetry solutes in zero efg mixtures

3.1 Introduction

The study of intermolecular forces in liquid crystals is a complicated problem. A system of a small solute as a probe molecule dissolved in a liquid crystal can be a good starting point to understand the nature of intermolecular forces. The system can be further simplified by choosing zero efg mixtures as liquid crystal solvents, where only the short-range interactions are present to orient the probe solute molecule. In this chapter, several C_{2V} and D_{2h} symmetry solutes are investigated in two zero efg mixtures 56.5% 1132/EBBA at 323K and 70% 5CB/EBBA at 316K. The solutes studied are ortho dichlorobenzene (ODCB), meta dichlorobenzene (MDCB), para dichlorobenzene (PDCB), furan (FUR), ortho dicyanobenzene (ODCyB), tetrathiofulvalene (TTF) and fluorobenzene (FB).

Section 3.2.1 deals with how the dipolar couplings, D_{ij}, and order parameters, $S_{\alpha\beta}$, can be obtained from ^{1}H-NMR spectra. Section 3.2.2 compares the orientation of solutes in the zero efg mixtures. Section 3.3 deals with comparison of short range interactions in the zero efg mixtures in terms of model parameters.

3.2 Results

3.2.1 Analysis

The total Hamiltonian, H_T, including Chemical shift, Dipolar and indirect-dipolar Hamiltonians of the solute molecule in the nematic phase can be written as:

$$H_T = -\sum_i \nu_i I_{Zi} + \sum_i \sum_{j>i} D_{ij}(3\hat{I_{Zi}}\hat{I_{Zj}} - \hat{I}_i.\hat{I}_j) + \sum_i \sum_{j>i} \frac{1}{3} \sum_k J_{kk,ij}\hat{I}_i.\hat{I}_j \qquad (3.31)$$

where the first two terms on the right hand side of eqn. (3.31) are the Chemical shift and Dipolar Hamiltonians respectively. The third term is the isotropic part of indirect scalar Hamiltonian, where the anisotropic contribution to the indirect scalar Hamiltonian is neglected [54]. The programme LEQUOR [55] is used to determine the Dipolar couplings, D_{ij}'s, and Chemical shifts, ν_i's, from the ^{1}H-NMR spectra, where the indirect scalar couplings J_{ij}'s are fixed to their isotropic values [56]. The main theme of this programme is briefly described in next paragraph.

Using a suitable set of basis functions, the matrix elements of the total Hamiltonian, H_T, are calculated. Then, the Hamiltonian matrix is diagonalised to obtain eigenvalues and eigenfunctions of the Hamiltonian. These eigenvalues are the energy levels of the molecule. Based on the selection rules and symmetry of the molecule, all possible transition frequencies and their corresponding intensities are calculated. These calculated line frequencies and intensities are matched with those of the experimental spectrum to assign the corresponding lines. The summation of squares of differences between experimental and calculated transition frequencies are minimized by varying the parameters ν_i and D_{ij}. The fitted D_{ij}'s for the C_{2V} and D_{2h} symmetry solutes are reported in Table 3.1.

The dipolar couplings D_{ij} of the solutes with C_{2V} and D_{2h} symmetry can be related to the solute geometry and orientation by the equation

$$D_{ij} = \frac{-\gamma_i\gamma_j h}{8\pi^2 r_{ij}^3}[S_{zz}(3\cos^2\theta_{ijz} - 1) + (S_{yy} - S_{xx})(\cos^2\theta_{ijy} - \cos^2\theta_{ijx})] \qquad (3.32)$$

Table 3.1: Dipolar couplings obtained from the ^{1}H-NMR spectra for C_{2V} and D_{2h} symmetry solutes.

Solute	D_{ij}	70%5$CB/EBBA$	56.5%1132/$EBBA$
metadichlorobenzene	D_{12}=D_{14}	-67.79 ±0.36	-82.86±0.26
	D_{13}	-19.52 ±0.60	-22.87±0.46
	D_{23}=D_{34}	-725.95 ±0.82	-920.02±0.30
	D_{24}	-179.7 ±1.2	-225.07 ±0.59
orthodichlorobenzene	D_{12}=D_{34}	-772.76 ±0.13	-1023.59 ±0.16
	D_{13}=D_{24}	-97.53 ±0.16	-132.28±0.17
	D_{14}	-46.66 ±0.36	-65.33 ±0.37
	D_{23}	-361.81 ±0.35	-500.20 ±0.40
paradichlorobenzene	D_{12}=D_{34}	-1745.74 ±0.48	-2320.71 ±0.16
	D_{13}=D_{24}	-20.98 ±0.67	-25.60±0.19
	D_{14}=D_{23}	74.96 ±0.65	101.05 ±0.19
orthodicyanobenzene	D_{12}=D_{34}	-807.82 ±0.14	-1028.38 ±0.12
	D_{13}=D_{24}	-108.23±0.14	-124.88±0.14
	D_{14}	-54.73 ±0.34	-57.46 ±0.37
	D_{23}	-423.42±0.33	-441.54 ±0.34
furan	D_{12}=D_{34}	-215.42 ±0.24	-249.29 ±0.26
	D_{13}=D_{24}	-74.11±0.28	-88.13 ±0.27
	D_{14}	-102.92 ±0.25	-123.81 ±0.27
	D_{23}	-339.67 ±0.42	-409.64 ±0.34
tetrathiofulvalene (TTF)	D_{12}=D_{34}	338.03 ±0.04	470.44 ±0.17
	D_{13}=D_{24}	-43.42 ±0.05	-55.43 ±0.20
	D_{14}=D_{23}	-56.57 ±0.05	-72.30 ±0.20
fluorobenzene	D_{12}=D_{16}	-328.61 ±0.41	-491.99 ±0.78
	D_{13}=D_{15}	-99.45 ±0.43	-139.09±0.78
	D_{14}	-75.20 ±0.23	-105.66 ±0.51
	D_{23}=D_{56}	-711.78±0.16	-1020.64 ±0.20
	D_{24}=D_{46}	-116.09±0.26	-169.38 ±0.43
	D_{25}=D_{36}	-46.07±0.14	-68.51 ±0.19
	D_{26}	-47.95 ±0.35	-76.10 ±0.46
	D_{34}=D_{45}	-363.74±0.33	-539.09 ±0.50
	D_{35}	-46.79 ±0.32	-72.25 ±0.35

Dipolar couplings in Hz for solutes in 70% 5CB/EBBA at 316K and in 56.5% 1132/EBBA at 323K obtained from the computer programme LEQUOR.

Table 3.2: Order Parameters of the solutes in the 70% 5CB/EBBA

70% 5CB/EBBA				
Solute	D_{HH}(TCB) /Hz	S_{zz}	$S_{yy} - S_{xx}$	RMS/Hz
metadichlorobenzene	109.37	-0.1370	0.0954	0.8
orthodichlorobenzene	129.51	-0.1619	0.0693	0.9
paradichlorobenzene	129.51	-0.1732	-0.2708	1.3
orthodicyanobenzene	117.52	-0.1717	0.0637	1.5
furan	126.17	-0.0944	0.0239	0.3
tetrathiofulvalene	116.43	-0.1906	-0.2794	0.14
fluorobenzene	116.99	-0.1236	-0.0627	0.5

Experimental order parameters S_{zz} and $S_{yy} - S_{xx}$ of solutes in the zero efg mixture 70% 5CB/EBBA obtained from the computer programme SHAPE.

where the molecule-fixed axes x, y and z are defined in Figure 3.5. S_{zz} and S_{yy}-S_{xx} are the order parameters of the solute in the liquid crystal mixture. The angle $\theta_{ij\alpha}$ represents the angle between the ij direction and the molecule-fixed axis α. The programme SHAPE [58] was used to obtain these order parameters from the dipolar couplings and the geometries [57] of the solutes. These experimental order parameters are reported in Tables 3.2 and 3.3.

3.2.2 Orientation in Zero efg mixtures

The orientation of the solutes in the zero efg mixtures can be compared at a certain experimental condition such as a temperature or a given splitting of a reference compound. In this thesis, trichlorobenzene, TCB, is chosen as the reference compound, and TCB splittings are used as a reference point for comparison purpose. It shall be shown in the next chapter that the TCB dipolar coupling in zero efg mixtures can be used as an internal measure of reduced temperature. All samples contain a little TCB, and the dipolar coupling of TCB, D_{HH}(TCB), has been measured from the same spectrum as the solute. Although all the sample tubes with the same liquid crystal mixture were studied

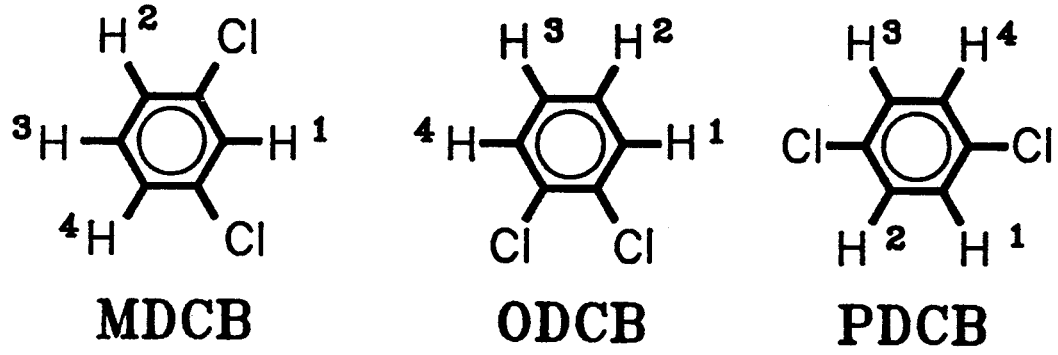

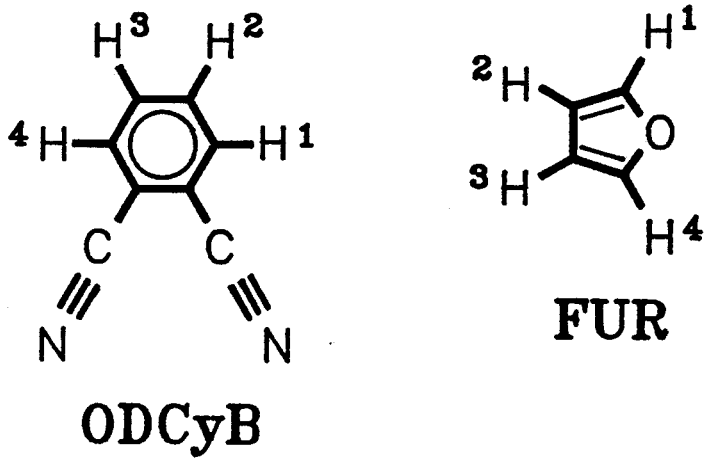

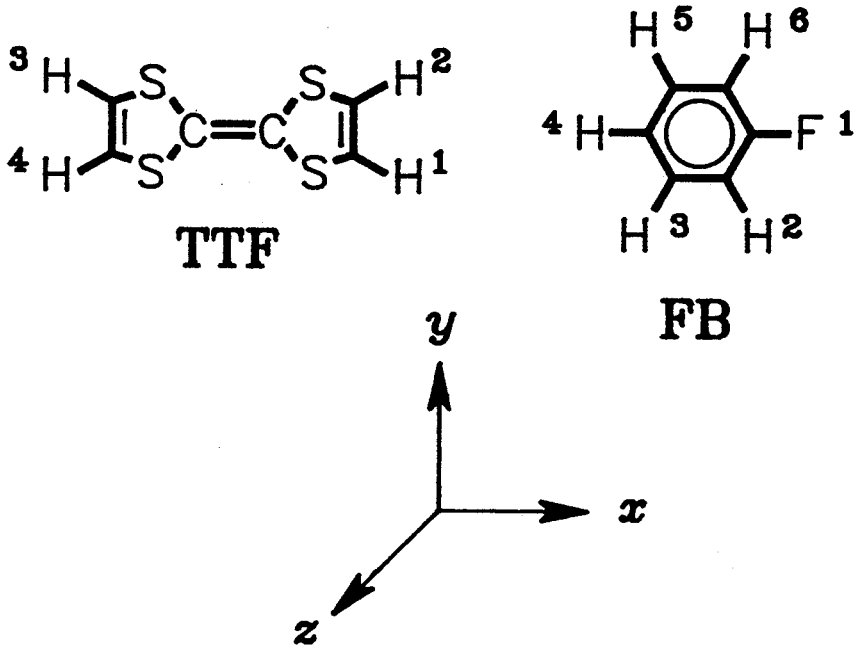

Figure 3.5: The coordinate system and atom numbering of the solute molecules studied.

Table 3.3: Order Parameters of the solutes in the 56.5% 1132/EBBA

56.5% 1132/EBBA				
Solute	D_{HH}(TCB) /Hz	S_{zz}	$S_{yy} - S_{xx}$	RMS/Hz
metadichlorobenzene	136.39	-0.1717	0.1246	0.21
orthodichlorobenzene	171.04	-0.2163	0.0882	1.6
paradichlorobenzene	171.04	-0.2290	-0.3614	1.1
orthodicyanobenzene	151.21	-0.2104	0.0976	1.6
furan	149.03	-0.1119	0.0307	0.5
tetrathiofulvalene	148.45	-0.2386	-0.3622	0.17
fluorobenzene	167.21	-0.1806	-0.0864	1.3

Experimental order parameters S_{zz} and $S_{yy} - S_{xx}$ of solutes in the zero efg mixture 56.5% 1132/EBBA obtained from the computer programme SHAPE.

at the same temperature, there is a slight deviation in the TCB dipolar coupling from one sample tube to another due to factors such as concentration and nature of the solute. These factors also influence the nematic — isotropic transition temperature, T_{NI}.

In order to compare results between the two zero efg mixtures, a new quantity, the order parameter ratio, $S^{tcb}_{\alpha\beta} = S_{\alpha\beta}/D_{HH}$(TCB), is defined as a ratio between the order parameter of the solute, $S_{\alpha\beta}$, and the dipolar coupling of TCB, D_{HH}(TCB), in the same sample tube. The order parameter ratios, $S^{tcb}_{\alpha\beta}$, of 70 % 5CB/EBBA are plotted against those of 56.5 % 1132/EBBA in Figures 3.6 and 3.7. The ratios $S^{tcb}_{\alpha\beta}$ of the 70 % 5CB/EBBA agree very well with those of the 56.5 % 1132/EBBA. Based on this agreement within experimental error, it can be written for any given order parameter of any given solute

$$(S^{tcb}_{\alpha\beta})_{70} = (S^{tcb}_{\alpha\beta})_{56.5} \tag{3.33}$$

where the subscripts 70 and 56.5 stand for the liquid crystal mixtures 70% 5CB/EBBA and 56.5% 1132/EBBA. This result is interesting because the order parameter ratios are found to be equal within experimental error in two different zero efg mixtures. In other words, as long as the TCB dipolar couplings have been measured in both zero

efg mixtures, the order parameters $S_{\alpha\beta}$ of any solute with C_{2V} and D_{2h} symmetry can be predicted in a zero efg mixture if the order parameter of that solute in another zero efg mixture is known. It is worth while to further analyse the results given by equation (3.33).

As described in section 1.2.3, the orientation of a probe solute depends on the mean field potential experienced by the solute. Therefore, we shall now analyse the potential in the zero efg mixtures to understand the transferability of the order parameters. In the zero efg mixtures, the intermolecular potential is assumed to be the short-range potential, $U_{sr}(\Omega)$.

The orientation of the solute can be related to the short-range potential by equation A.51. The order parameter $S_{\alpha\beta}$ is proportional to $e^{-U_{sr}/kT}$. We shall now analyse the transferability of the order parameters in the zero efg mixtures in terms of the short-range potential, $U_{sr}(\Omega)$.

3.3 Comparison of short-range interactions

Since the precise nature of the short-range potential is not well known, a one-parameter model is used to describe the short-range potential. The reason to choose the one-parameter model is that it can be tested on the two independent experimental order parameters. We chose the one-parameter model, discussed in Chapter 1, and rewrite as:

$$U_{sr}(\Omega) = \frac{1}{2} k_s \int_{Z_{min}}^{Z_{max}} C_Z(\Omega) dZ \tag{3.34}$$

To calculate the $C_Z(\Omega)$, the solute molecule is taken as a collection of van der Waals spheres, and van der Waals radii are taken from Bondi *et al.*[59].

The two independent experimental order parameters S_{zz} and S_{yy}-S_{xx} were used to obtain the best fit model parameter k_s for each solute independently. The best fit model parameter k_s was then used to recalculate the order parameters S_{zz} and S_{yy}-S_{xx}. These

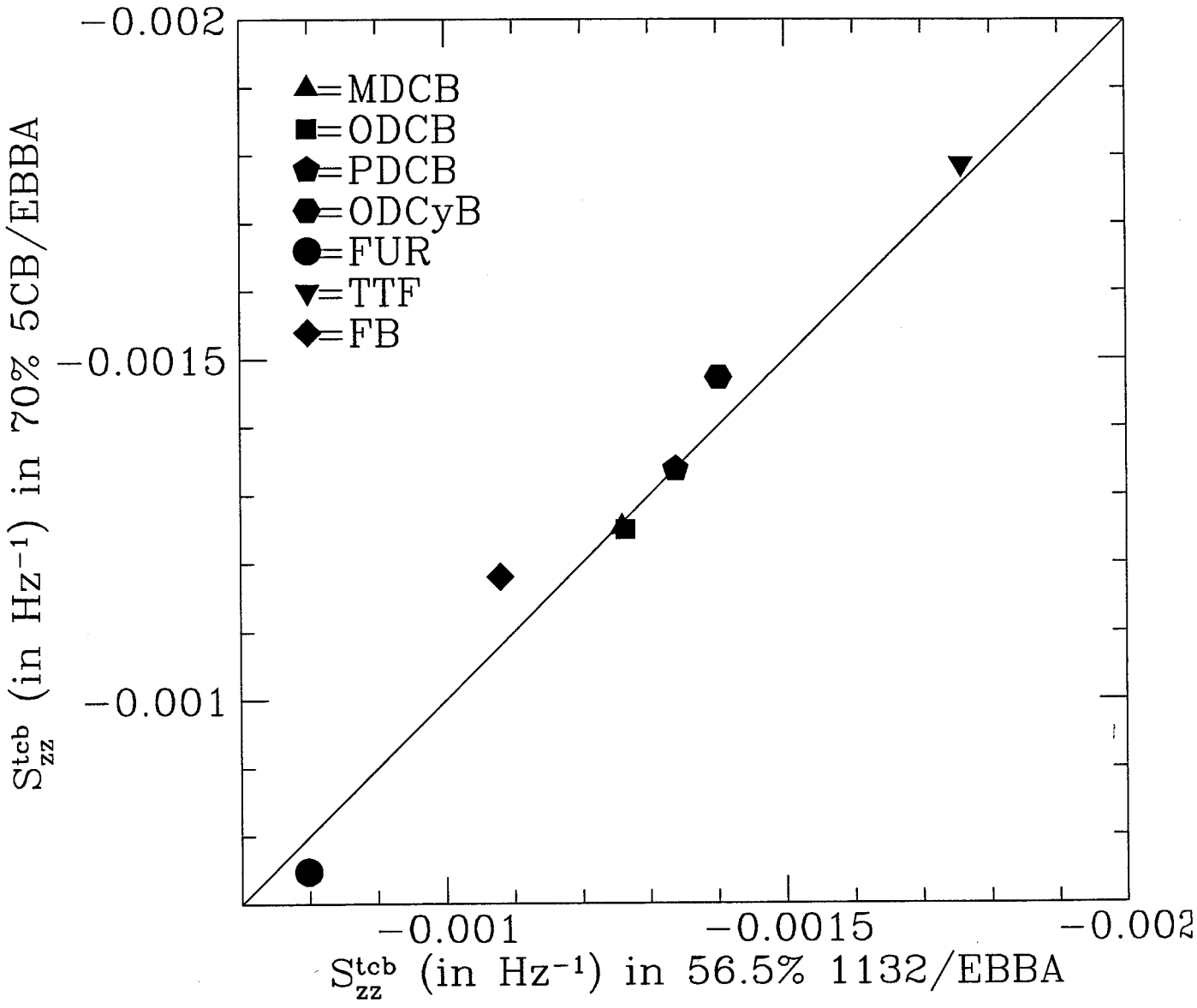

Figure 3.6: The order parameter ratios, $S_{zz}^{tcb} = S_{zz}/D_{HH}(\text{TCB})$, of the solutes in 70 % 5CB/EBBA against those in 56.5 % 1132/EBBA.

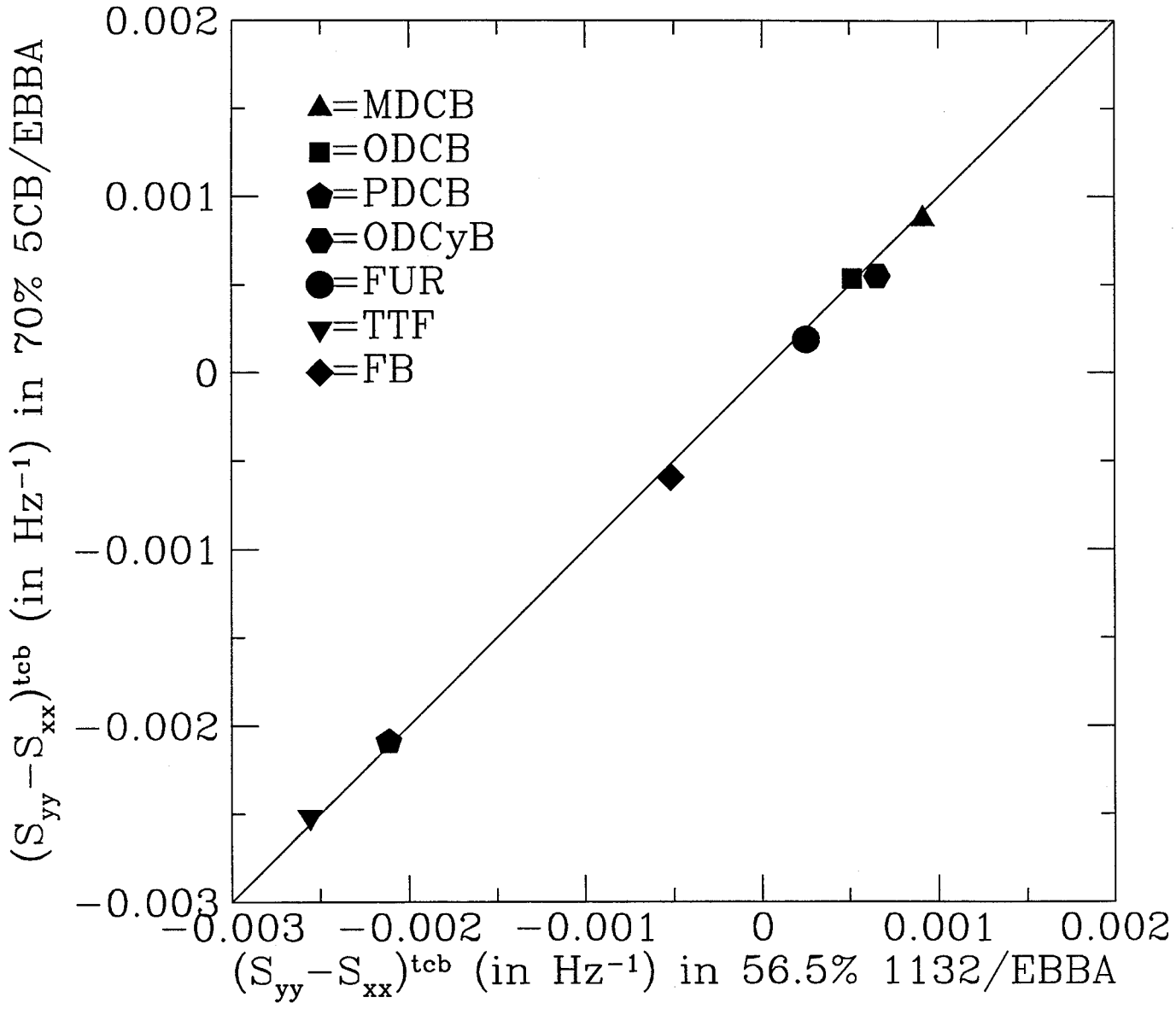

Figure 3.7: The order parameter ratios, $(S_{yy} - S_{xx})^{tcb} = (S_{yy} - S_{xx})/D_{HH}(\mathrm{TCB})$, of the solutes in 70 % 5CB/EBBA against those in 56.5 % 1132/EBBA.

Table 3.4: model parameters for the C_{2V} and D_{2h} symmetry solutes

	70% 5CB/EBBA		56.5% 1132/EBBA	
Solute	k_s/dyn cm^{-1}	k'_s/dyn cm^{-1}	k_s/dyn cm^{-1}	k'_s/dyn cm^{-1}
metadichlorobenzene	40 ±3	35.62 ±0.04	54 ±3	48.35 ±0.07
orthodichlorobenzene	47 ±3	44.17 ±0.06	71 ±3	66.84 ±0.13
paradichlorobenzene	59 ±6	44.17 ±0.06	85 ±5	66.84 ±0.13
orthodicyanobenzene	42.4 ±0.9	38.96 ±0.05	57.8 ±0.2	55.75±0.09
furan	53.95 ±0.13	42.69 ±0.05	67.0 ±0.5	54.62 ±0.09
tetrathiofulvalene	53 ±11	38.50 ±0.05	77 ±13	54.31 ±0.08
fluorobenzene	46 ±3	38.73 ±0.05	74 ±2	64.57 ±0.12

Fitted k_s values from equation. 1.28 of the solutes, with the corresponding k'_s values of trichlorobenzene in the same sample tube, in the zero efg mixtures 70% 5CB/EBBA and 56.5% 1132/EBBA.

recalculated order parameters are plotted against the experimental ones in Figures 3.8 and 3.9. The recalculated order parameters agree well with the experimental ones. The relative errors are generally less than 10% for all solutes. Therefore, the fits are of sufficient quality that this one-parameter model is useful for making comparisons between mixtures.

The one-parmeter model gives the k_s value which is directly proportional to the U_{sr} experienced by the solute. The fitted k_s values, along with the short-range potential parameter of TCB , k'_s, are reported in Table 3.4 for all solutes in both zero efg mixtures. The k'_s was calculated from the TCB dipolar coupling, D_{HH}(TCB), using eqns. (3.32), (A.51) and (3.34). As can be seen in Table 3.4, the k_s values vary among the solutes.

To demonstrate the transferability of the short-range potentials between the two zero efg mixtures, the ratios k_s/k'_s for all solutes in the 70% 5CB/EBBA mixture are plotted against those in the 56.5% 1132/EBBA mixture in Figure 3.10. The ratios are used to account for differences among sample tubes containing the same liquid crystal mixture. The ratios k_s/k'_s vary from one solute to another up to 20%. This large difference mainly

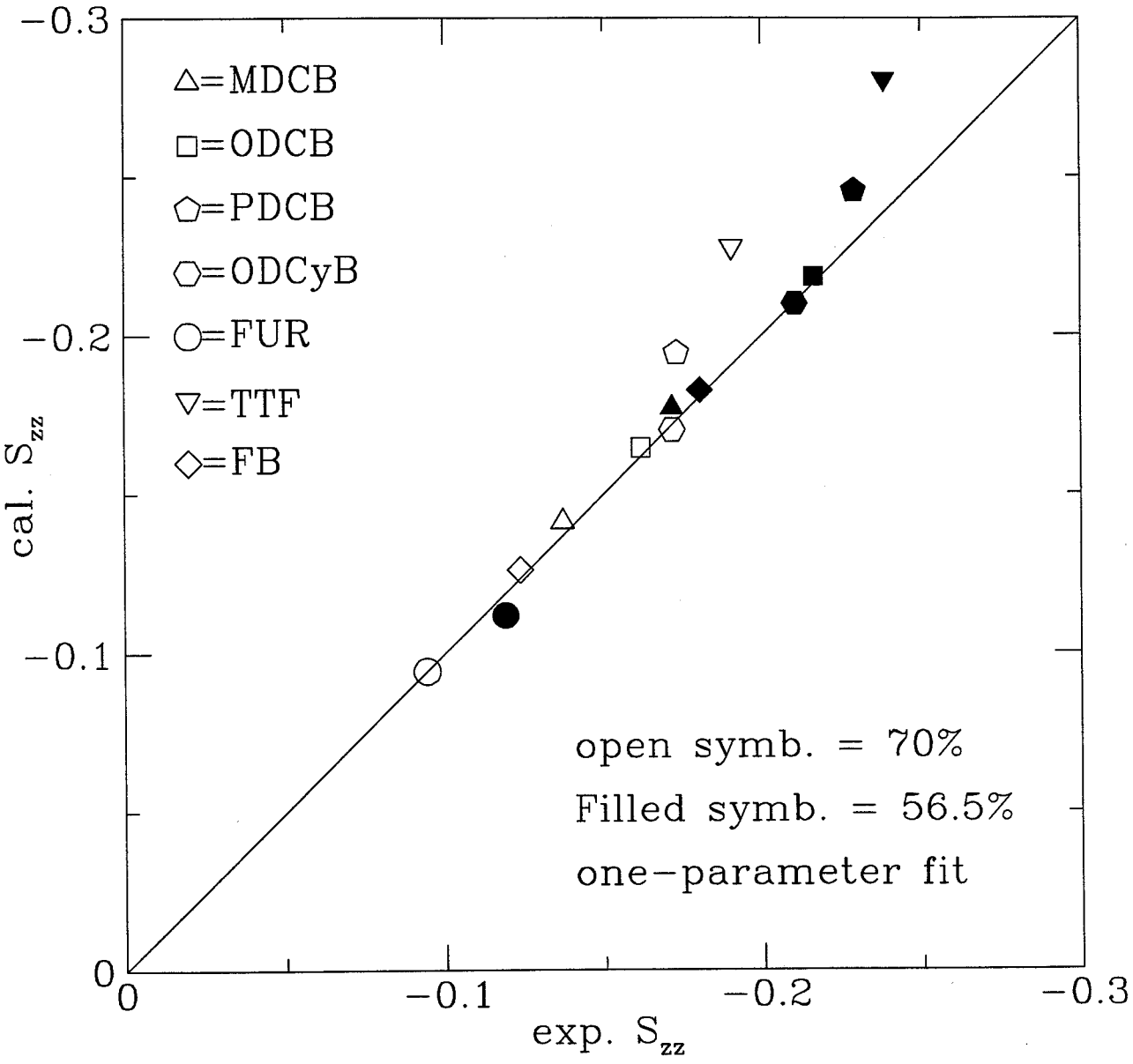

Figure 3.8: Calculated versus experimental order parameters S_{zz}. Open symbols represent 70 % 5CB/EBBA, and filled symbols 56.5 % 1132/EBBA.

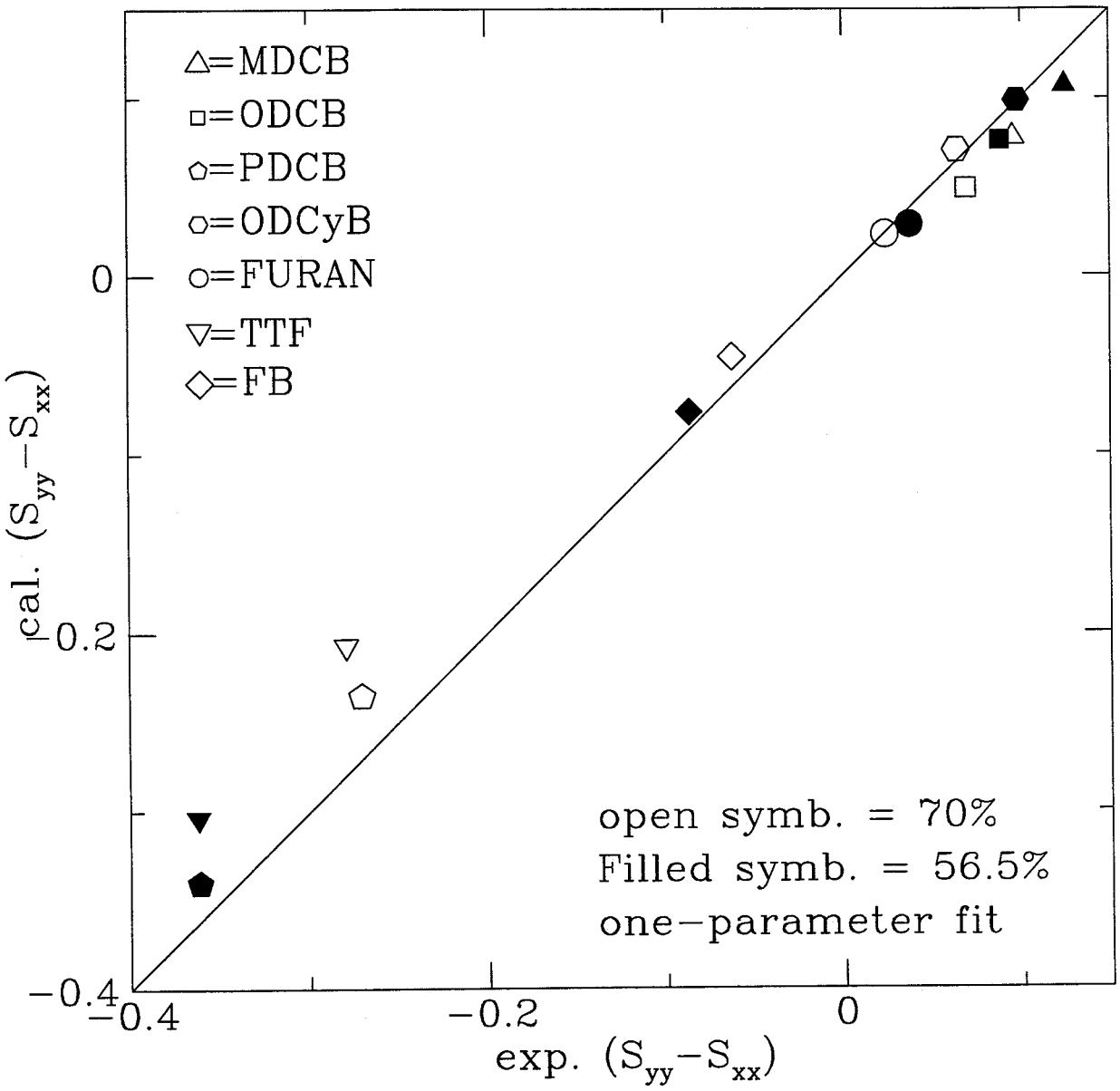

Figure 3.9: Calculated versus experimental order parameters S_{yy}-S_{xx}. Open symbols represent 70 % 5CB/EBBA, and filled symbols 56.5 % 1132/EBBA.

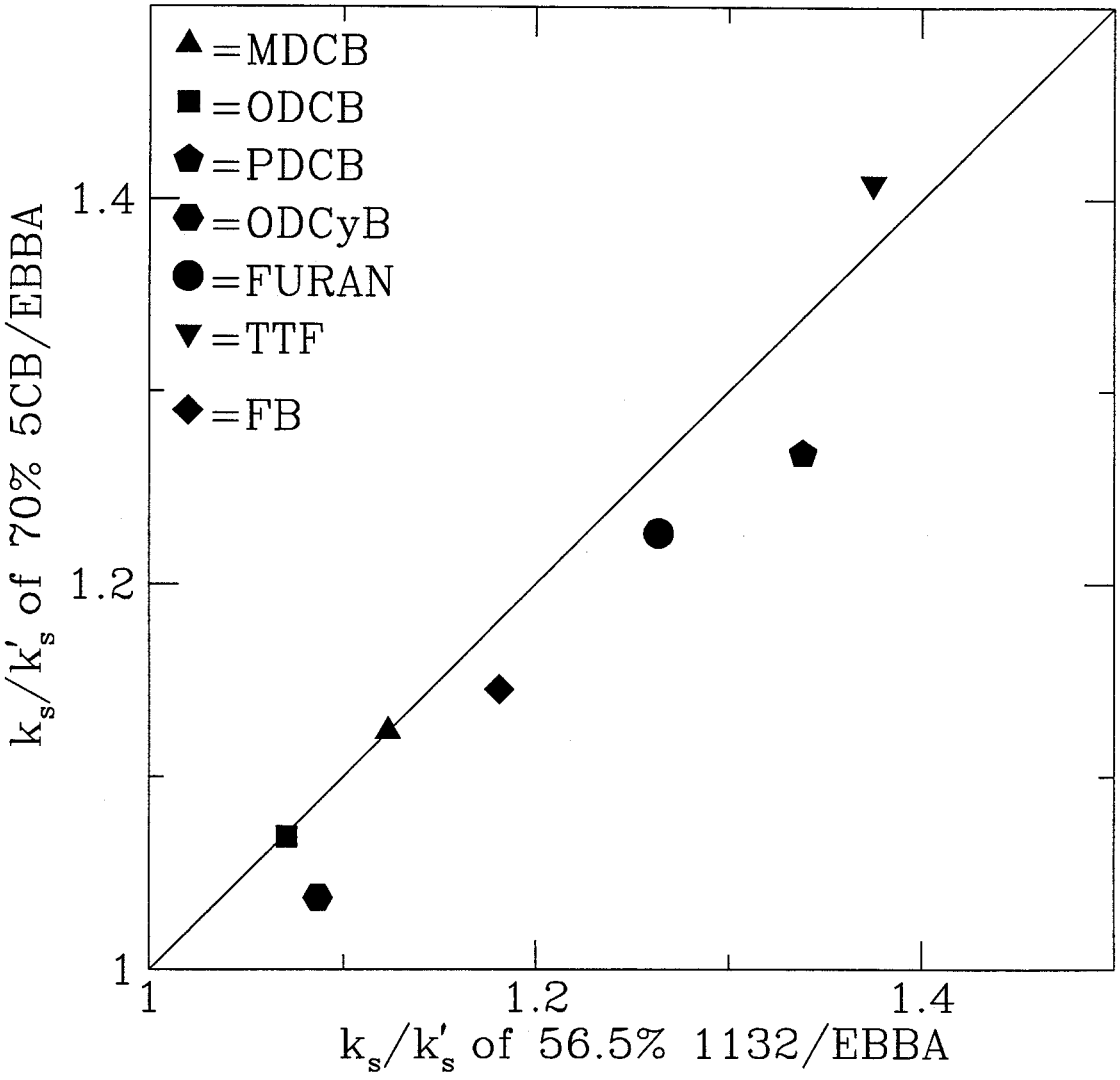

Figure 3.10: k_s/k'_s ratios of the 70% 5CB/EBBA mixture against those of the 56.5% 1132/EBBA mixture, where k_s and k'_s are the model parameters for the solute and for the TCB in the same sample tube.

stems from the fact the model fits some solutes better than the other solutes. However, the agreement between the ratios k_s/k'_s in both mixtures is within 7% for all solutes. This suggests that for a given k'_s the model parameters k_s are transferable from one of these mixtures to the other. Therefore, the short-range potentials of these two zero efg mixtures are similiar for a given k'_s.

3.4 Summary

For a given TCB dipolar coupling, the order parameters $S_{\alpha\beta}$ of C_{2V} and D_{2h} symmetry solutes are transferable from one zero efg mixture to another. The short-range potential represented by a one-parameter model in eq. (3.34) is quite sufficient to calculate the order parameters $S_{\alpha\beta}$, which are in good agreement with the experimental order parameters. The one-parameter model k_s values are used to compare the short-range potentials of the solutes in the two zero efg mixtures. For a given k'_s, the model parameter of TCB, the ratios k_s/k'_s in one zero efg mixture are in good agreement with those in the other mixture. This suggests that the form of the short-range potentials experienced by C_{2V} and D_{2h} symmetry solutes in the two zero efg mixtures is the same.

Chapter 4

Temperature dependence study of small solutes in the zero efg mixtures

4.1 Introduction

The temperature dependence study of small solutes in the zero efg mixtures is important to understand the temperature effect on the short-range interactions. The study is also convenient to compare the short-range potentials in the zero efg mixtures. In this chapter, the temperature dependence of a few small solutes, having different shape and symmetry, is studied in the zero efg mixtures 55% 1132/EBBA and 70% 5CB/EBBA. The one-parameter model (eqn. 1.28) is used to describe the short-range potential. The study also focuses on biaxial order parameter, $S_{xx} - S_{yy}$, and on how the model fits to the experimental order parameters, with the variation of temperature. The solutes studied are as follows: benzene (BENZ) and 2-butyne(2-BUTY) with C_3 and higher symmetry, orthodichloro benzene (ODCB) and metadichloro benzene (MDCB) with C_{2V} symmetry and 1,3- bromochloro benzene (1,3-BrCl) with C_S symmetry.

Section 4.2 discusses the temperature dependence of trichloro benzene (TCB) in three zero efg mixtures and in a non-zero efg mixture. Section 4.3.1 briefly describes the geometries of BENZ and 2-BUTY needed to determine the order parameter, S_{zz}. Similarly, section 4.3.2 briefly mentions the geometries of ODCB, MDCB and 1,3-BrCl. Section 4.4 compares the short-range potentials in the zero efg mixtures. Finally, section 4.5 discusses the temperature dependence of S_{xx}-S_{yy} and S_{zz}.

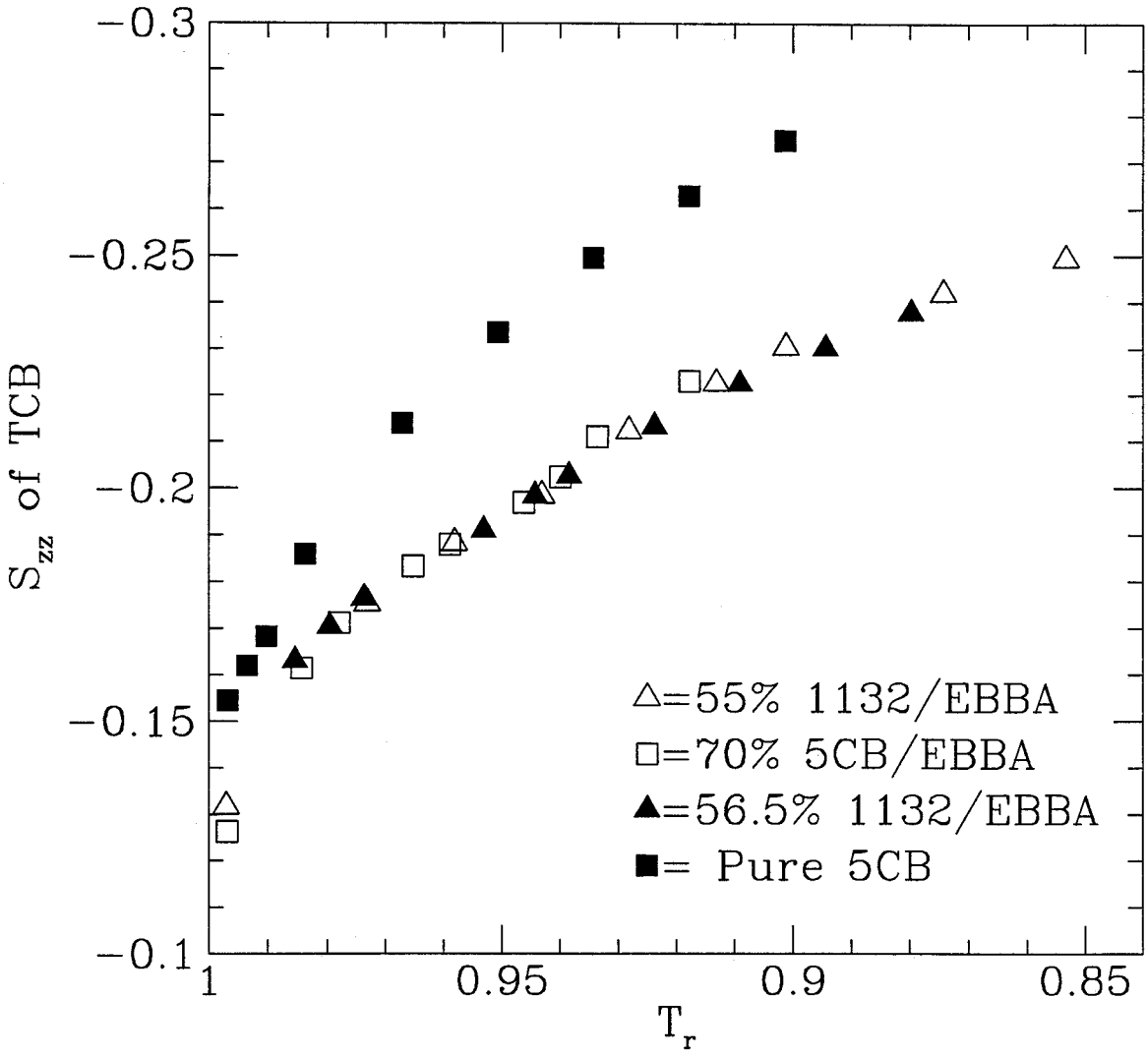

Figure 4.11: The order parameter S_{zz} of TCB vs. reduced temp.

4.2 Temperature dependence study of trichloro benzene

This section describes how the TCB dipolar coupling in zero efg mixtures can be used as an internal measure of reduced temperature, T_r. To show this, the temperature dependence of TCB was studied in three zero efg mixtures 70% 5CB/EBBA, 56.5% 1132/EBBA and 55% 1132/EBBA and for the pure liquid crystal 5CB. The order parameters S_{zz} of TCB are plotted against T_r, where T_r is defined as $T_r = T/T_{NI}$, for the three zero efg mixtures 70% 5CB/EBBA, 56.5% 1132/EBBA and 55% 1132/EBBA and for the pure liquid crystal 5CB. In figure 4.11 it is found that for a given T_r the order parameter S_{zz} of TCB for the three zero efg mixtures are equal within experimental error. Therefore, a given D_{HH}(TCB), which is directly proportional to S_{zz} of TCB, can be used as an internal measure of T_r in these zero efg mixtures. However, as demonstrated in Figure 4.11, this argument is not valid for non-zero efg mixtures such as the pure liquid crystal 5CB. Therefore, D_{HH}(TCB) cannot be used as a measure of T_r in non-zero efg mixtures.

4.3 Structure

4.3.1 C_3 and higher symmetry solutes

An aromatic planar solute, BENZ, and a non-aromatic molecule 2-BUTY are studied as a function of temperature. The solute BENZ was chosen for its simple geometrical structure, and 2-BUTY was chosen because it is a molecule having a different shape from the other solutes studied. Due to the higher symmetry of these two molecules, they have only one independent order parameter, S_{zz}, in the nematic phase. The order parameter, S_{zz}, can be related to the dipolar couplings D_{ij} by the equation (1.5). The molecule-fixed axes x, y and z are defined in Figure 4.12, and D_{ij}'s were determined using the programme LEQUOR [55] and are reported in Appendix B.

The programme SHAPE [58] was used to obtain the order parameter, S_{zz}, from the dipolar couplings, D_{ij}. The geometry of BENZ and 2-BUTY were taken from ref. [57, 60] respectively, where the geometry of BENZ is a regular hexagon. In 2-BUTY, the two methyl groups are separated far enough that the methyl groups undergo free rotation about the C-C bond [61]. For simplicity, we assume that the 2-BUTY undergoes 18-steps during its free rotation (18-site jump). Although the angle α (see Fig. 4.12) determined by electron diffraction study was found to be 110.9^0 [60], the RMS error in our study was the lowest when α was fixed to 109.9^0. Therefore, we used the value of 109.9^0 for α to calculate the order parameters. The order parameters S_{zz} of BENZ and 2-BUTY are tabulated in Appendix C as a function of temperature.

4.3.2 C_{2V} and C_S symmetry solutes

The C_{2V} symmetry solutes ODCB and MDCB dissolved in liquid crystals give information about two independent order parameters S_{zz} and S_{xx}-S_{yy}. The solutes ODCB and MDCB have only 4 spin $\frac{1}{2}$ nuclei, therefore, the spectra are not complicated. The dipolar couplings D_{ij} of ODCB and MDCB in the zero efg mixtures can be related to the geometry and orientation by the equation (1.5). The molecule-fixed axes x, y and z are defined in Figure 4.12 such that the S_{zz} is major order parameter. The S_{xx}-S_{yy} is the biaxial order parameter of these two solutes in the nematic phase.

The geometries of ODCB and MDCB were taken from ref. [57]. The SHAPE programme was used to obtain the order parameters S_{zz} and S_{xx}-S_{yy} from the dipolar couplings D_{ij}. The order parameters S_{zz} and S_{xx}-S_{yy} as a function of temperature are tabulated in Appendix C.

A C_S symmetry solute in a nematic phase gives information about the order parameters, S_{zz}, S_{xx}-S_{yy} and S_{xy}. The solute 1,3-BrCl is chosen in this study, and the geometry of 1,3-BrCl differs from that of MDCB by replacing one of the Cl atoms by a Br atom.

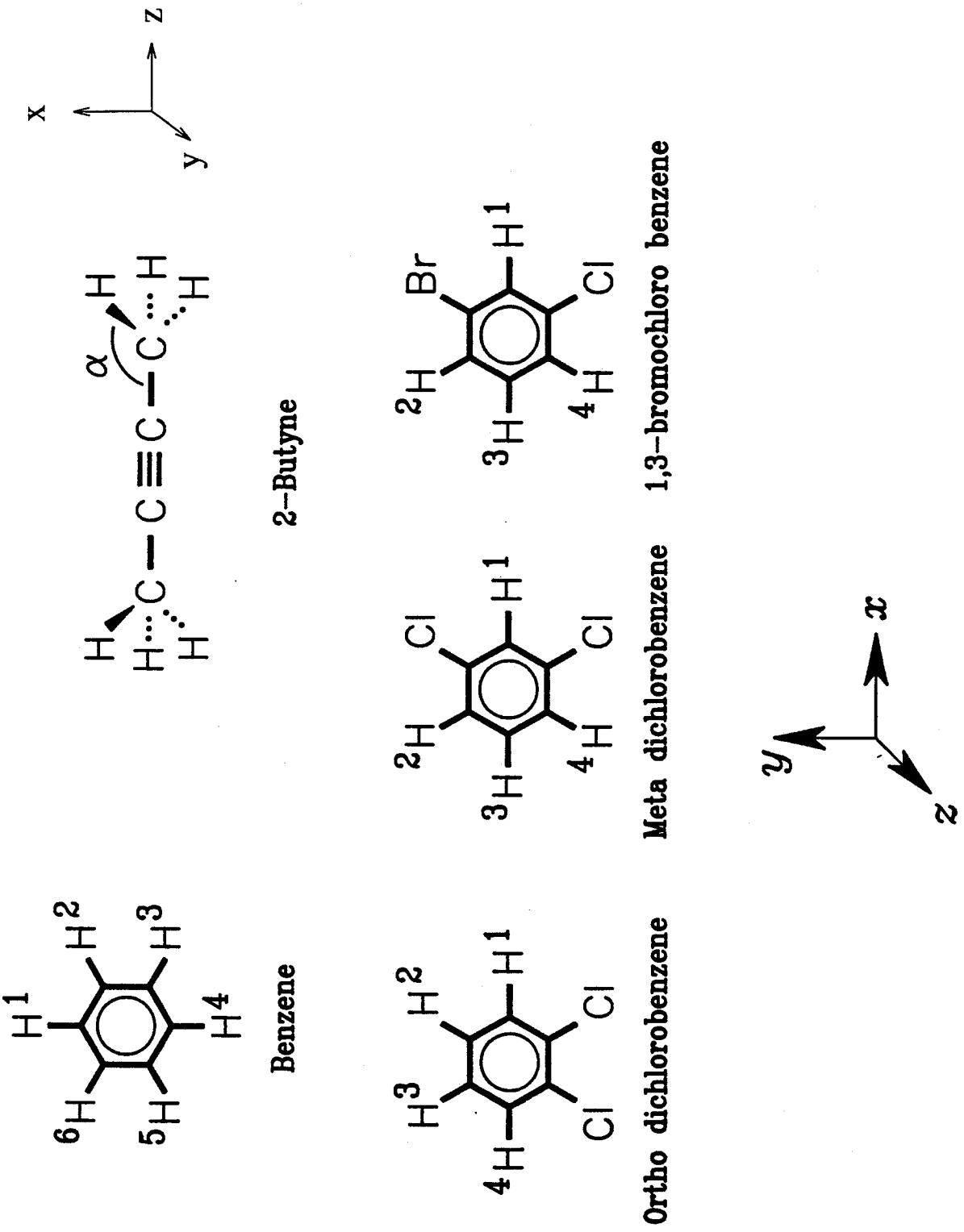

Figure 4.12: The coordinate system and atom numbering of the solute molecules studied.

The dipolar couplings D_{ij} of 1,3-BrCl are related to its geometry and orientation by equation (1.5). The molecule-fixed axes x, y and z are defined in Figure 4.12 . The geometry of 1,3-BrCl is taken from ref [57]. The order parameters S_{zz}, S_{xx}-S_{yy} and S_{xy} as a function of temperature are tabulated in Appendix C.

4.4 Comparison of short-range interactions

All samples contain a little TCB, and the dipolar coupling of TCB, D_{HH}(TCB), has been measured from the same spectrum as the solute. In this section, the short-range potentials in the zero efg mixtures are compared at the same TCB splitting.

The order parameters $S_{\alpha\beta}$ are plotted against D_{HH}(TCB) in Figures 4.13 - 4.17. The order parameters S_{zz} in 70% 5CB/EBBA agree well with those of the 55% 1132/EBBA for all solutes. The agreement between biaxial order parameters, S_{xx}-S_{yy}, is close in mixtures 55% 1132/EBBA and 70% 5CB/EBBA, but it is not as good as that for S_{zz}. Although the magnitude of S_{xy} is very small, the agreement between the S_{xy} in mixtures 55% 1132/EBBA and 70% 5CB/EBBA is good. It is interesting to obtain the same magnitude of order parameters for a solute in the two different zero efg mixtures. What does this result tell about the zero efg mixtures? To further understand this, we shall relate the order parameters to the intermolecular potential and analyse the results in terms of intermolecular potentials of the mixtures. The intermolecular potential is assumed to have only contributions from the short-range potential at all temperatures studied (shall be discussed in Chapter 5). Therefore, to understand the transferability of the order parameters $S_{\alpha\beta}$, we relate the order parameters to the short-range potential using equation (A.51). The short-range potential is described by the one-parameter model given by equation (1.28).

A least-squares fit is done on the experimental order parameters for each molecule at

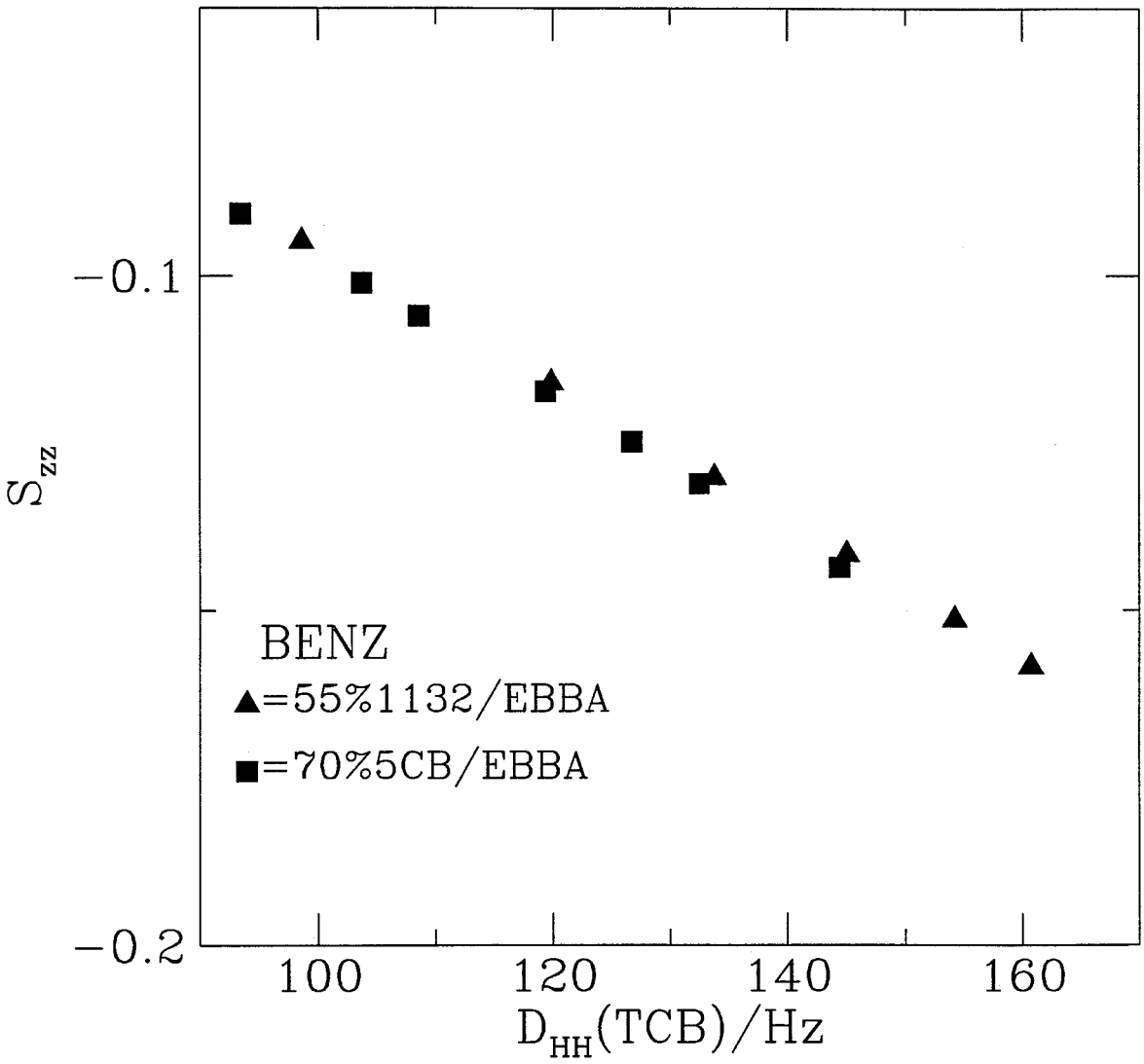

Figure 4.13: Order parameters *vs.* D_{HH}(TCB) for BENZENE.

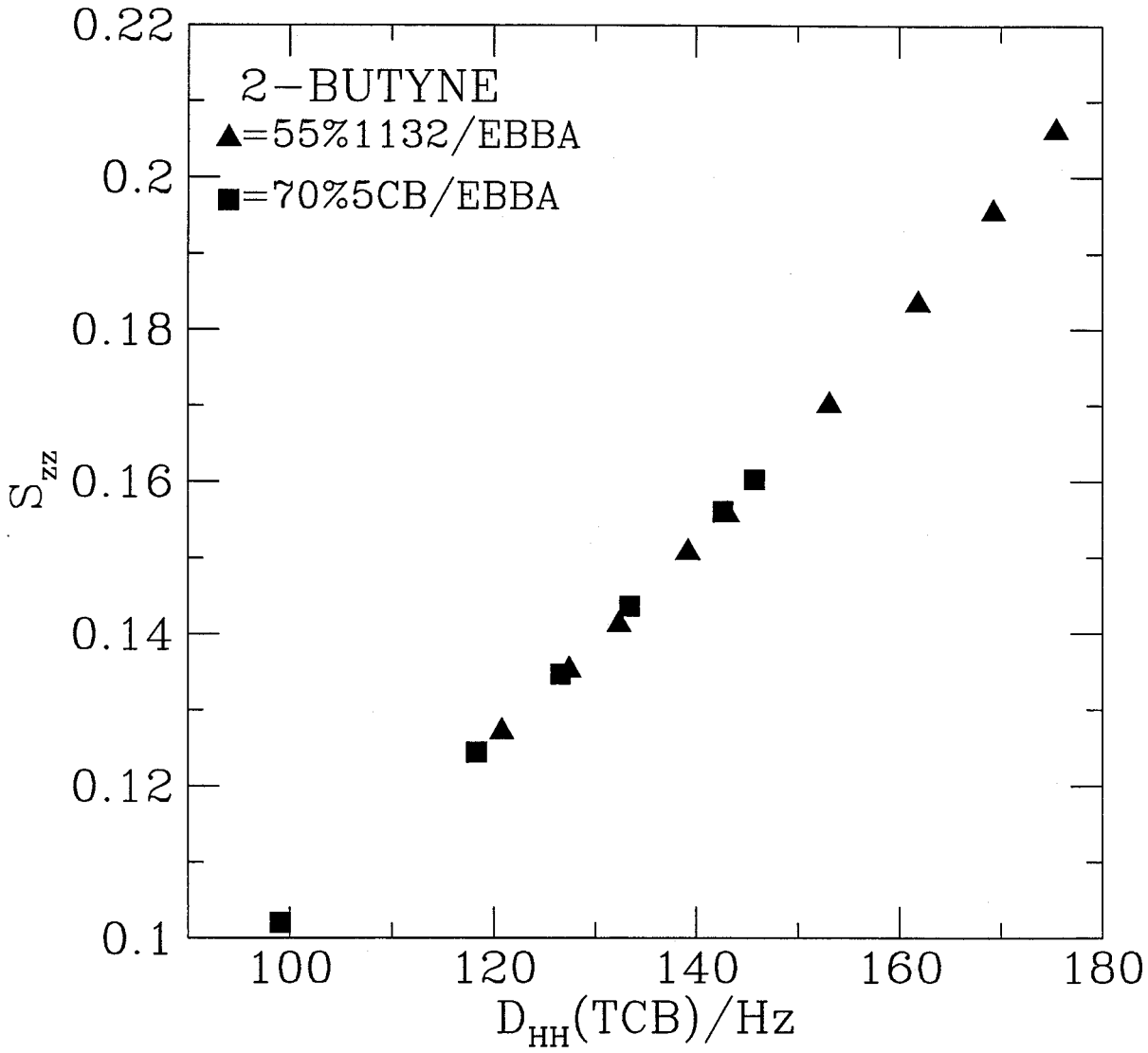

Figure 4.14: Order parameters *vs.* D_{HH}(TCB) for 2-BUTYNE.

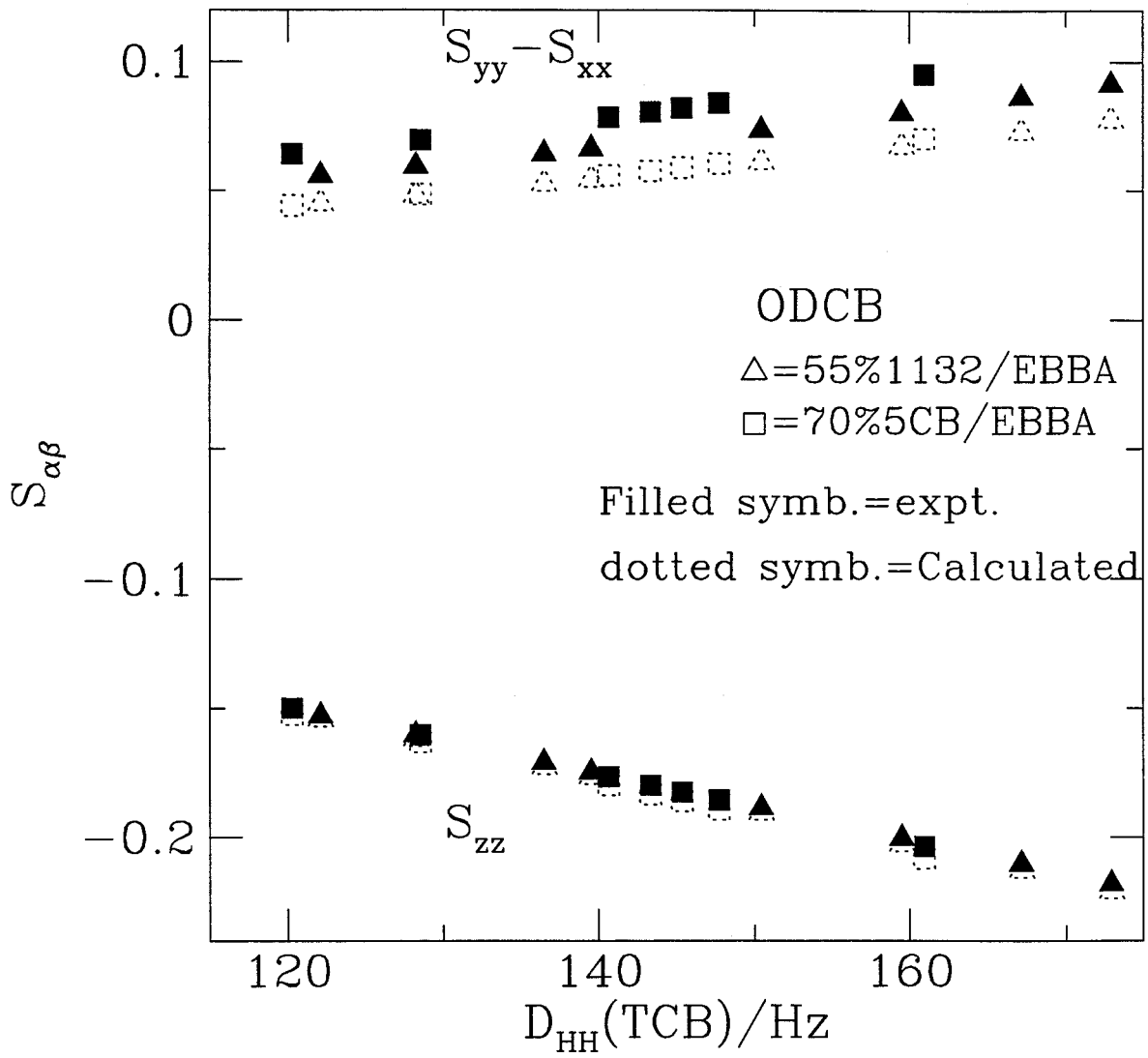

Figure 4.15: Order parameters *vs.* D_{HH}(TCB) for ODCB.

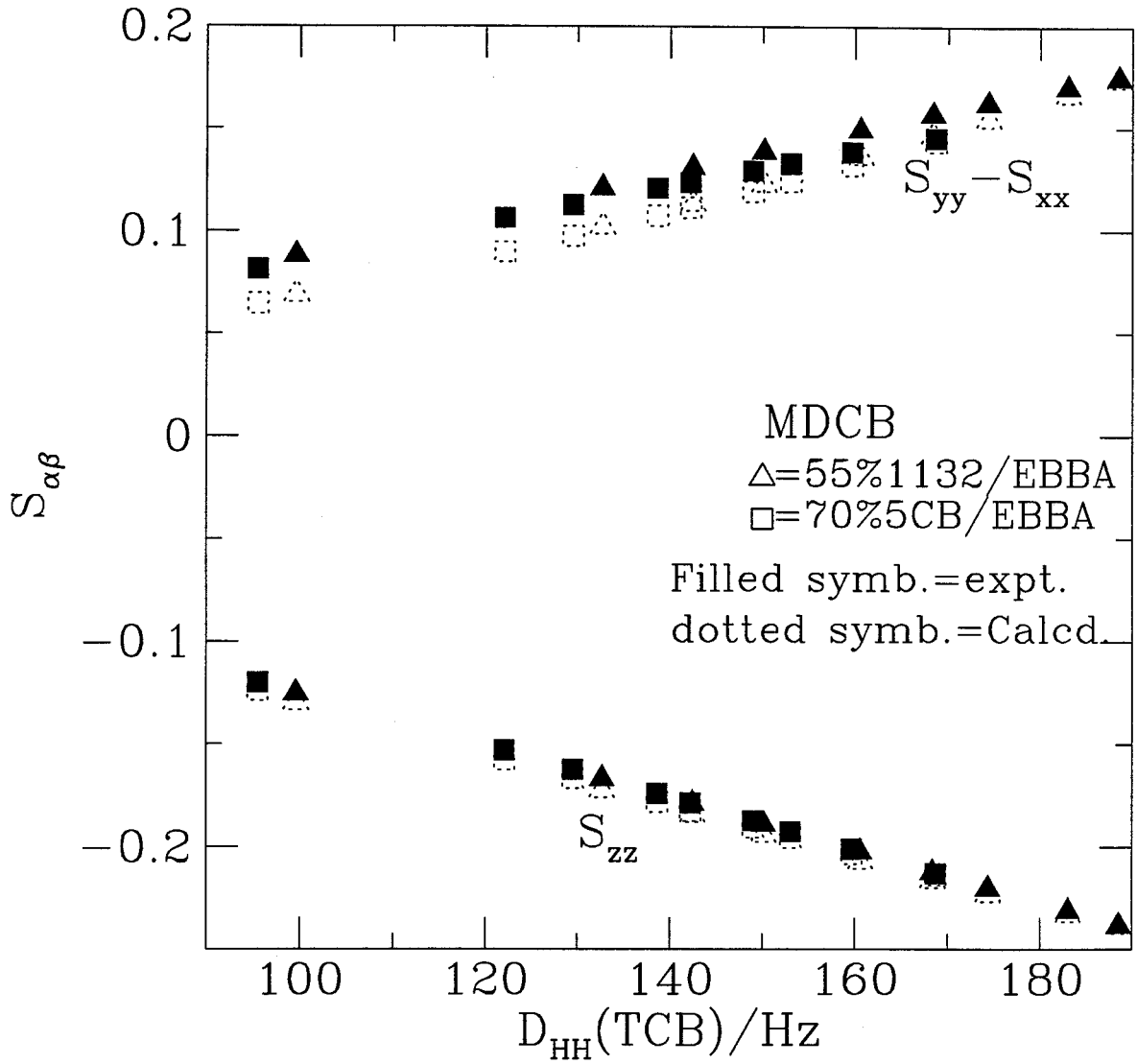

Figure 4.16: Order parameters *vs.* D_{HH}(TCB) for MDCB.

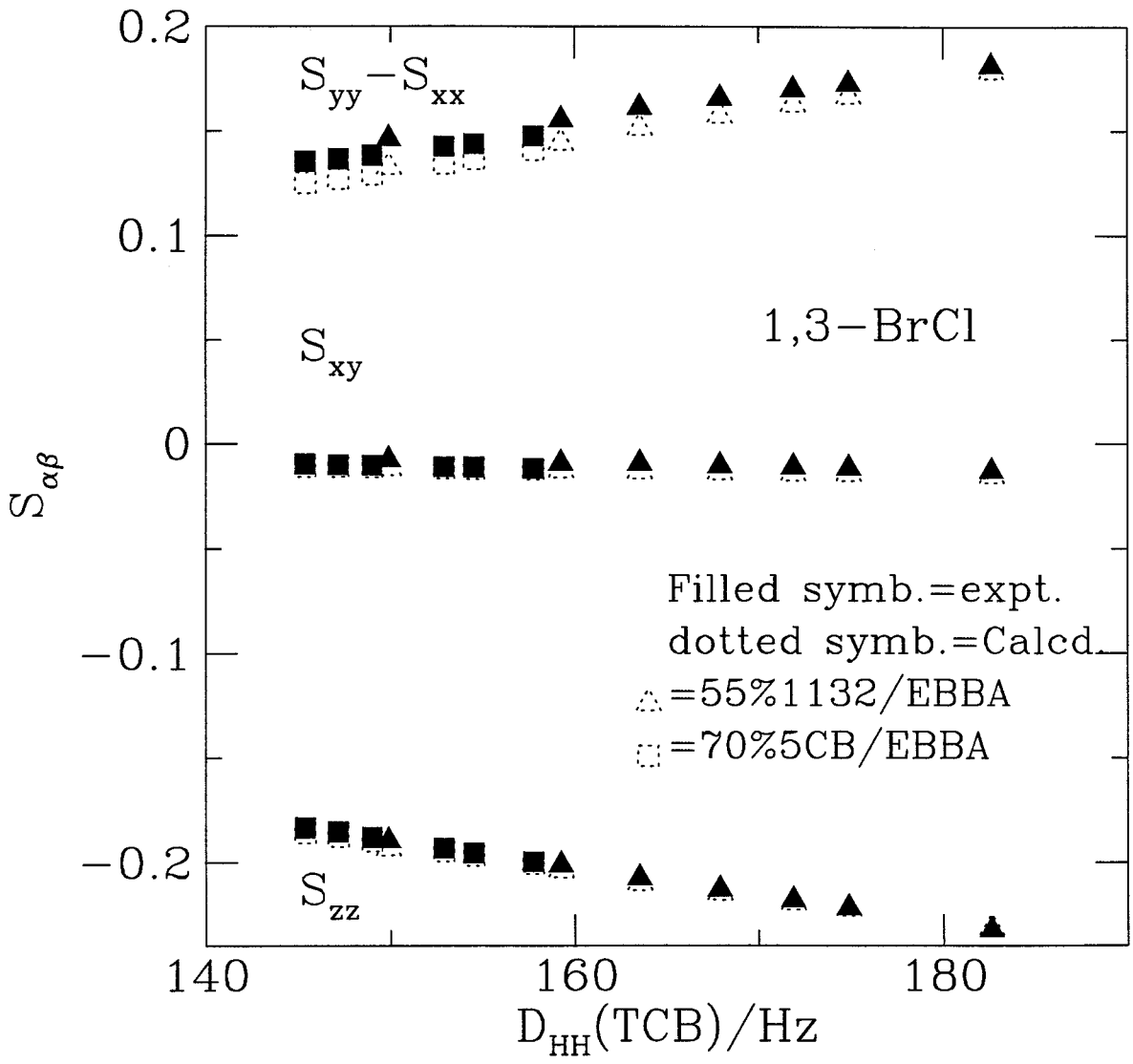

Figure 4.17: Order parameters *vs.* D_{HH}(TCB) for 1,3- Bromochloro benzene.

each temperature to obtain the best fit model parameter k_s. The k_s values are reported in Appendix C. The best fit model parameter was then used to obtain the recalculated order parameters $S_{\alpha\beta}$ for all solutes. In Figures. 4.13 - 4.17, the recalculated order parameters are plotted (open triangles and squares) to see the agreement with the experimental order parameters. The agreement between the experimental and recalculated order parameter S_{zz} is very good. Although the recalculated S_{xx}-S_{yy} values are close to the experimental values, the agreement is not as good as for S_{zz}. However, the relative errors between the experimental and calculated order parameters are generally less than 10% for all solutes. Therefore, the short-range potential, U_{sr}, can well be represented by the model parameter k_s. We shall use the model parameter k_s to explain the transferability of the order parameters in the two zero efg mixtures 55% 1132/EBBA and 70% 5CB/EBBA.

Based on equations. (A.51) and eq. (1.28), we note that the order parameter $S_{\alpha\beta}$ depends on k_s/T. Thus, $S_{\alpha\beta}$ can be written as:

$$S_{\alpha\beta} = f(k_s/T) \tag{4.35}$$

To examine the dependence of the quantity k_s/T on liquid crystal environment, k_s/T is plotted against D_{HH}(TCB) for both liquid crystal mixtures in Figures. 4.18 - 4.22 for all solutes. The plots show that there is very good agreement between the k_s/T values for 55% 1132/EBBA and 70% 5CB/EBBA. Based on this agreement, we write the following relationship

$$(k_s/T)_{55} = (k_s/T)_{70} \tag{4.36}$$

for a given D_{HH}(TCB), where the subscripts 55 and 70 stand for the liquid crystal mixtures 55% 1132/EBBA and 70% 5CB/EBBA. Sustituting eq. (4.36) into eq. (1.28), we get the relationship

$$(U_{sr}/T)_{55} = (U_{sr}/T)_{70} \tag{4.37}$$

Table 4.5: T_{NI} values for the solute-liquid crystal mixtures.

	T_{NI} values	
Solute	55% 1132/EBBA	70% 5CB/EBBA
ortho dichlorobenzene	333K	318K
meta dichlorobenzene	334K	316K
1,3-bromochlorobenzene	339K	320K
benzene	329K	314K
2-butyne	333K	313K

The reduced temperatures, T_r, are calculated using the relationship $T_r = T/T_{NI}$.

In order to simplify the notation, new quantities reduced short-range potential, U^r_{sr}, and reduced model parameter, k^r_s, are defined by $U^r_{sr} = U_{sr}/T$ and $k^r_s = k_s/T$. Equations (4.36) and (4.37) suggest that at a given D_{HH}(TCB) the reduced short-range potential, U^r_{sr}, and the reduced model parameter, k^r_s, are transferable from one of these two mixtures to the other. This explains why the order parameters, $S_{\alpha\beta}$, are transferable from one zero efg mixture to another.

We further investigate the temperature dependence of the short-range potentials in the zero efg mixtures. In figure 4.23, we plot k_s/T against T_r for all the solutes. The reduced temperatures, T_r, are calculated using the relationship $T_r = T/T_{NI}$, where the nematic - isotropic transition temperatures, T_{NI}, for all sample tubes are tabulated in Table 4.5. The lowest temperature at which the isotropic peak appears is taken to be T_{NI}. The figure shows that the magnitude of the reduced model parameters for all the aromatic solutes are in good agreement within experimental error. The magnitude of the k^r_s for the non-aromatic molecule 2-butyne, however, is higher than those of the aromatic solutes. It should also be noted that the reduced model parameters for a particular solute in the two zero efg mixtures are in good agreement for a given T_r. We shall further discuss the temperature dependence study of the solutes in the Chapter 7.

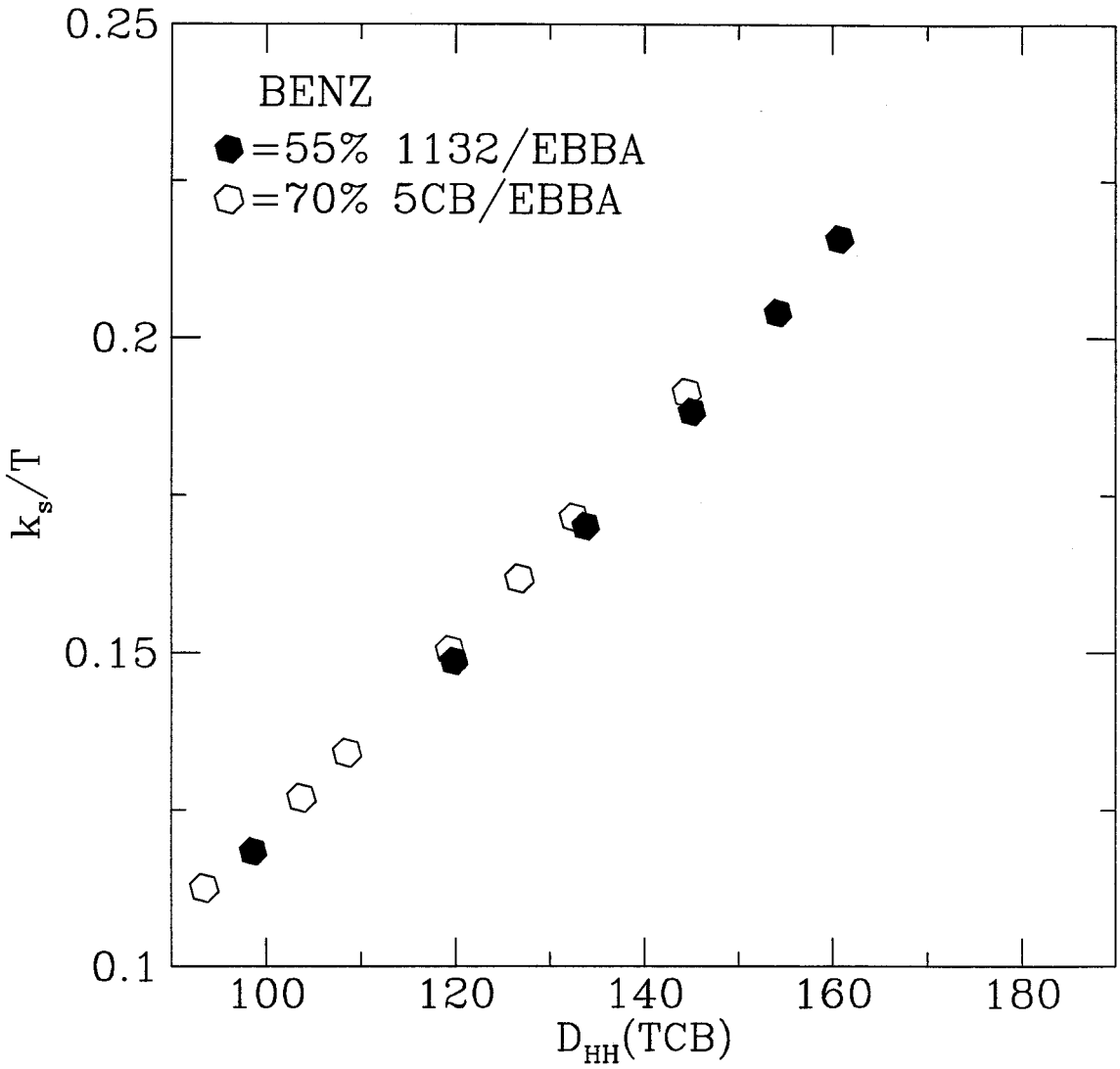

Figure 4.18: Reduced model parameter, k_s/T *vs.* D_{HH}(TCB) for BENZENE.

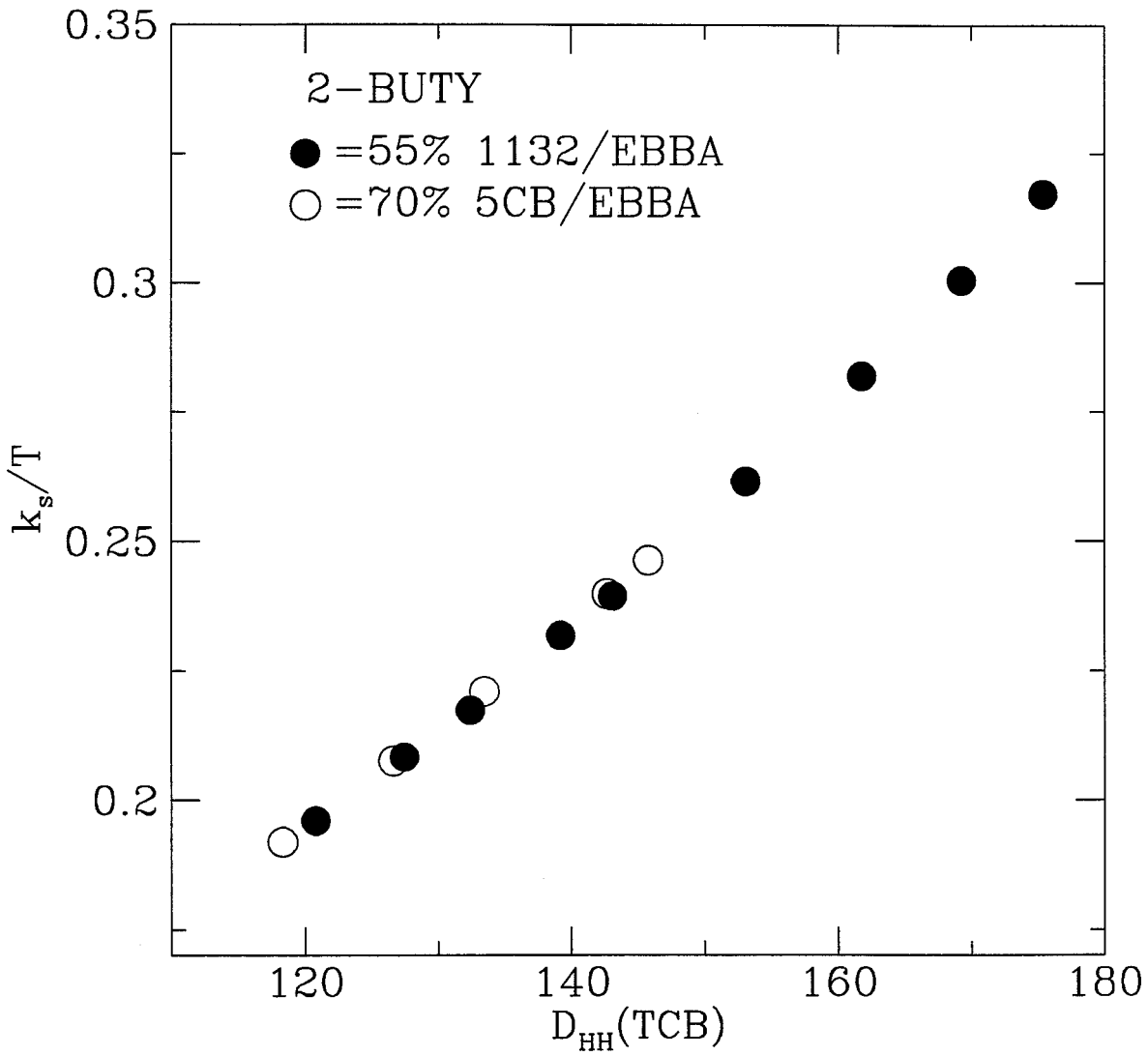

Figure 4.19: Reduced model parameter, k_s/T *vs.* D_{HH}(TCB) for 2-BUTYNE.

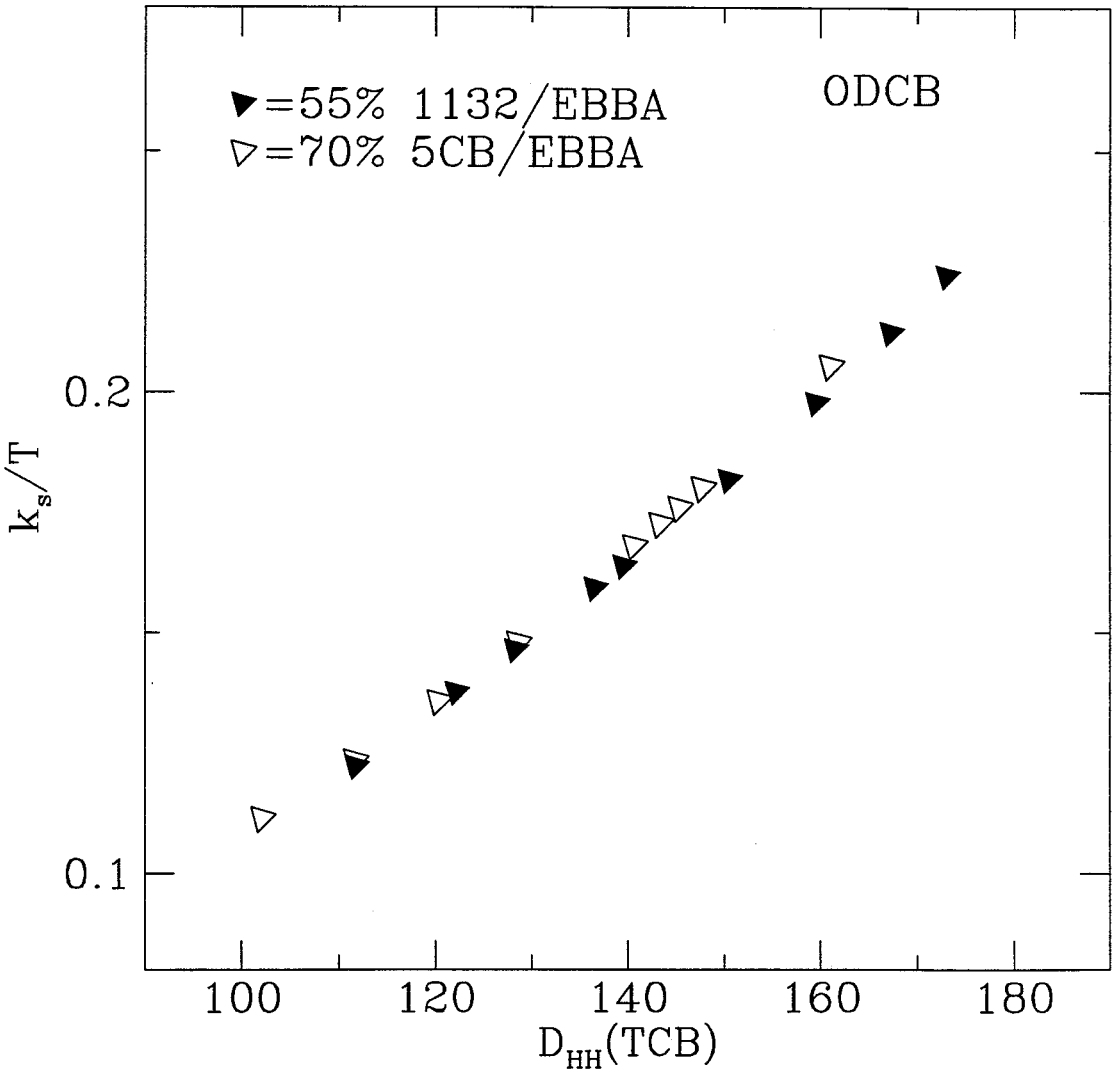

Figure 4.20: Reduced model parameter, k_s/T *vs.* D_{HH}(TCB) for ODCB.

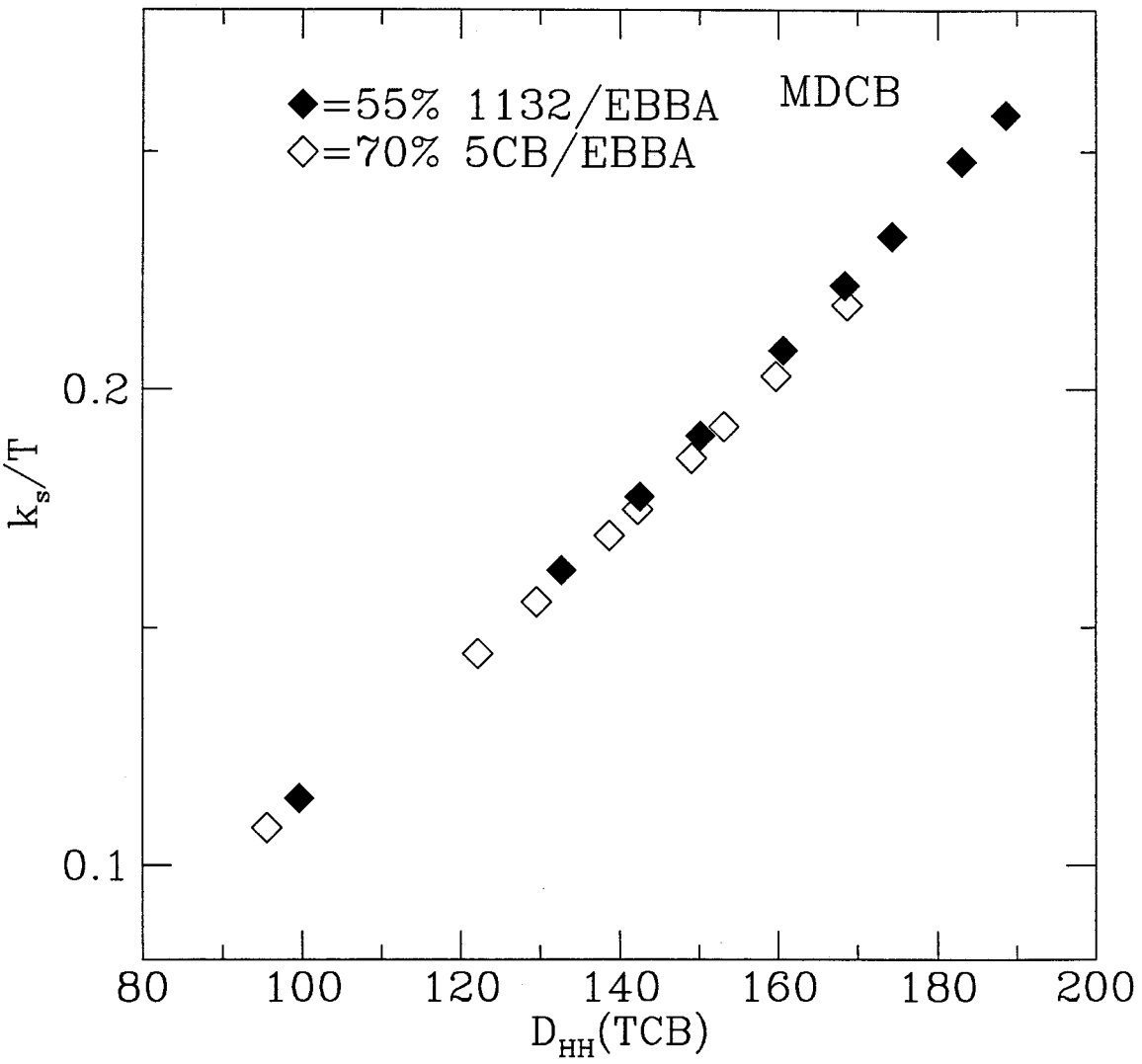

Figure 4.21: Reduced model parameter, k_s/T *vs.* D_{HH}(TCB) for MDCB.

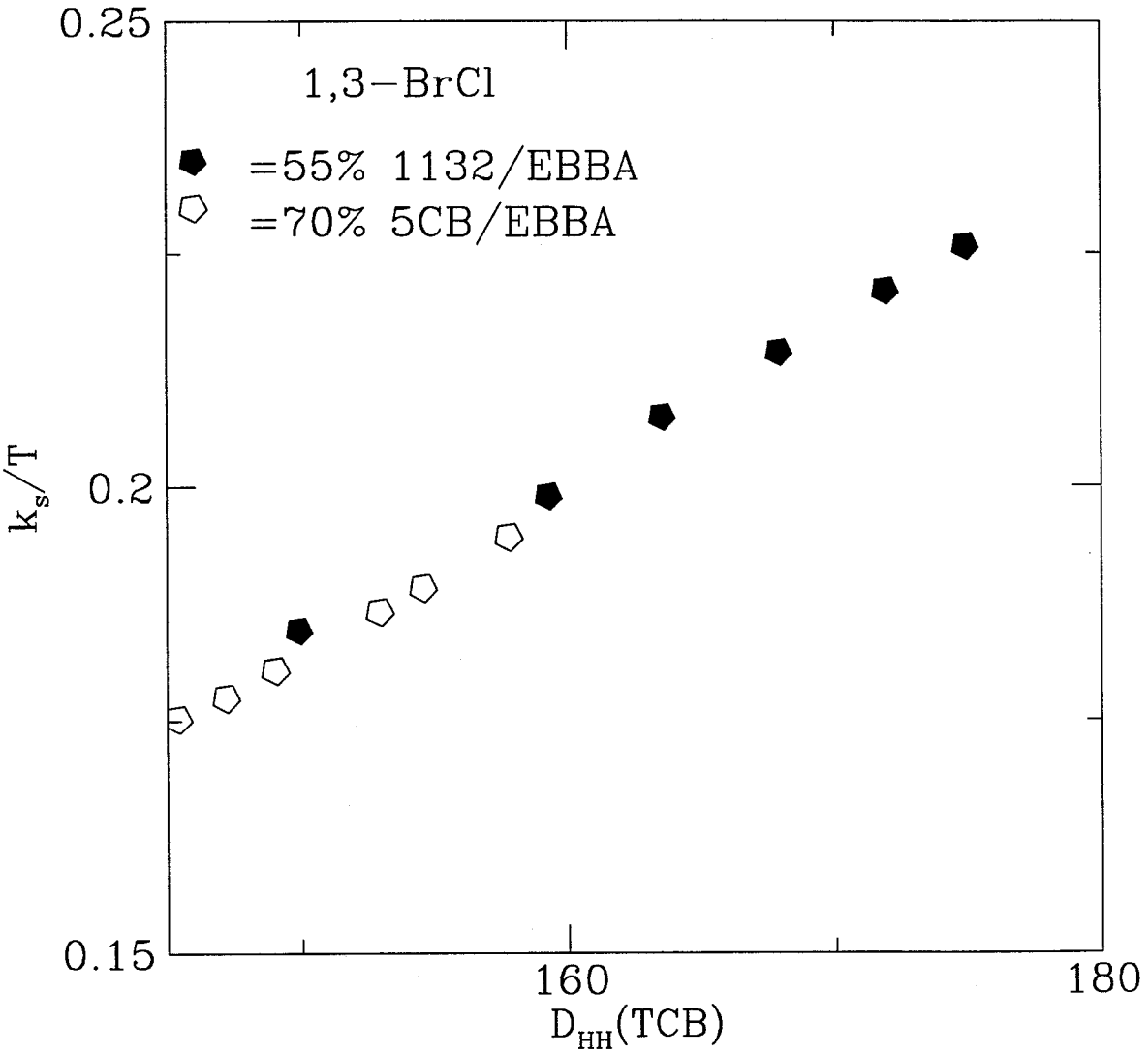

Figure 4.22: Reduced model parameter, k_s/T *vs.* D_{HH}(TCB) for 1,3- Bromochloro benzene.

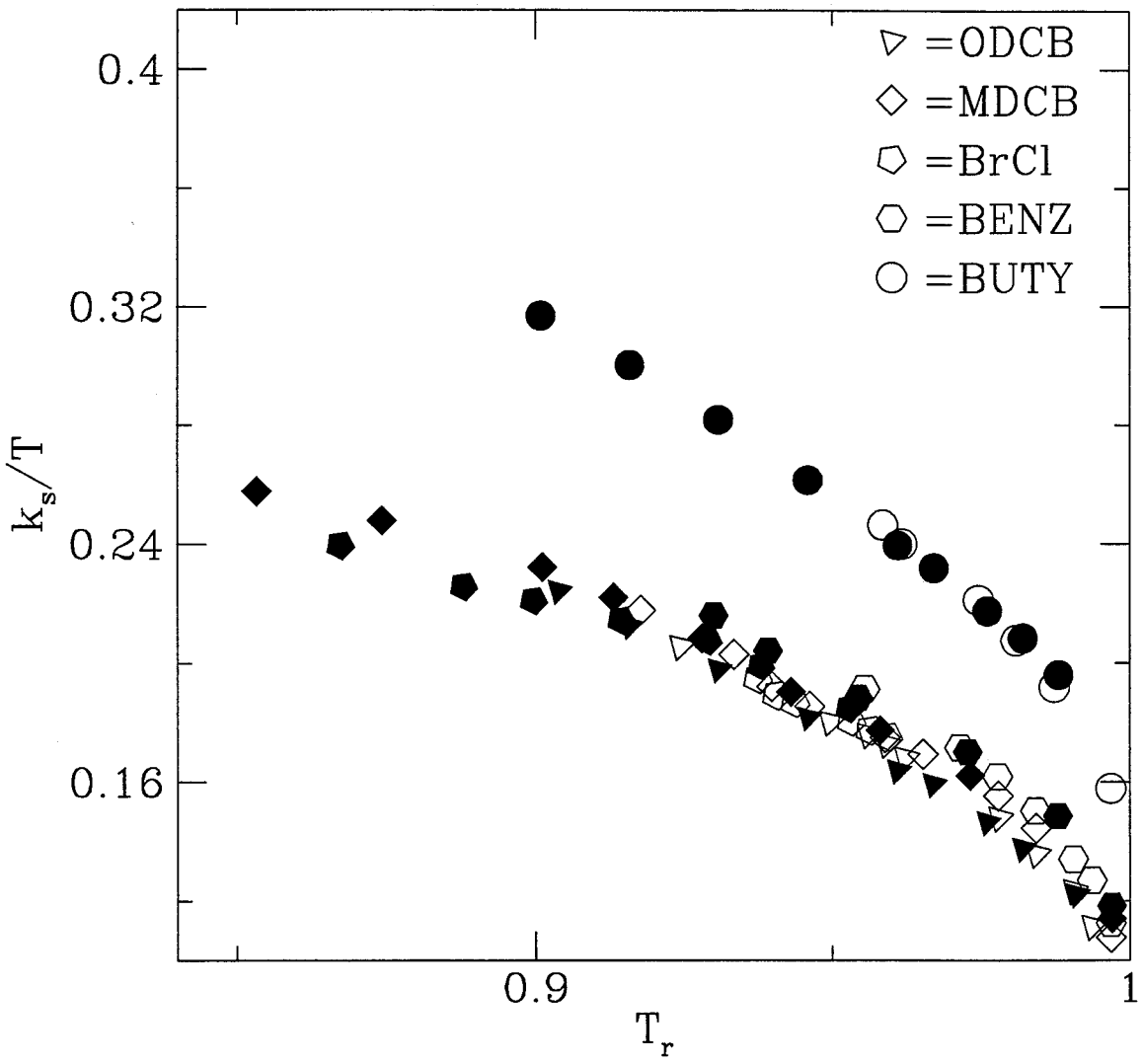

Figure 4.23: Reduced model parameter, k_s/T *vs.* T_r for all the solutes.

4.5 Biaxial order parameter

The biaxial order parameter , S_{xx}-S_{yy}, expresses the asymmetry in the order of the molecular long axis. The temperature dependencies of S_{xx}-S_{yy} and S_{zz} have been analysed in detail in the studies [62, 63]. In this thesis, S_{xx}-S_{yy} has been measured for the solutes ODCB, MDCB and 1,3-BrCl in the zero efg mixtures. The S_{xx}-S_{yy} dependence on S_{zz} shall be compared with that predicted by the model.

In Figures. 4.24 - 4.26, the variation of S_{xx}-S_{yy} with S_{zz} is shown for the solutes ODCB, MDCB and 1,3-BrCl in the solvents 55% 1132/EBBA and 70% 5CB/EBBA. The dotted symbols on the figures represent the calculated S_{xx}-S_{yy} dependence on S_{zz}. In the following, we shall refer to the experimental S_{xx}-S_{yy} *vs.* S_{zz} plots as "experimental profile" and those of calculated S_{xx}-S_{yy} *vs.* S_{zz} as "calculated profile". Figures. 4.24 - 4.26 show that the "experimental profile" has a weak solvent dependence.

The difference between the "experimental profile"s of the two mixtures is not consistent from one solute to another. The difference is the smallest for the solute MDCB and the largest for the ODCB. Further, for the solute ODCB the magnitude of the "experimental profile" of 70% 5CB/EBBA is larger than that of 55% 1132/EBBA, whereas it is opposite for the solutes MDCB and 1,3-BrCl. If the discrepancies between the "experimental profile"s of the two mixtures were systematic for all three solutes, then it could be argued that there is an additional contribution to the intermolecular potential in one zero efg mixture, whereas it is absent in the other mixture. Since discrepancies between the "experimental profile"s for the solutes appear to be random, it is not clear why there is a significant difference between the 'experimental profile"s of the mixtures 55% 1132/EBBA and 70% 5CB/EBBA.

The "calculated profile"s are compared with those of the "experimental profile"s. It is found that the "calculated profile"s are always underestimated for all three solutes.

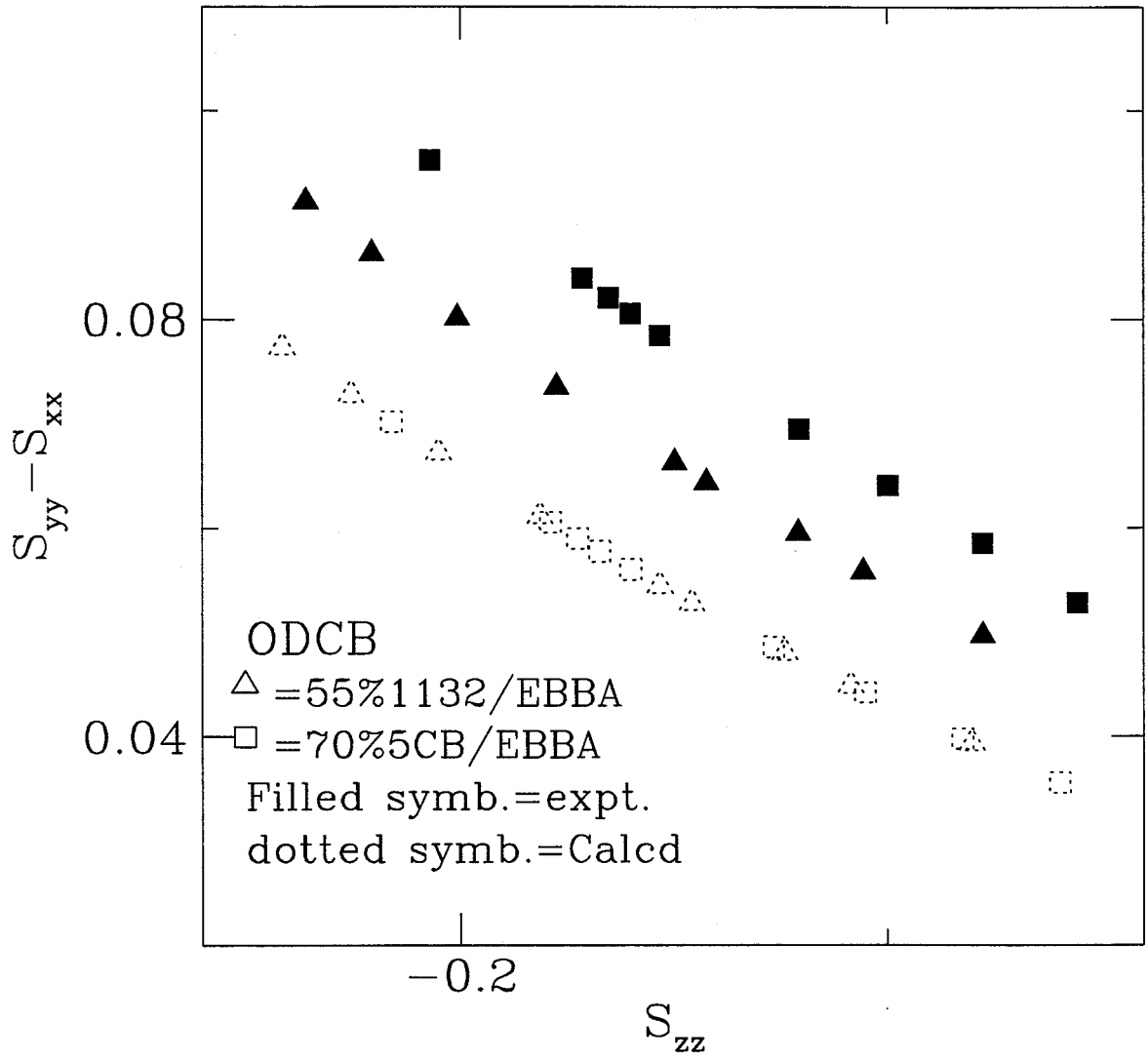

Figure 4.24: S_{xx}-S_{yy} dependence on S_{zz} for the solute ODCB.

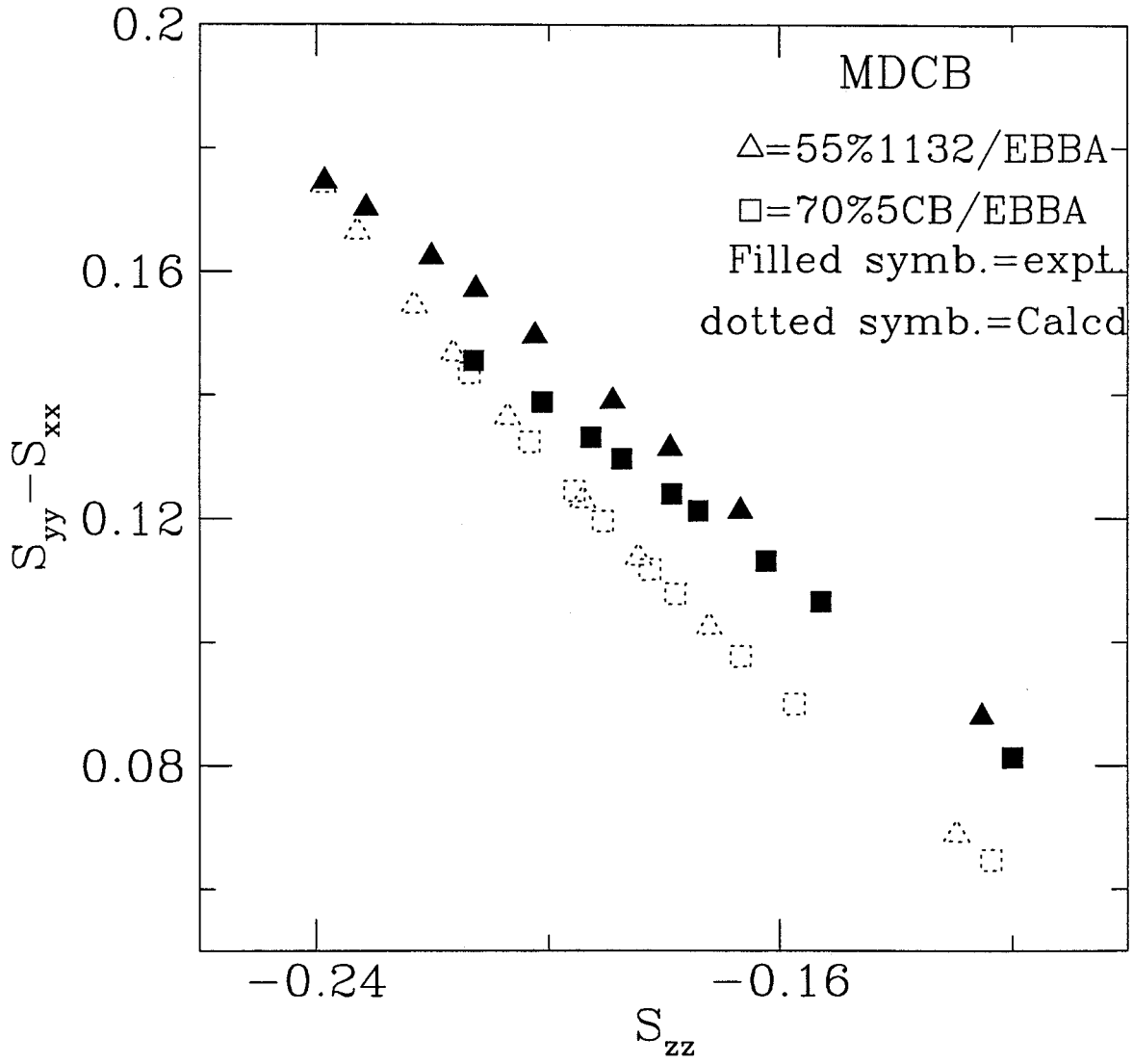

Figure 4.25: S_{xx}-S_{yy} dependence on S_{zz} for the solute MDCB.

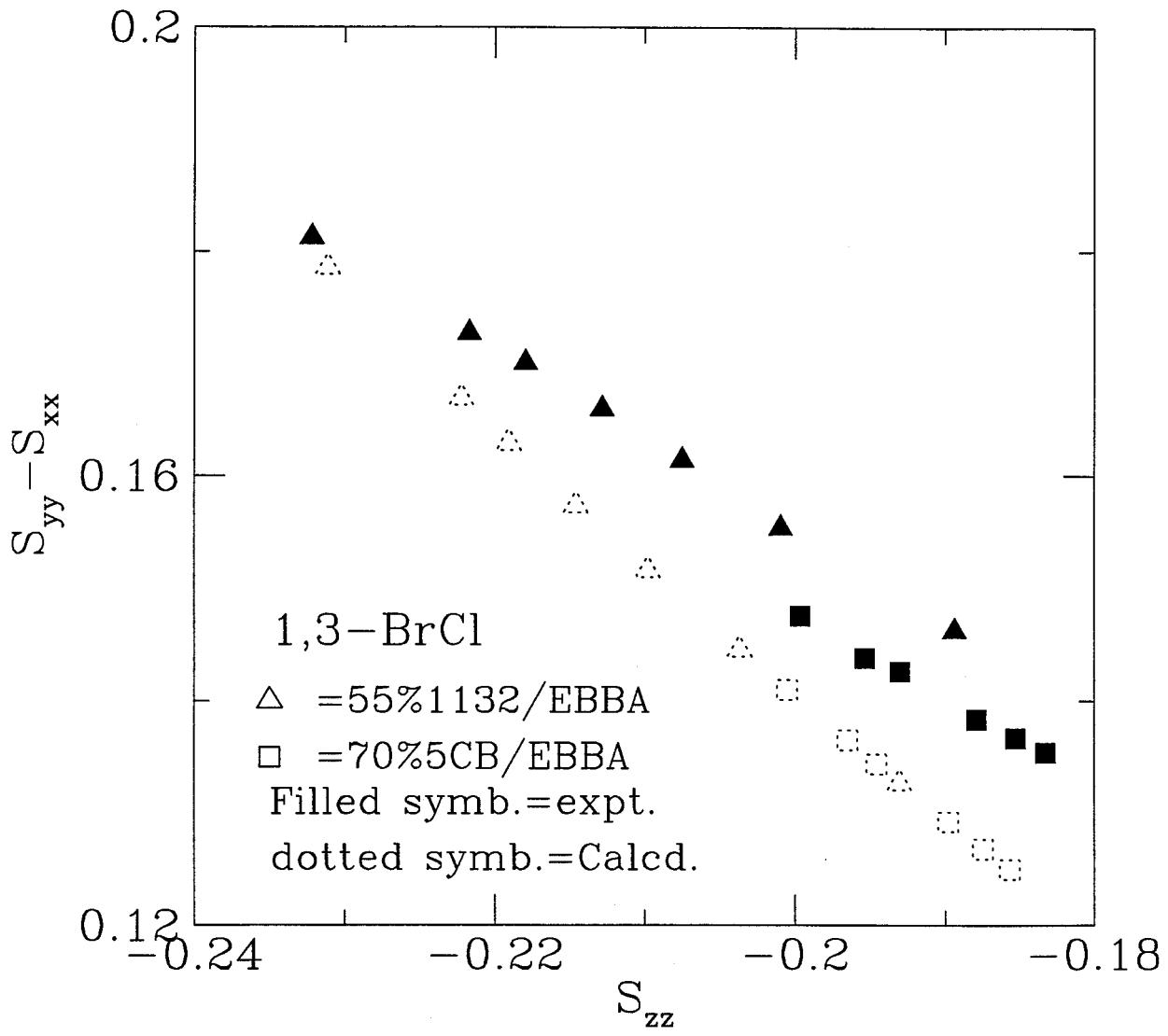

Figure 4.26: S_{xx}-S_{yy} dependence on S_{zz} for the solute 1,3- Bromochloro benzene.

This underestimation could be due to two possiblities. First, the model used for the short-range interaction does not fit the biaxial order parameter, S_{xx}-S_{yy}, as well as it does to S_{zz}. This observation was also noted in Figures. 4.13 - 4.17.

The other possiblity is that if there still exists a residual electric field gradient present at temperatures other than 301K for 55% 1132/EBBA and 316K for 70% 5CB/EBBA, then the residual electric field gradient — electric quadrupole moment interaction contributes to the potential. If this is the case, there should be a much better agreement between the experimental and calculated order parameters at temperature 301K for 55% 1132/EBBA and 316K for 70% 5CB/EBBA than that at other temperatures. However, the quality of agreement between the "experimental profile" and the "calculated profile" at all temperatures is more or less the same. This suggests that the same type mechanism is responsible for the intermolecular potential in the zero efg mixtures at all temperatures studied and that the temperature effect on the electric field gradient is negligibly small in the zero efg mixtures. Therefore, it must be concluded that the discrepancies between the "experimental profile" and the "calculated profile" is mainly due to the fact that the model does not fit the biaxial order parameter, S_{xx}-S_{yy}, very well. The temperature effect on the residual electric field gradient shall be investigated further in the next chapter.

4.6 Summary

The TCB dipolar coupling is a good measure of reduced temperature, T_r, in zero efg mixtures. The order parameters, $S_{\alpha\beta}$, are in good agreement in the two zero efg mixtures for a given TCB splitting. The origin of this transferability of the order parameters between the two mixtures comes from the short-range potential. It has been found that reduced short-range potentials in the two zero efg mixtures 55% 1132/EBBA and 70% 5CB/EBBA are the same. The short-range potential is quite sufficient to describe the

orientation of the solutes having different shape and symmetry in the zero efg mixtures 55% 1132/EBBA and 70% 5CB/EBBA at all temperatures studied.

Chapter 5

A ^{2}H NMR study of 5CB – d_{19} in zero electric field gradient nematic mixtures

5.1 Introduction

The nature of intermolecular forces among constituent liquid crystal molecules is a fascinating problem. As a starting point, it is convenient to use small solutes as probes to understand the intermolecular forces. In Chapter 3, small C_{2V} symmetry solutes as probes were studied in the zero efg mixtures 56.5% 1132/EBBA and 70% 5CB/EBBA at certain temperatures. As an extension to this study, the temperature dependence of different-shape-solutes were undertaken in the zero efg mixtures 55% 1132/EBBA and 70% 5CB/EBBA in Chapter 4. To further extend the understanding of intermolecular forces among liquid crystal molecules, it is appropriate to study a liquid crystal as a probe molecule.

In this chapter, the molecule 5CB – d_{19} (Figure 5.27) is studied in the three zero efg mixtures 55% 1132/EBBA, 56.5% 1132/EBBA and 70% 5CB/EBBA. 5CB is interesting because it exhibits a nematic phase, and is in fact one of the components of one of the mixtures used. The spectra of 5CB – d_{19} at the same temperature are not the same in the different mixtures. To understand the differences, a model is used for the short-range interactions to calculate the spectrum. Two different models, CZ and CI, are used for the calculation. The reason to use two different models is to confirm the experimental results independent of model. The calculations are also repeated for different E_{tg} values to choose an appropriate trans-gauche energy difference, E_{tg}, value.

Section 5.2 briefly reviews the theory needed to calculate the quadrupolar splittings of 5CB $-$ d_{19} in the zero efg mixtures. Section 5.3 describes the spectral analysis of the 5CB $-$ d_{19} spectra. Section 5.4.1 discusses the temperature effect on residual electric field gradient in the mixtures 55% 1132/EBBA and 56.5% 1132/EBBA. Section 5.4.2 mainly deals with the geometry of the 5CB $-$ d_{19} molecule. Section 5.4.3 describes the calculation of quadrupolar splittings using the CZ and CI models at each individual temperature (Individual Fit). In these calculations, the model parameters are obtained at each temperature. Section 5.4.4 discusses the temperature dependence of the individual fit model parameters. Section 5.4.5 describes how the parameters E_{tg} and the ratios of the model parameters, ξ and ξ', can be calculated for a particular mixture in a single fit, where the quadrupolar splittings of all temperatures are included.

5.2 Review of Theory

The solute 5CB $-$ d_{19} has a rigid ring part and a flexible chain part. According to the RIS approximation [64], each C-C bond has three discrete rotational states: trans, t, and two gauche, $g+$ and $g-$. Thus, there are 27 conformer states for 5CB $-$ d_{19}. The total energy, $U_{T,i}(\Omega)$, of conformer i in orientation Ω is a sum of two terms [65]:

$$U_{T,i}(\Omega) = U_{int,i} + U_i(\Omega) \tag{5.38}$$

$U_{int,i}$, which is assumed to be independent of orientation [66], describes the internal energy of conformer i. $U_i(\Omega)$ is an orientation dependent part of the interaction potential. The internal energy, $U_{int,i}$, is given by:

$$U_{int,i} = n_g E_{tg} + n_{g+g-} E_{g+g-} \tag{5.39}$$

where E_{tg} is the trans-gauche energy difference, n_g is the number of gauche rotations and n_{g+g-} is the number of gauche+ followed by gauche$-$ rotations in the conformer. The

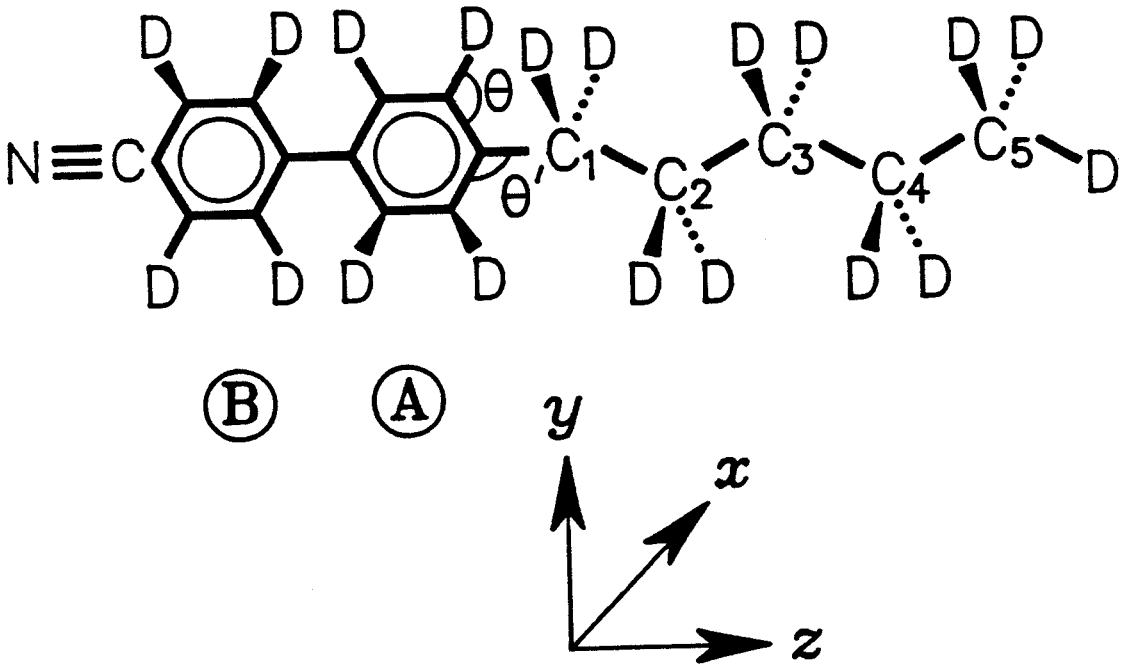

Figure 5.27: The coordinate system and atom numbering scheme of the 5CB $-$ d_{19} molecule.

energy E_{g+g-} is the additional energy required to inhibit successive gauche+ gauche− bonds which include large steric interactions. E_{g+g-} is taken as 1.5 kcal/mol [52, 64]. The probability of conformer i, p_i, is given by:

$$p_i = \frac{\exp(\frac{-U_{int,i}}{kT}) \int \exp(\frac{-U_{sr,i}(\Omega)}{kT}) d\Omega}{\sum_i \exp(\frac{-U_{int,i}}{kT}) \int \exp(\frac{-U_{sr,i}(\Omega)}{kT}) d\Omega} \tag{5.40}$$

where the integration is over all orientations Ω. For a nematic liquid crystal with the director aligned parallel to the magnetic field direction the Quadrupolar splitting of a deuteron in conformer i, $\nu_{Q,i}$, is given by:

$$\nu_{Q,i} = \sum_{\alpha} \sum_{\beta} \frac{e^2 Q}{h} q_{\alpha\beta,i} S_{\alpha\beta,i} \tag{5.41}$$

where eQ is the quadrupole moment of the ^{2}H nucleus, $S_{\alpha\beta,i}$ and $q_{\alpha\beta,i}$ are the $\alpha\beta$ components of the order matrix and the electric field gradient of the deuteron nucleus in a conformer coordinate frame. The components of the order matrix for conformer i, $S_{\alpha\beta,i}$, are given by:

$$S_{\alpha\beta,i} = \frac{\int (3\cos\theta_\alpha \cos\theta_\beta - \delta_{\alpha\beta}) exp(-U_i(\Omega)/kT) d\Omega}{2 \int exp(-U_i(\Omega)/kT) d\Omega} \tag{5.42}$$

where $\cos\theta_\alpha$, $\cos\theta_\beta$ are the direction cosines of the α, β axes with respect to the Z, director, axis. The calculated quadrupolar splitting, $\Delta\nu_Q$, is then:

$$\Delta\nu_Q = \sum_i \nu_{Q,i} p_i \tag{5.43}$$

The principal axes, a, b, c, of the intramolecular electric field gradient tensor of the ring deuterons have axis b along the C-D bond and axis a in the plane of the ring. The quadrupolar splitting of conformer i, $\nu_{Q,i}$, is then written in terms of the quadrupolar coupling constant, $\frac{e^2 Q q_{bb}}{h}$, and the asymmetry parameter, $\eta = (q_{aa} - q_{cc})/q_{bb}$. The quadrupolar coupling constant for ring deuterons is 185 KHz, and η is 0.04 [67]. For the flexible chain part, the quadrupolar coupling constant is taken as 168 KHz and η is taken as zero [68].

Table 5.6: Quadrupolar splittings (in kHz) of 5CB-d_{19} in 55% 1132/EBBA.

Temp./K	$\Delta\nu_1$	$\Delta\nu_2$	$\Delta\nu_3$	$\Delta\nu_4$	$\Delta\nu_5$	Ring A	Ring B
251.4	77.782	63.768	65.233	49.559	35.790	21.728	17.577
256.1	77.050	62.255	63.719	47.899	34.569	21.435	17.430
261.1	75.878	60.887	62.597	46.142	33.446	21.240	17.236
265.3	75.048	59.569	61.327	44.823	32.568	20.946	17.040
270.7	74.267	58.251	59.960	43.066	31.396	20.946	16.893
275.8	73.974	57.177	58.739	41.747	30.663	20.702	16.699
281.5	72.314	55.028	56.688	39.745	29.199	20.263	16.161
285.3	70.898	53.319	55.077	38.329	28.173	19.725	15.721
292.1	68.309	50.438	52.489	35.936	26.366	18.896	14.941
296.4	66.796	48.730	50.634	34.520	25.292	18.310	14.501
302.1	64.697	46.337	48.339	32.616	23.827	17.577	13.818
307.1	62.743	44.189	46.239	30.858	22.606	16.698	13.232
312.7	59.911	41.308	43.456	28.612	20.995	15.770	12.352
317.0	57.079	38.768	41.014	26.757	19.579	14.843	11.572
323.1	53.368	35.448	37.646	24.218	17.724	13.524	10.497
327.0	49.316	32.079	34.276	21.776	15.917	12.255	9.325
332.6	42.333	26.806	28.661	18.017	13.182	10.156	7.567
334.6	38.622	24.315	25.927	16.307	11.962	9.130	6.786

5.3 Results

5.3.1 General

Figure 5.28 shows the spectra of 5CB $-$ d_{19} in 55 % 1132/EBBA at 307.1 K and in 70% 5CB/EBBA at 306.8 K. The quadrupolar lines are broadened due to the dipole-dipole coupling between deuterons. Quadrupolar splittings were measured in a manner consistent with line shape simulations. Measurements were carried out at temperatures ranging from 250K to the isotropic temperature on the mixtures 55% 1132/EBBA, 70% 5CB/EBBA and 56.5% 1132/EBBA. Measured line positions are tabulated in Tables 5.6 to 5.8. Spectral line assignments are discussed in detail in section 5.3.2.

As the temperature approaches T_{NI}, the spectra begin to appear as a superposition

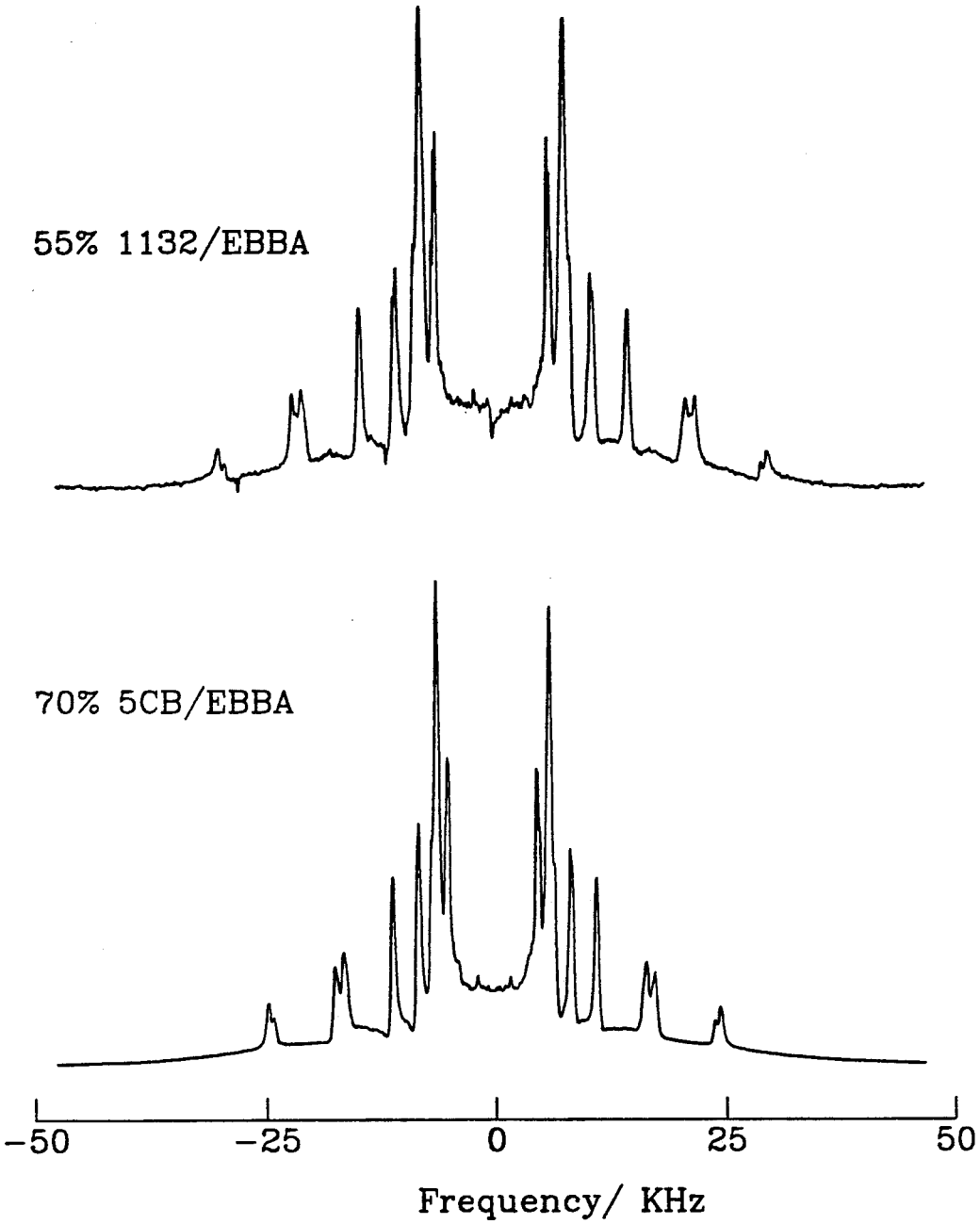

Figure 5.28: Experimental ^{2}H-NMR spectra of 5CB – d_{19} dissolved in the zero efg mixtures 55% 1132/EBBA, at 307.1K, and 70% 5CB/EBBA at 306.8K.

Table 5.7: Quadrupolar splittings (in kHz) of 5CB-d_{19} in 70% 5CB/EBBA.

Temp./K	$\Delta\nu_1$	$\Delta\nu_2$	$\Delta\nu_3$	$\Delta\nu_4$	$\Delta\nu_5$	Ring A	Ring B
251.9	72.509	57.812	59.569	44.140	32.031	19.725	15.966
255.9	70.702	55.663	57.958	42.626	30.956	19.189	15.526
261.2	69.579	53.564	55.712	40.233	29.345	18.652	14.940
265.3	68.163	52.148	54.101	38.720	28.271	18.212	14.550
271.1	65.868	49.511	51.513	36.230	26.513	17.528	13.963
276.1	64.550	47.704	49.755	34.569	25.438	17.040	13.524
281.9	62.108	44.921	46.972	32.177	23.827	16.258	12.841
285.9	60.399	43.017	45.116	30.517	22.704	15.721	12.352
292.1	57.861	40.331	42.626	28.319	21.044	15.038	11.766
296.6	56.298	38.671	40.819	26.854	20.018	14.452	11.425
302.0	53.906	36.620	38.573	24.999	18.700	13.866	10.937
306.8	51.563	34.570	36.524	23.438	17.480	13.232	10.400
308.8	49.462	32.909	34.813	22.118	16.551	12.597	9.764
310.8	46.728	30.859	32.714	20.702	15.477	11.816	9.130
312.7	42.968	28.026	29.736	18.700	14.013	10.595	8.153
313.7	40.624	26.464	28.075	17.578	13.134	10.008	7.616
314.7	37.646	24.608	25.976	16.210	12.059	9.228	6.982
315.7	34.130	21.678	22.704	14.404	10.839	8.104	6.201

Table 5.8: Quadrupolar splittings (in kHz) of 5CB-d_{19} in 56.5% 1132/EBBA.

Temp./K	$\Delta\nu_1$	$\Delta\nu_2$	$\Delta\nu_3$	$\Delta\nu_4$	$\Delta\nu_5$	Ring A	Ring B
261.4	75.927	61.156	62.987	46.569	33.691	21.239	17.211
266.1	75.255	59.997	61.827	45.349	32.714	20.995	16.966
271.7	74.340	58.287	60.180	43.334	31.616	20.812	16.783
276.0	73.791	57.311	59.143	42.236	30.821	20.751	16.722
281.9	72.630	55.480	57.067	40.160	29.479	20.201	16.234
286.1	71.044	53.649	55.541	38.695	28.441	19.713	15.929
292.5	69.029	50.963	53.222	36.620	26.854	19.042	15.075
296.7	67.321	49.133	51.390	35.095	25.634	18.432	14.587
302.0	65.123	46.813	48.889	33.080	24.169	17.638	13.915
307.1	63.415	44.615	46.752	31.372	22.887	16.844	13.304
312.6	60.851	41.870	44.249	29.235	21.362	15.990	12.511
317.1	58.226	39.489	41.869	27.403	20.018	15.075	11.718
323.1	54.686	36.376	38.513	24.963	18.249	13.854	10.742
327.6	50.963	33.263	35.522	22.704	16.600	12.633	9.764
328.6	50.109	32.653	34.972	22.277	16.234	12.389	9.459
330.1	48.095	31.127	33.202	21.117	15.380	11.779	8.971
330.6	47.057	30.089	32.226	20.446	14.892	11.413	8.666
332.6	44.799	28.502	30.517	19.286	14.037	10.802	8.056
333.6	43.578	27.648	29.601	18.676	13.610	10.436	7.812
334.6	42.296	26.732	28.747	18.065	13.183	10.070	7.507
335.1	40.526	25.573	27.465	17.272	12.572	9.642	7.140
336.1	38.207	23.864	25.817	16.112	11.718	8.971	6.591
337.1	36.193	22.460	23.925	15.075	11.046	8.300	6.163
338.1	33.019	20.263	21.422	13.732	10.009	7.446	5.553

of nematic and isotropic peaks. The lowest temperature at which the isotropic peak appears is taken to be T_{NI}. The T_{NI} of 55% 1132/EBBA and 56.5% 1132/EBBA are 337K and 339K respectively, and the T_{NI} of 70% 5CB/EBBA is 316K. These numbers differ slightly from those of the microscopic study (Chapter 2) because the samples used for NMR contain deuteriated materials.

The measured quadrupolar splittings at position 1, $\Delta\nu_1$, are plotted against temperature in Figure 5.29. The curves corresponding to 55% 1132/EBBA and 56.5% 1132/EBBA are similar. However, the curve corresponding to the mixture 70% 5CB/EBBA appears to have a break at 307K(see Figure 5.29). Below this temperature the quadrupolar splitting changes linearly with temperature. However, the microscope study indicates that there is no phase transition taking place near 307K in this mixture. Thus, the liquid crystal mixtures are nematic for all points given in Figure 5.29.

5.3.2 Analysis of 5CB-d_{19} spectra

The ^2H-NMR spectrum of 5CB-d_{19} in the nematic phase has 7 pairs of quadrupolar lines, each pair corresponding to its C-D bond site. The assignment of each pair to its corresponding site is described below.

As described in section 1.2.2, the quadrupolar splitting, $\Delta\nu_Q$, depends on the order parameter, S_{CD}, of the C-D bond. In other words, the quadrupolar splitting depends on the angle between the C-D bond and the director axis, Z. In order to relate the quadrupolar splitting to the geometrical features of 5CB-d_{19} molecule, it is convenient to describe the quadrupolar Hamiltonian in terms of an intermediate frame. The intermediate frame is usually chosen such that the long molecular axis is one of the axis in the intermediate frame. For 5CB-d_{19} molecule, the para axis, the axis connecting two phenyl group, is chosen as one of the axis in the intermediate frame.

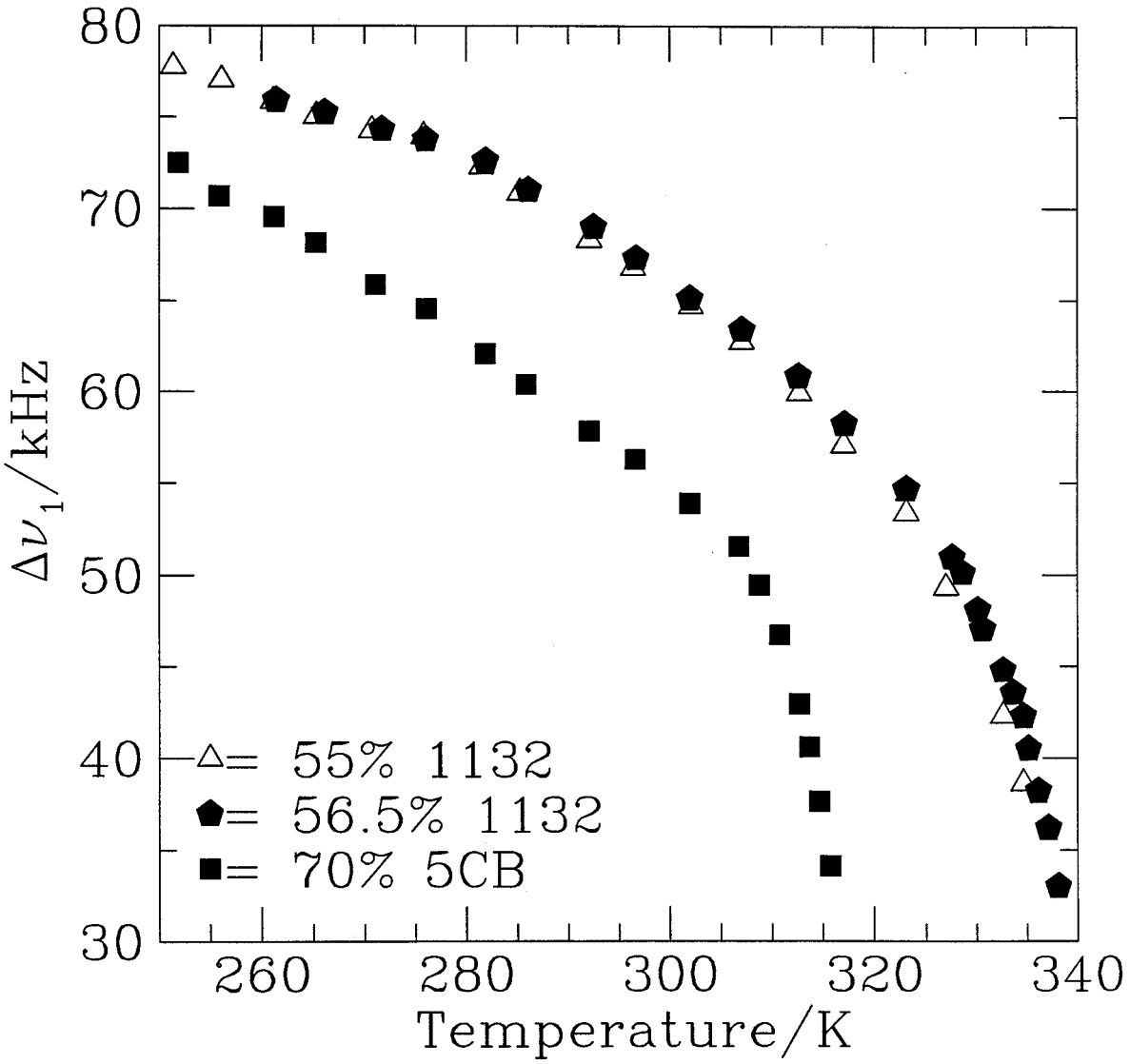

Figure 5.29: The quadrupolar splitting $\Delta\nu_1$ versus temperature for the mixtures 55% 1132/EBBA, 70% 5CB/EBBA and 56.5% 1132/EBBA.

To a good approximation, the quadrupolar splitting, $\Delta\nu_Q$, can be described as

$$\Delta\nu_Q = \frac{3e^2qQ}{4h} < \frac{(3\cos^2\theta' - 1)}{2} >< \frac{(3\cos^2\theta'' - 1)}{2} >, \tag{5.44}$$

where the term $< \frac{(3\cos^2\theta''-1)}{2} >$ is the transformation from the principal axis system of the C-D bond to the intermediate frame of the molecule. The term $< \frac{(3\cos^2\theta'-1)}{2} >$ is the transformation from the intermediate frame to the lab-fixed axis system of the molecule. Since θ' is the angle between the para axis of 5CB-d_{19} molecule and the lab-fixed axis, Z, the term $< \frac{(3\cos^2\theta'-1)}{2} >$ is the same for all 7 different sites of the C-D bond. On the other hand, the term $< \frac{(3\cos^2\theta''-1)}{2} >$ varies from one C-D bond to another due to the geometrical features.

We shall now correlate the assignment of the quadrupolar splitting to its C-D bond site based on the angle θ''. First, we look at the quadrupolar splitting corresponding to C_1 position (Figure 5.27). Since the bond attaching C_1 with aromatic ring is fixed, the angle θ'' is very close to 109^0. This causes the term $< \frac{(3\cos^2\theta''-1)}{2} >$ to have a large magnitude. As a result, the quadrupolar splitting at C_1 position has the largest magnitude.

Next, we assign the quadrupolar splitting due to the methyl group. The methyl group of the alkyl chain undergoes a fast free rotation along the C_4-C_5 bond. Due to this extra motion, the quadrupolar splitting needs to be described in two intermediate frames. As a result, the expression for the quadrupolar splitting (eq. 5.44) has an extra term $< \frac{(3\cos^2\beta-1)}{2} >$, , where β is the angle between C_4-C_5 bond and C-D bond in the methyl group. The angle β takes a value of 70.5^0. Consequently, the term $< \frac{(3\cos^2\beta-1)}{2} >$ reduces the magnitude of the quadrupolar splitting of the methyl group. Therefore, the quadrupolar splitting of the methyl group is the narrowest among chain deuterons.

The rotation along the C-C bonds of C_1-C_2, C_2-C_3 and C_3-C_4 leads to 27 conformational states. This extra motion causes an additional motional narrowing. As a result, the quadrupolar splittings at the C_2, C_3 and C_4 positions are smaller in magnitude than that

at C_1 position, but larger than at C_5 position. In general, the magnitude of quadrupolar splittings has the tendency to decrease towards the end of the chain since the order decreases from rigid ring part to the tail chain part. Due to the odd-even effect [69], however, the quadrupolar splitting at C_3 position has a larger magnitude than that at C_2 and C_4 positions. The spectral line assignments for the chain deuterons agree exactly with the previous work [70]. The assignment of the quadrupolar lines corresponding to the ring deuterons is described in the next paragraph.

In order to assign the quadrapolar lines corresponding to Ring A and Ring B (see Figure 5.27), the experimental quadrupolar splittings for the flexible chain were assigned first for the room temperature spectrum. These assigned experimental quadrupolar splittings were fitted to calculate the quadrupolar splittings at all 7 different sites, using the CZ model for the short-range potential. (calculation shall be described in sections 5.4.2 and 5.4.3). These calculated quadrupolar splittings for ring deuterons are matched with the experimental ones to assign the experimental quadrupolar lines of Ring A and Ring B.

The assignment of ring deuterons shows that the two inner pairs of quadrupolar lines correspond to the aromatic deuterons. This can be understood in terms of the θ'' angle. The angle θ'' between aromatic C-D bond and the molecular para axis is close to 60^0. Therefore, $< \frac{(3\cos^2\theta''-1)}{2} >$ term becomes very small. As a result, the quadrupolar splittings of aromatic deuterons are small.

5.4 Discussion

5.4.1 General

The purpose of this section is to examine several zero efg mixtures. One way of emphasizing small differences among the zero efg mixtures is to plot ratios of the quadrupolar

splittings, such as $\Delta\nu_5/\Delta\nu_1$, against $\Delta\nu_1$. These plots shall be referred to as ratio plots. Ratio plots for 5CB $-$ d_{19} were previously used to illustrate differences among the liquid crystals 1132, EBBA, 5CB and 55% 1132/EBBA [52]. In that study, the differences were ascribed to the presence of a non-zero electric field gradient in the various liquid crystals.

A plot of $\Delta\nu_5/\Delta\nu_1$ against $\Delta\nu_1$ is shown in Figure 5.30. Intuitively, one might expect that ratio plots for all zero efg mixtures would be similar. However, the differences between 55% 1132/EBBA and 70% 5CB/EBBA are large and comparable to those between the liquid crystals 1132 and EBBA in ref [52]. On the other hand, the ratio plots of 5CB $-$ d_{19} in 55% 1132/EBBA and in 56.5% 1132/EBBA are superimposable. This latter fact allows us to evaluate the effect of a small residual electric field gradient present in the mixtures 55% 1132/EBBA and 56.5% 1132/EBBA at temperatures other than 301.4K and 322K where the electric field gradient is zero.

In such zero efg mixtures, the average electric field gradient measured using D_2 changes sign and magnitude with changing temperature. At any given temperature, the average electric field gradient in the 55% 1132/EBBA mixture differs from that in the 56.5% 1132/EBBA mixture. If these small efg's made a significant contribution to the anisotropic orientational potential, the ^{2}H spectra of 5CB $-$ d_{19} should differ between the two mixtures. However, the ratio plots in Figure 5.30 show that the quadrupolar splitting ratios $\Delta\nu_5/\Delta\nu_1$ are identical for the two mixtures over the temperature range 250K-337K. This result, together with the equivalence of the $\Delta\nu_1$ for the two 1132/EBBA mixtures in Figure 5.29, shows that the small electric field gradients present in these mixtures have a negligible effect on the spectra. The quadrupole moment - electric field gradient mechanism can be neglected as an important orientational mechanism in these mixtures. Thus, when we refer to a zero efg mixture, we include the entire nematic range of a mixture that has a precisely zero efg at one specific temperature. Note that van der Est *et al.* [71] have reported a quantitative temperature dependence study of the efg in the

55% 1132/EBBA mixture, and found that the magnitude of the measured electric field gradient does not change much with temperature.

We shall also assume that the contribution of the electric field gradient-electric quadrupole moment interaction to $U_{T,i}(\Omega)$ is negligible throughout the nematic range of the zero efg mixture 70% 5CB/EBBA. Thus the differences in Figure 5.30 between 70% 5CB/EBBA and the other zero efg mixtures do not arise from the electric field gradient - molecular quadrupole moment mechanism. Do these differences imply that the details of the short-range potential are liquid crystal dependent? We shall attempt to answer this question below.

To proceed, it is useful to introduce a model for the short-range potential, $U_{sr,i}(\Omega)$. It seems sensible to choose a model that provides a successful fit to the orientational order parameters measured for a range of rigid solutes in a zero efg nematic solvent [39, 40, 41]. Because we wish to draw meaningful conclusions from our work, we shall investigate two different models, CZ model and CI model, for the short-range potential in an attempt to come up with a comparison among mixtures that is independent, as far as possible, of the model chosen. Since no significant differences between the zero efg mixtures 55% 1132/EBBA and 56.5% 1132/EBBA are observed, only the zero efg mixtures 55% 1132/EBBA and 70% 5CB/EBBA shall be compared in the following sections.

5.4.2 RIS parameter and molecular geometry

One of the complexities of the 5CB $-$ d_{19} molecule is the presence of the flexible hydrocarbon chain which introduces the additional parameter, E_{tg}, the trans-gauche energy difference. Since E_{tg} is an intramolecular property, it should be independent of temperature and environment. E_{tg} values have been measured for n-butane in isotropic solvents and it would seem reasonable to use these values for 5CB $-$ d_{19} in zero efg mixtures. Literature values of E_{tg} for n-butane vary from 400 to 900 cal/mol [64, 72, 73, 74, 75, 76, 77, 78].

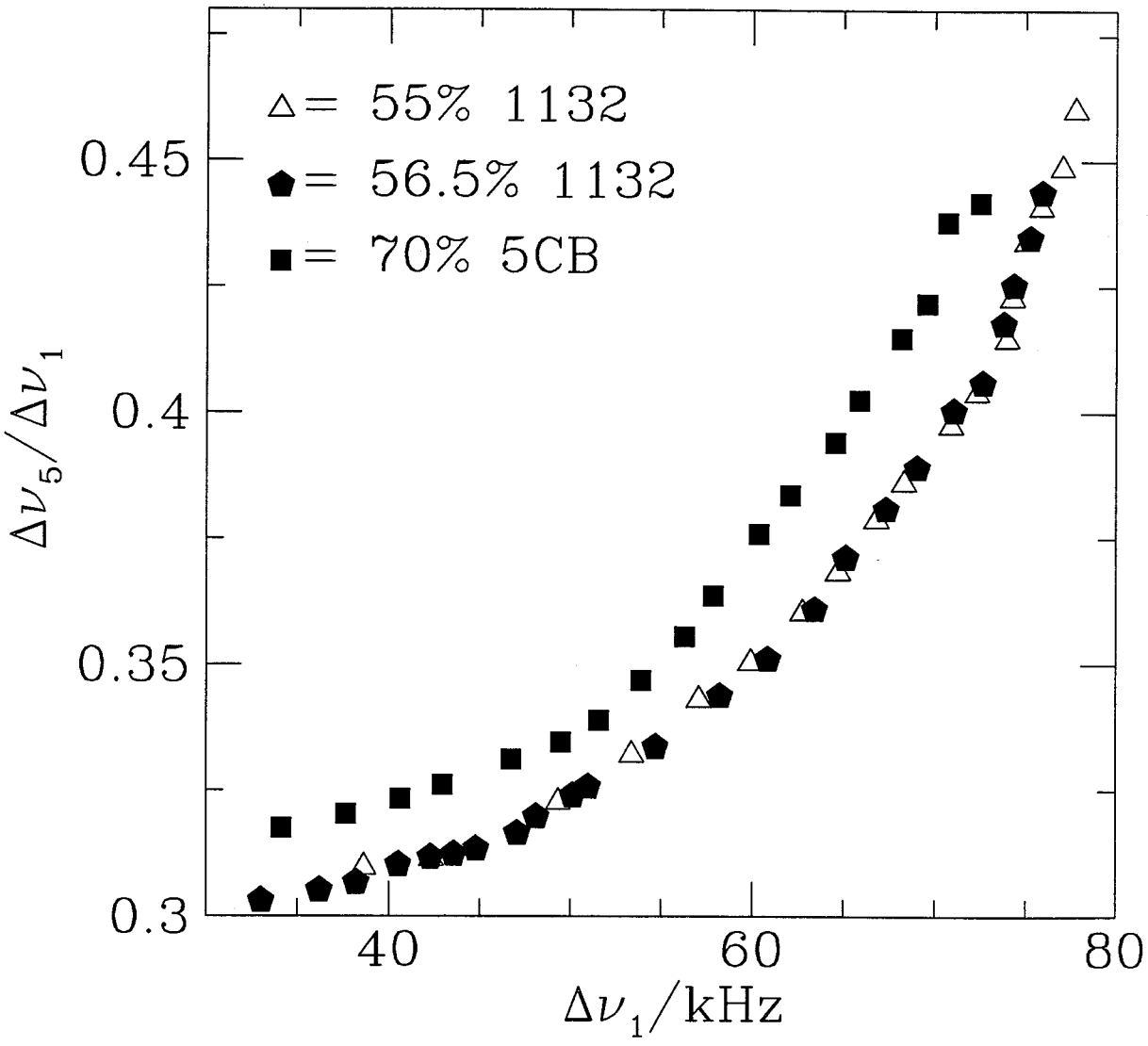

Figure 5.30: Quadrupolar splitting ratios $\Delta\nu_5/\Delta\nu_1$ versus $\Delta\nu_1$ of 5CB – d_{19} in the zero efg mixtures 55% 1132/EBBA, 70% 5CB/EBBA and 56.5% 1132/EBBA.

Most of the literature values of liquid n-butane are close to 500 cal/mol [74, 75, 76, 77]. However, one study [73] reports a value of 966 cal/mol for gaseous n-butane. Since there are a range of E_{tg} values in the literature, we shall explore calculations using E_{tg} values of 500, 700 and 900 cal/mol.

In addition, the geometry of 5CB $-$ d_{19} must be known in order to calculate the quadrupolar splittings. The parameters C and Z in the equations for $U_{sr}(\Omega)$ depend on the bond lengths, and the quadrupolar splittings depend on the bond angles. We assume that the benzene rings are regular hexagonal, and that the angle between the normals to the two benzene rings is 30^0 [45]. In addition, we assume that all the methylene groups are described by the CCC and CCD bond angles 112.5^0 and 108.82^0. The DCD plane in each CD_2 group is assumed to bisect the CCC angle. The dihedral angle for a trans – gauche conformational change is 112.0^0.

Two additional unknowns in the molecular geometry of 5CB $-$ d_{19} are the angles θ' (see Figure5.27) and θ_d, where θ_d is the dihedral angle between the C_1C_2 bond and the plane of benzene ring A. Most studies of 5CB assume that the angle θ' is 120^0. However, Photinos *et al.* [43] used the value 124^0 from X-ray studies on 5-OCB for their calculations of N-CB and N-OCB liquid crystals. While 5-OCB and 5-CB will have different geometries, it nevertheless seems worthwhile to explore the possibility of a value of θ' different from 120^0 for 5CB. Of the many possibilities, we perform four different calculations corresponding to four different geometries: the four geometries are (1) $\theta' = 120^0$, $\theta_d = 0^0$ (the bond C_1C_2 is coplanar to the benzene ring A — this geometry shall be referred as PL-0); (2) $\theta' = 124^0$, $\theta_d = 0^0$ (this geometry shall be referred as PL-4); (3) $\theta' = 120^0$, $\theta_d = 90^0$ (the ring-C_1 bond lies along the para axis of ring A and the bond C_1C_2 is perpendicular to the benzene ring A — this geometry shall be referred as PERP-0); (4) $\theta' = 124^0$, $\theta_d = 90^0$ (starting from the PL-4 geometry, the hydrocarbon chain is rotated 90^o about the para axis of ring A — this geometry shall be referred as

PERP-4).

5.4.3 Individual Fit Model parameters

A least squares minimization routine was used to obtain best fit model parameters for each experimental spectrum from a minimization of the differences between experimental and calculated quadrupolar splittings of 5CB $-$ d_{19} as solute in the zero efg mixtures 55% 1132/EBBA and 70% 5CB/EBBA. The quality of the fit is judged mainly from RMS (root mean square deviation) values — i.e. the lower the RMS the better the quality of the fit. We find that the quality of the fit depends on the parameters θ (see Figure 5.27) and E_{tg}. When the angle θ was varied, the calculated quadrupolar splittings agreed very well with the experimental quadrupolar splittings at the ring positions. However, the variation of θ did not change much the calculated quadrupolar splittings at the chain positions. Hoatson *et al.* [52] also allowed θ to vary and obtained a good fit for the ring deuterons in their study of 5CB $-$ d_{19} in liquid crystals. When the parameter E_{tg} was varied for each individual temperature, the fitted E_{tg} values varied with temperature. This contradicts the fact that the intramolecular property E_{tg} should be independent of temperature. Therefore, we decided to fix the parameter E_{tg} to certain values, 500, 700 and 900 cal/mol, at all temperatures. These values span the range of literature E_{tg} values [64, 72, 73, 74, 75, 76, 77, 78]

Separate calculations were performed for both the CZ and CI models for the four geometries PL-0, PL-4, PERP-0 and PERP-4 and for the three E_{tg} values 500, 700 and 900 cal/mol. The model parameters k_z, k_{xy} and θ were fitted in the CZ model calculations. The CI model calculation gives k, k_s and θ values. Therefore, we obtain 12 sets of (k_z, k_{xy}, θ) and of (k, k_s, θ) values for each spectrum. The fitted θ value ranges are reported in Table 5.9. The θ values obtained are consistent with the value reported in reference [70]. In order to reduce the number of possible calculations in the following,

Table 5.9: Fitted θ values for different geometries and models

Model and Geometry	E_{tg}cal mol^{-1}	θ/deg of 55% 1132/EBBA	θ/deg of 70% 5CB/EBBA
COZ	500	118.88 — 117.48	118.70 — 117.48
	700	118.96 — 117.90	118.80 — 118.00
PERP-0	900	119.02 — 118.28	118.90 — 118.44
COZ	500	119.00 — 117.48	118.80 - 117.48
	700	119.14 — 118.04	118.96 — 118.18
PERP-4	900	119.26 — 118.58	119.14 — 118.78
CAI	500	119.76 — 122.20	119.94 — 122.68
	700	119.60 — 121.00	119.72 — 121.06
PERP-0	900	119.38 — 119.52	119.42 — 119.00
COZ	500	120.38 — 123.26	120.62 — 123.82
	700	120.18 — 121.88	120.34 — 122.00
PERP-0	900	119.88 — 120.12	119.90 — 120.04

Fitted ranges for θ of 5CB (Figure 5.27) in 55% 1132/EBBA and 70% 5CB/EBBA.

we shall examine the quality of these fits and choose one set of k_z, k_{xy} and one set of k, k_s values. We shall choose the geometry and E_{tg} values that fit best the experimental quadrupolar splittings as the most appropriate basis.

The quality of the fit (RMS) to the 55% 1132/EBBA mixture for the four different geometries using the two different models and three different E_{tg} values is shown in Figure 5.31 - 5.33. While some fits are obviously much better than others, most of these fits are acceptable considering the many assumptions involved in the modelling process. It is unfortunate that the parameters are correlated such that it is not possible to choose a definitive value of E_{tg} from these calculations. However, calculations that use a value of E_{tg} of order 500 cal/mol are generally considered preferable [43]. In all cases for the CI model, the PERP-4 geometry gives the best fit. For the CZ model, the PERP-0 geometry gives the best fit except for E_{tg} of 900 cal/mol at low temperatures, where the PERP-4 geometry gives the best fit. Similar results were obtained for the 70% 5CB/EBBA

mixture. Based on these plots, we decided to choose the PERP-0 geometry for the CZ model and the PERP-4 geometry for the CI model. Henceforth, whenever we refer to CZ model parameters, it implies the parameters calculated with the CZ model using the PERP-0 geometry. Similarly, any reference to the CI model parameters implies that the parameters are calculated with the CI model using the PERP-4 geometry.

5.4.4 Temperature dependence of Individual Fit model parameters

The temperature dependence of the short-range potential is described by the temperature dependence of the CZ and CI model parameters. We use the parameters k_z and k_s to characterize the magnitude of the short-range potentials. The parameters ξ and ξ' are ratios of model parameters. If all contributions to the potential scale the same way with temperature, these ratios would be independent of temperature. First, we shall analyse the temperature dependence of the model parameters k_z and k_s. Then, we shall examine the temperature dependence of the ratios ξ and ξ'.

k_z and k_s

Our main interest here is to see how the model parameters k_z and k_s depend on factors such as liquid crystal mixture, E_{tg} and temperature. The fitted k_z and k_s values obtained for each experimental temperature and for E_{tg} of 500, 700 and 900 cal/mol are plotted as reduced model parameters, k_i/T, against reduced temperature, $T_r = T/T_{NI}$, in Figure 5.34 - 5.35. We use reduced model parameters because in the calculation of quadrupolar splittings the k_i are always divided by temperature; we use reduced temperature because the liquid crystal mixtures 55% 1132/EBBA and 70% 5CB/EBBA have different T_{NI} values.

As temperature increases towards T_{NI}, the reduced model parameters decrease. The k_z/T values of 55% 1132/EBBA are higher than those of 70% 5CB/EBBA at reduced temperatures less than 0.95, and this is true for all three E_{tg} values. The k_s/T values are

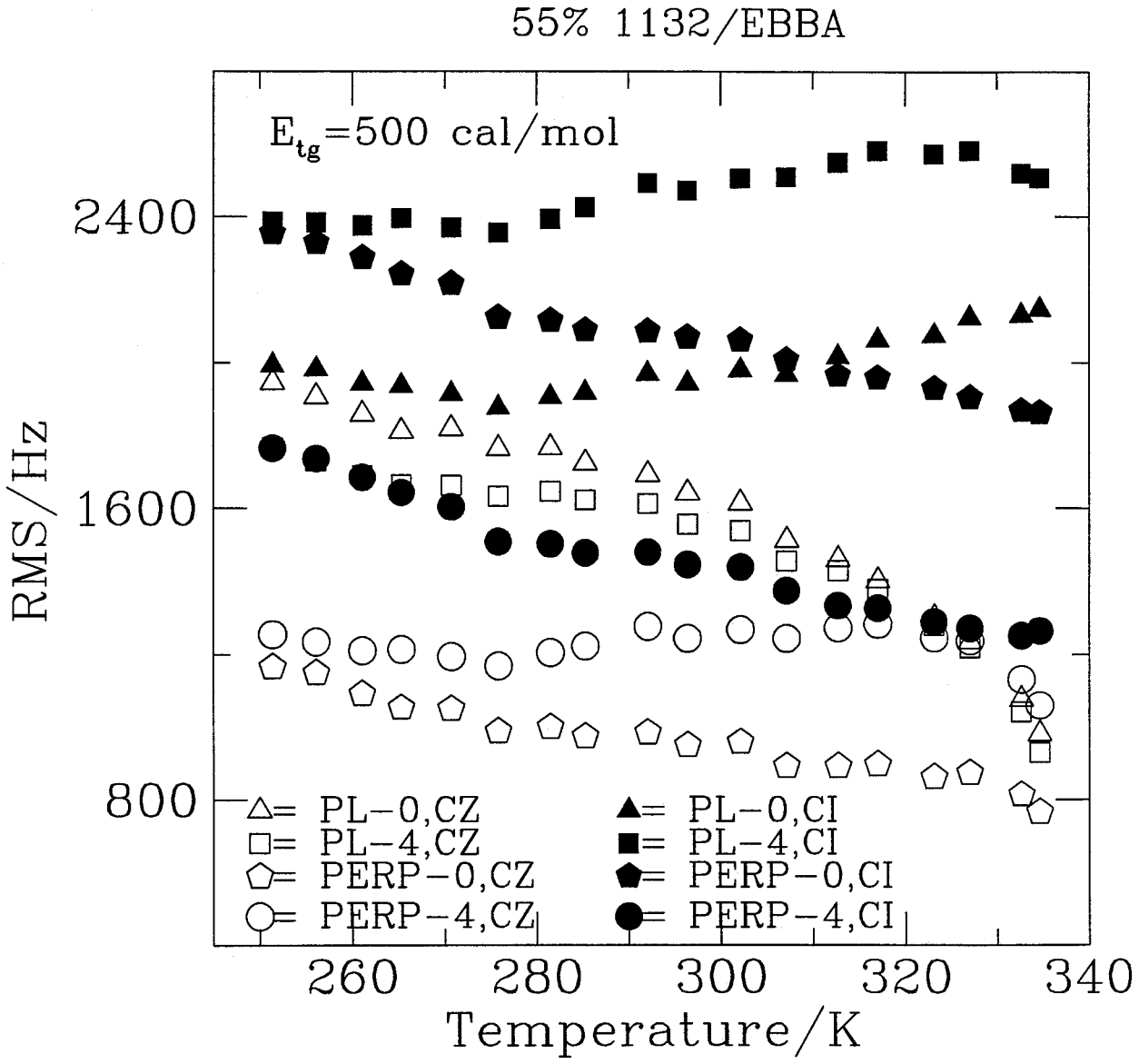

Figure 5.31: RMS (root mean squares deviation) versus temperature of the fits to individual spectra of 5CB in 55% 1132/EBBA for the different geometries PL-0, PL-4, PERP-0 and PERP-4 at E_{tg} equal 500 cal/mol.

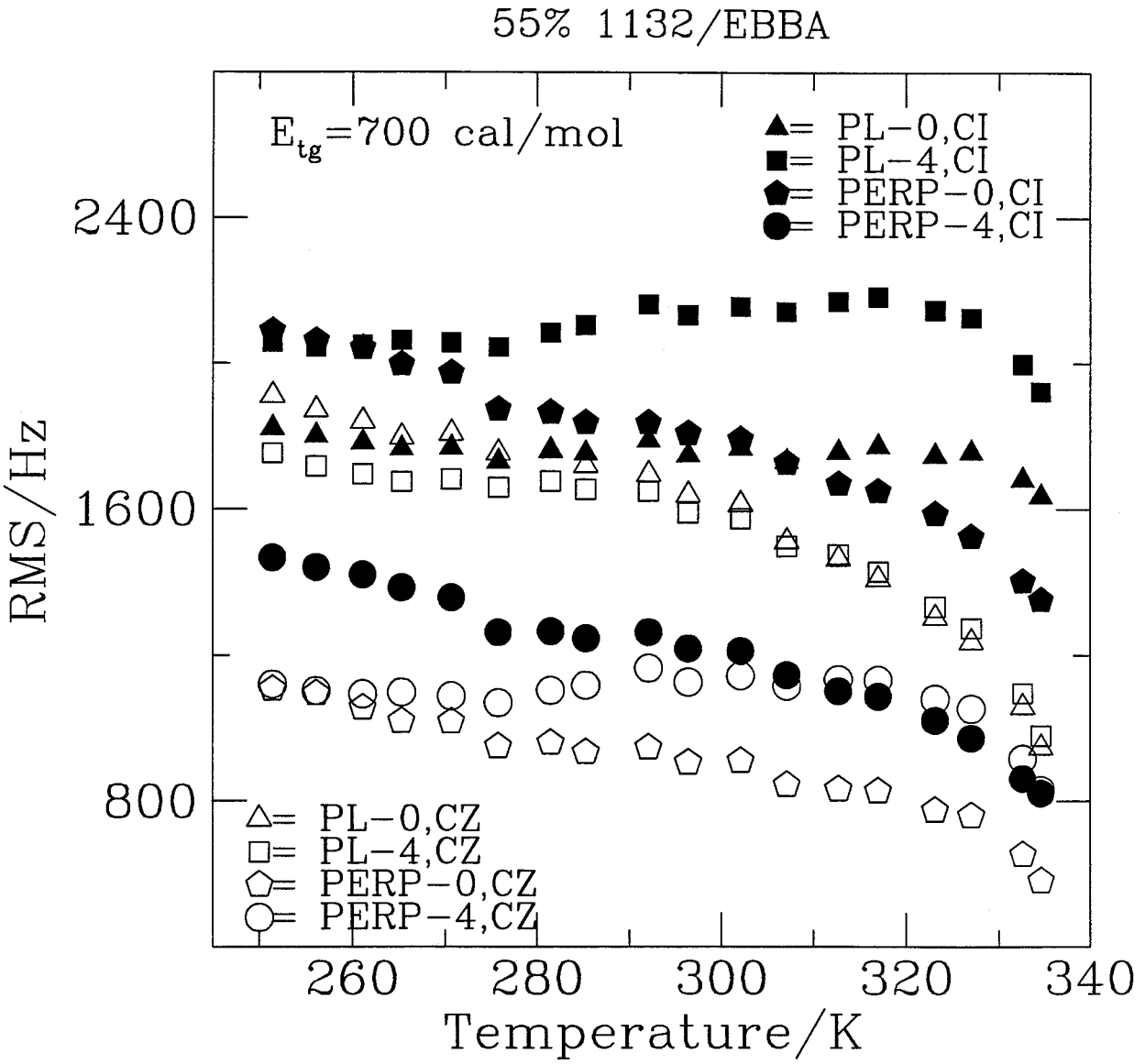

Figure 5.32: RMS (root mean squares deviation) versus temperature for E_{tg} equal 700 cal/mol.

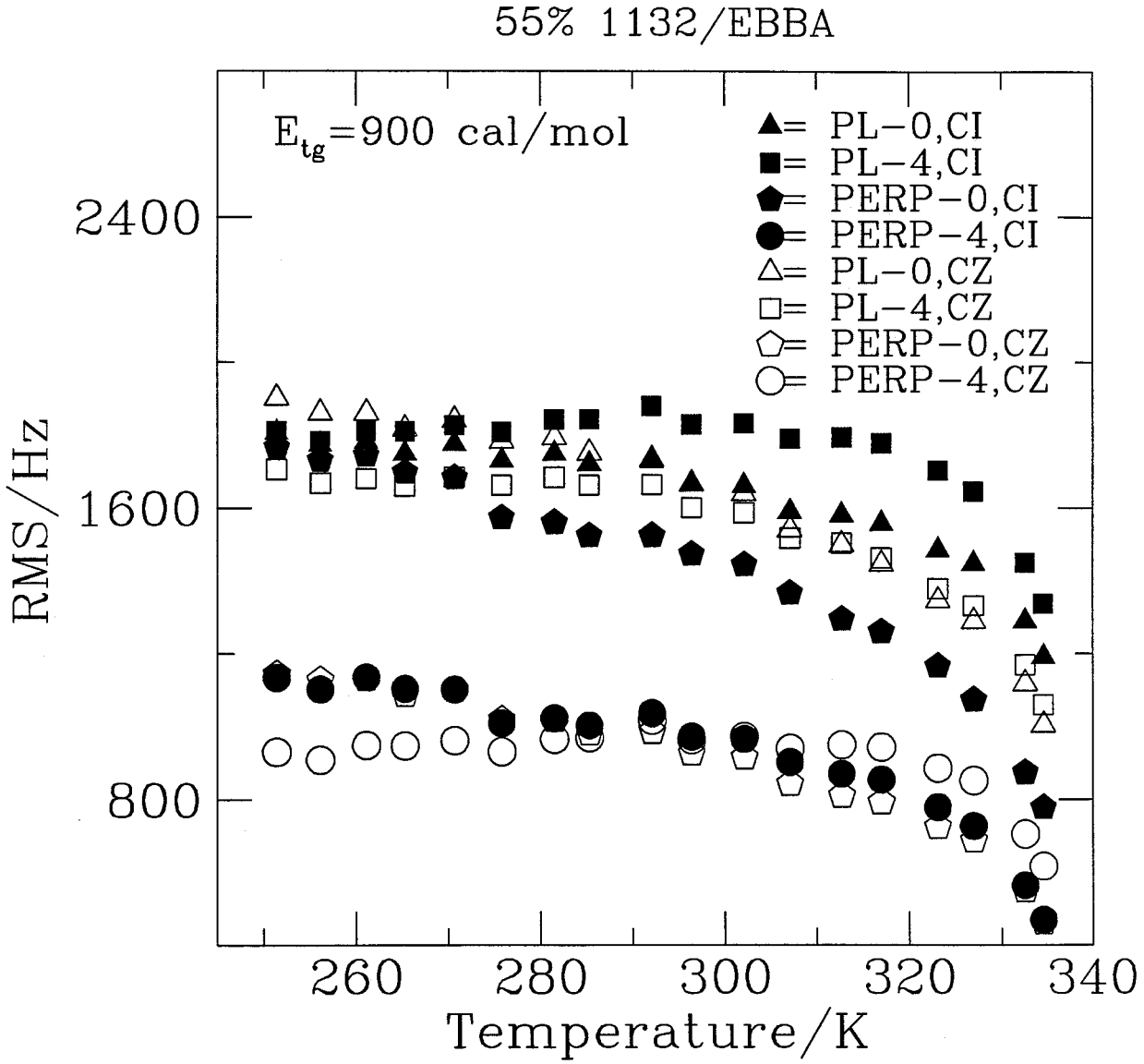

Figure 5.33: RMS (root mean squares deviation) versus temperature for E_{tg} equal 900 cal/mol.

quite similar in both mixtures. However, the break observed in Figure 5.29 for the 70% 5CB/EBBA mixture is also apparent in Figures 5.34 - 5.35.

ξ and ξ'

The ratios ξ and ξ' are plotted against reduced temperature in Figures 5.36 and 5.37. The similar result obtained for both mixtures, independent of model used, is striking. Thus the form of the short-range potential appears to be the same in both mixtures.

The temperature dependence of ξ depends on E_{tg}. The ratio ξ has a large temperature dependence for the E_{tg} value 500 cal/mol, is less dependent on temperature for the E_{tg} value 700 cal/mol, and is almost independent of temperature for the E_{tg} value 900 cal/mol. On the other hand, the ratio ξ' is small and has no significant temperature dependence for all E_{tg} values. Except for the CZ calculations at 500 and 700 cal/mol, these results are consistent with all terms in the potential having the same temperature dependence.

The small value of ξ' suggests that using only the second term of equation 1.28 or 1.29 would provide an excellent fit to the experimental results. It is precisely this term that provides the best one parameter fit to a collection of 46 solutes in the 55% 1132/EBBA mixture [40].

5.4.5 Global Fit

In section 5.4.3, we have seen that the ratio ξ is independent of temperature for E_{tg} values close to 900 cal/mol, and ξ' is independent of temperature for E_{tg} values of 500 to 900 cal/mol. Constant values of ξ and ξ' are consistent with the reasonable guess that all contributions to the short-range anisotropic potential have similar temperature dependence. In such a case, it is possible to calculate the parameters ξ and ξ' in a single least squares fit to all the experimental quadrupolar splittings at all temperatures for a given liquid crystal mixture. In addition, it is possible to determine the E_{tg} value in the

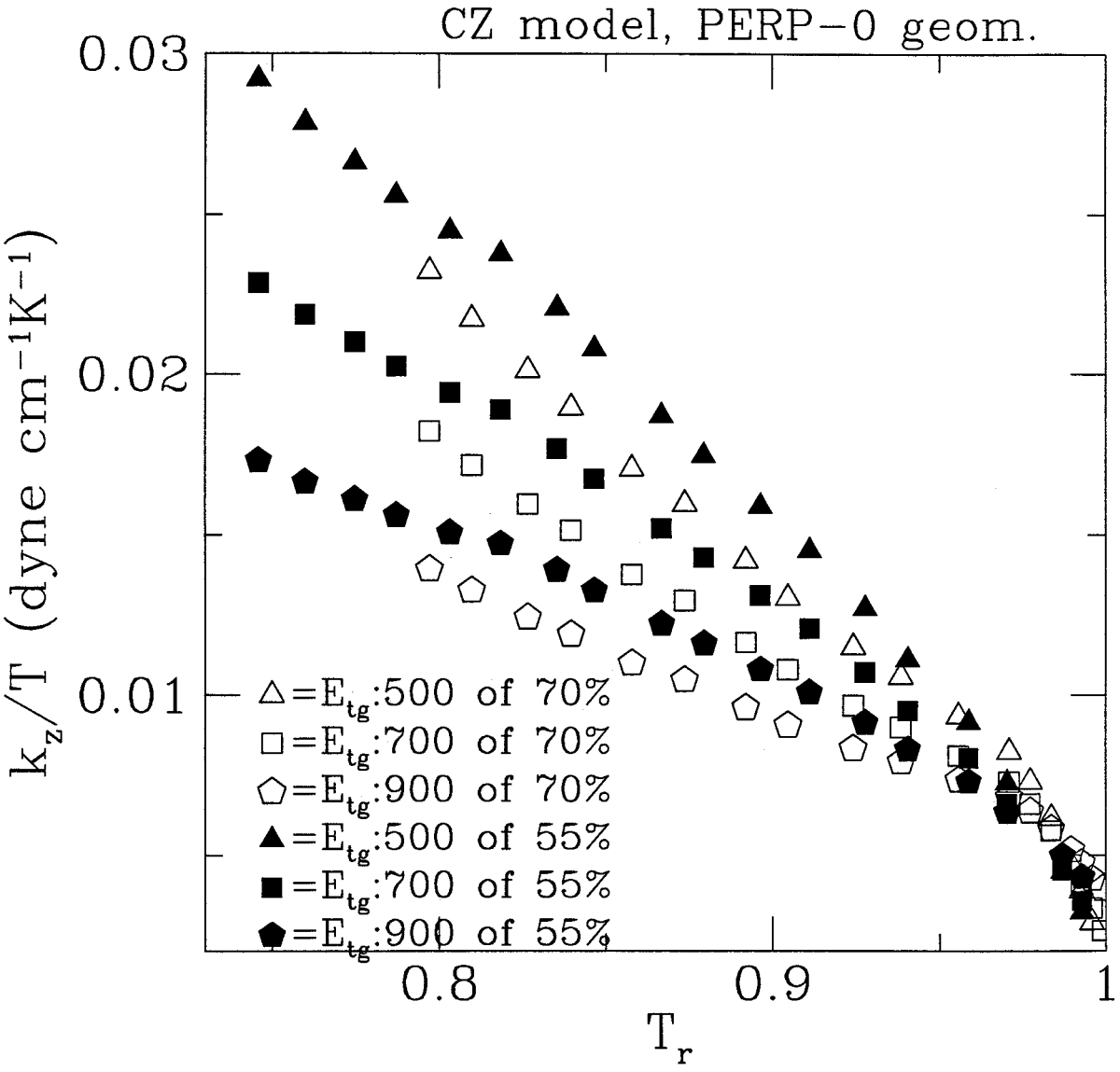

Figure 5.34: The reduced model parameter k_z/T versus reduced temperature.

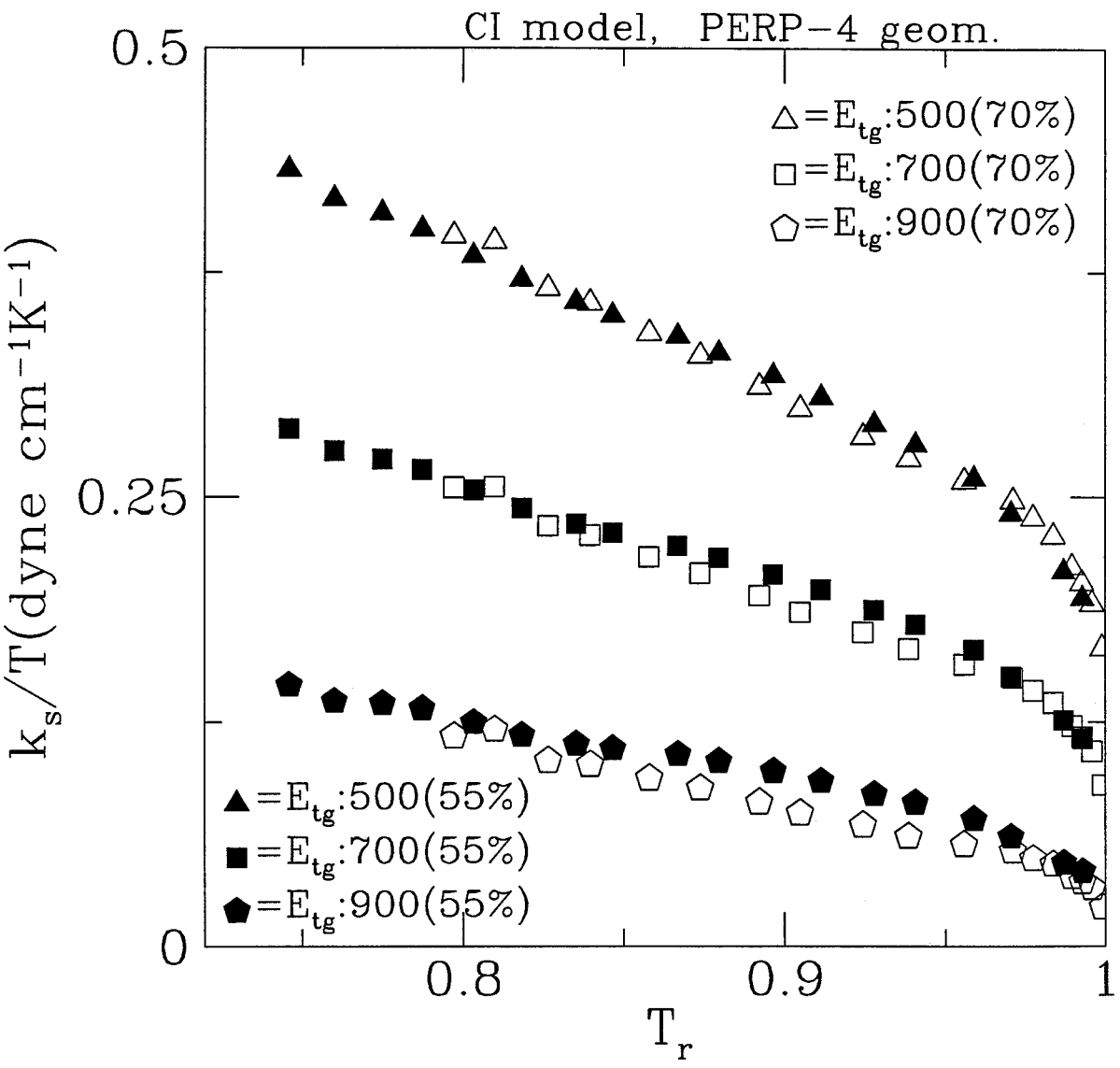

Figure 5.35: The reduced model parameter k_s/T versus reduced temperature.

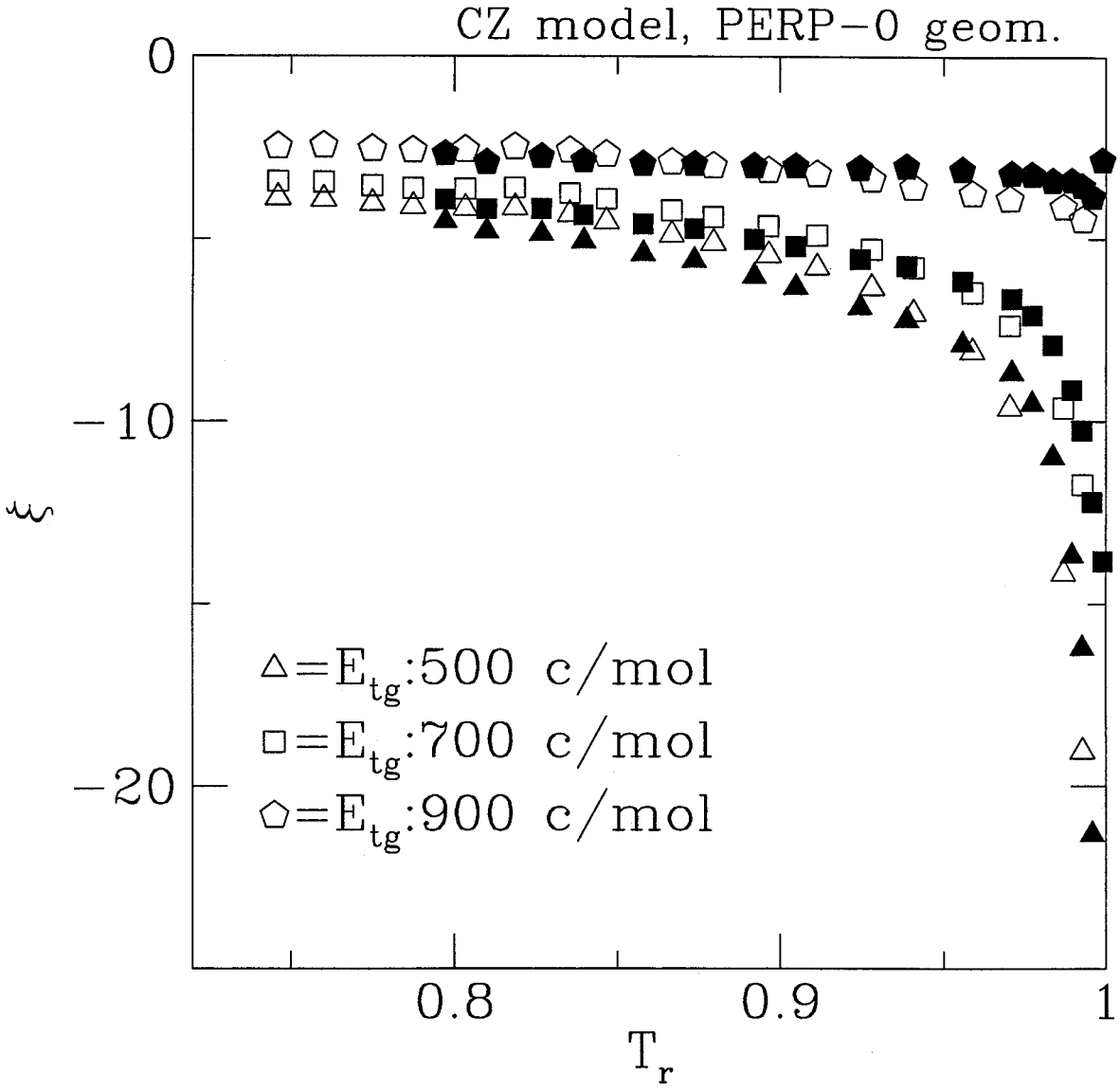

Figure 5.36: The ratio ξ versus reduced temperature .

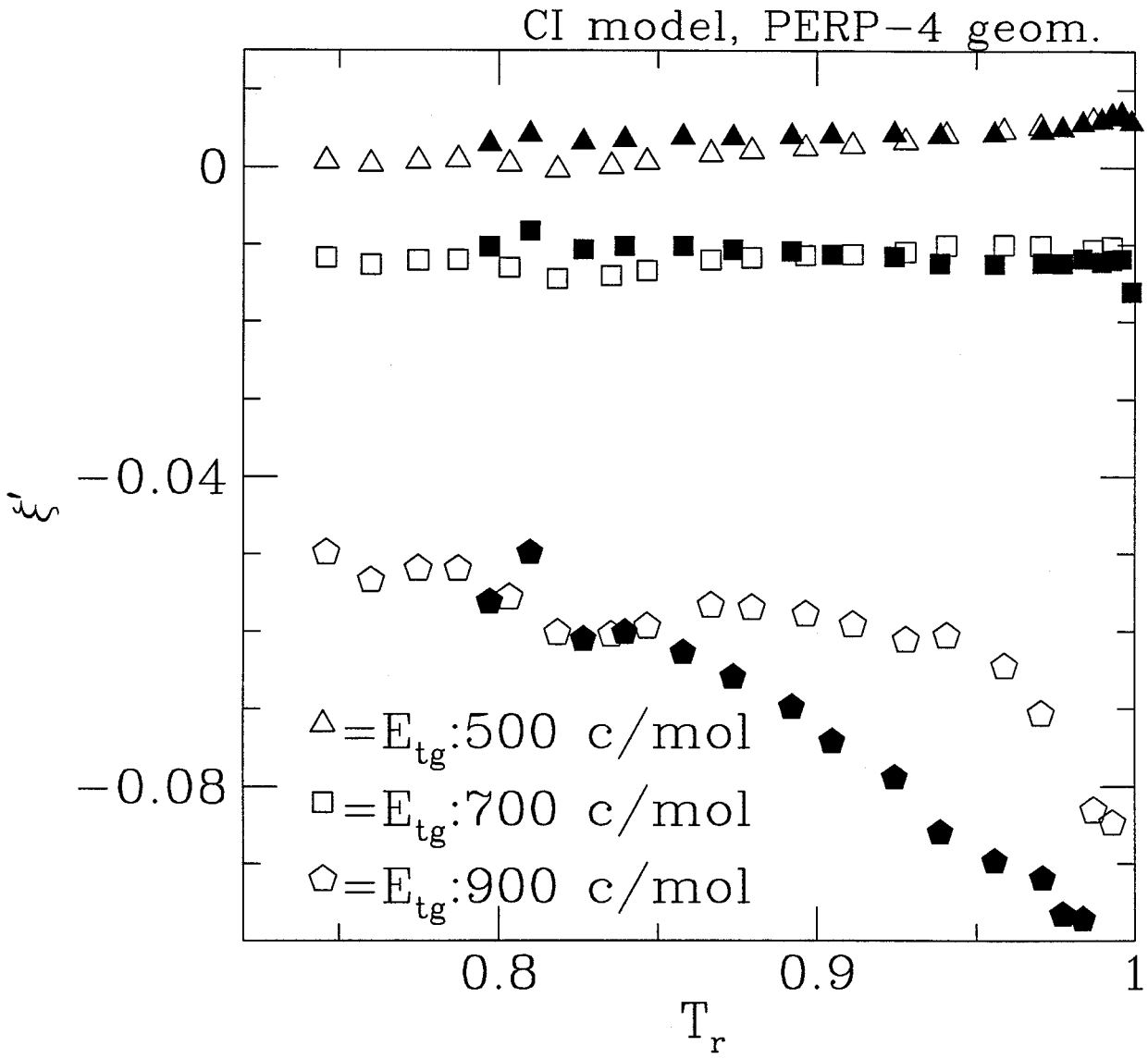

Figure 5.37: The ratio ξ' versus reduced temperature .

Table 5.10: Fitted values of k_0, k_0, k_0, ξ and E_{tg} using the CZ model.

Fitted parameters	55% 1132/EBBA	70% 5CB/EBBA
k_0 /dyne cm^{-1}	0.94 $\pm$0.06	1.11 $\pm$0.03
k_1 /dyne cm^{-1}	-2.28 $\pm$1.04	-1.05 $\pm$1.07
k_2 /dyne cm^{-1}	7.47 $\pm$0.50	5.41 $\pm$0.38
ξ	-2.20 $\pm$0.23	-2.73 $\pm$0.32
E_{tg} /cal mol^{-1}	952 $\pm$19	911 $\pm$21
θ /deg	118.94 $\pm$0.03	118.74 $\pm$0.03
RMS/Hz	1089	968

Fitted parameters of the CZ model using the PERP-0 geometry and varying E_{tg}. For a given liquid crystal mixture, the fit is to all experimental quadrupolar splittings at all temperatures. The k_i describe the temperature dependence of the model parameter k_z according to eq. 5.45.

same fit, since E_{tg} is independent of temperature. To reduce the number of adjustable parameters in such a fit it is useful to choose some functional form for the temperature dependence of k_z and k_s. The variations of k_z and k_s from the individual fits to each temperature above resemble parabolas. To an excellent approximation, these k_z and k_s can be approximated by

$$k_i = k_0 + k_1 * (1 - T_r) + k_2 * (1 - T_r)^{1/2}. \tag{5.45}$$

Using this functional form in a fit to all experiments for a given sample at all temperatures gives the fitted parameters k_0, k_1 and k_2, ξ (or ξ'), E_{tg} and θ in Table 5.10 for the CZ model and in Table 5.11 for the CI model.

Global Fit Model Parameters

It is instructive to compare the fitted parameters k_z (k_s), ξ (ξ') and E_{tg} to those from previous studies. First, we compare the parameters (k_z, ξ) and (k_s, ξ') to the values obtained from a study of 46 solutes in 55% 1132/EBBA at 301K [40]. The k_z value for the 55% 1132/EBBA at 301K in our study is 3.13 dyn/cm, which is close to the value

Table 5.11: Fitted values of k_0, k_0, k_0, ξ and E_{tg} using the CI model.

Fitted parameters	55% 1132/EBBA	70% 5CB/EBBA
k_0 /dyne cm^{-1}	-5.34 ±1.48	-5.57 ±2.00
k_1 /dyne cm^{-1}	30.68 ±8.27	18.63 ±6.73
k_2 /dyne cm^{-1}	-35.13±9.39	-21.84±7.71
ξ'	-0.16±0.05	-0.19±0.08
E_{tg} /cal mol^{-1}	1001±23	972±23
θ /deg	119.68 ±0.05	119.58 ±0.08
RMS/Hz	946	1006

Fitted parameters of the CI model using the PERP-4 geometry and varying E_{tg}. For a given liquid crystal mixture, the fit is to all experimental quadrupolar splittings at all temperatures. The k_i describe the temperature dependence of the model parameter k_s according to eq. 5.45.

3.92 dyn/cm found in the study of 46 solutes in 55% 1132/EBBA at 301K [40]. However, the ratio ξ is -2.20 in our study and -5.01 for the 46 solutes [40]. Although the k_z values in these two studies are close, the ratio ξ in our study is of much smaller magnitude than that for the 46 solutes [40]. Similarly, the fitted k and k_s values are 2.22 and 6.08 in our study compared to 2.04 and 48.4 for the 46 solutes in 55% 1132/EBBA at 301K [41].

Next, we compare the fitted E_{tg} values to those in the literature. The fitted E_{tg} values for 55% 1132/EBBA are 952 and 1001 cal/mol and those for 70% 5CB/EBBA are 911 and 972 cal/mol using the CZ (Tab.5.10) and CI (Tab.5.11) models. These E_{tg} values are high compared to most accepted literature values [64, 74, 75, 76, 77] which are close to 500 cal/mol. However, we note that one study reports the value 966 cal/mol for E_{tg} of gaseous n-butane [73].

Since the fitted E_{tg} values are high compared to commonly accepted literature values (400 − 700 cal/mol), we shall explore the possibility of using a more acceptable value. For this purpose, we consider the RMS plots given in Figures 5.31 - 5.33. For the CI model, the E_{tg} value 700 cal/mol gives acceptable fits, although larger E_{tg} values give better fits. Moreover, ξ' is independent of temperature when E_{tg} takes the value 700

Table 5.12: Fitted values of k_0, k_0, k_0 and ξ for E_{tg} = 700 cal/mol, using the CZ model.

Fitted parameters	55% 1132/EBBA	70% 5CB/EBBA
k_0 /dyne cm^{-1}	0.83 ±0.12	1.08 ±0.05
k_1 /dyne cm^{-1}	1.66 ±1.96	2.29 ±1.30
k_2 /dyne cm^{-1}	9.25 ±1.07	6.39±0.59
ξ	-4.02 ±0.11	-4.79 ±0.14
E_{tg} /cal mol^{-1}	700.00	700.00
θ /deg	119.38 ±0.04	119.27 ±0.04
RMS/Hz	1594	1405

Fitted parameters of the CZ model using the PERP-0 geometry and fixing E_{tg} at 700 cal/mol. For a given liquid crystal mixture, the fit is to all experimental quadrupolar splittings at all temperatures. The k_i describe the temperature dependence of the model parameter k_z according to eq. 5.45.

cal/mol. For the CZ model, the ratio ξ is independent of temperature for high E_{tg} values. However, the E_{tg} value 700 cal/mol gives acceptable fits, and the ratio ξ is less dependent on temperature than for E_{tg} of 500 cal/mol. As a result, we choose the E_{tg} value 700 cal/mol, which is also the upper limit of the acceptable E_{tg} range, and repeat the least squares minimization keeping the E_{tg} value fixed at 700 cal/mol and adjusting the parameters k_0, k_1, k_2, θ, and ξ or ξ'.

The fitted values of k_0, k_1, k_2, θ, and ξ or ξ' are reported in Table 5.12 or Table 5.13 for the E_{tg} value 700 cal/mol. The RMS deviation in these fits is larger than when E_{tg} was varied, but the fits are still quite acceptable. We again compare the fitted values with those from the study of 46 solutes in 55% 1132/EBBA. The k_z and ξ values are 4.03 and -4.02 in our study, whereas these values are 3.92 and -5.01 in the study of 46 solutes [40]. This is excellent agreement. In addition, the fitted k and k_s values in our study are -0.80 and 76.4 compared to 2.04 and 48.0 in ref [41]. However, the k_s value 76.4 dyn/cm is very close to the k_s value 76.7 dyn/cm [41] obtained for the 46 solutes when the short range potential, $U_{sr,i}(\Omega)$, is expressed only in terms of k_s (i.e. k=0). This is consistent

Table 5.13: Fitted values of k_0, k_0, k_0 and ξ for E_{tg} = 700 cal/mol, using the CI model.

Fitted parameters	55% 1132/EBBA	70% 5CB/EBBA
k_0 /dyne cm^{-1}	-25.27 ±1.49	-28.55 ±1.28
k_1 /dyne cm^{-1}	115.05 ±16.67	78.05 ±15.46
k_2 /dyne cm^{-1}	-147.87±10.39	-102.59±8.15
ξ'	-0.013±0.002	-0.013±0.002
E_{tg} /cal mol^{-1}	700.00	700.00
θ /deg	120.50 ±0.04	120.74±0.06
RMS/Hz	1390	1464

Fitted parameters of the CI model using the PERP-4 geometry and fixing E_{tg} at 700 cal/mol. For a given liquid crystal mixture, the fit is to all experimental quadrupolar splittings at all temperatures. The k_i describe the temperature dependence of the model parameter k_s according to eq. 5.45.

with the separate fits at each temperature of k and k_s, section 5.4.3, where it was found that the k_s term dominates the potential.

5.5 Summary

The quadrupolar splittings of 5CB – d_{19} in the zero efg mixtures 55% 1132/EBBA and 56.5% 1132/EBBA are almost equal at any given temperature. Therefore, the short-range potentials in these two mixtures are the same. However, the quadrupolar splittings of 5CB – d_{19} in the zero efg mixture 70% 5CB/EBBA are different from those of 55 % 1132/EBBA at any given temperature. These differences at a given temperature are due to the different magnitudes of the short-range potentials in these mixtures. The CZ and CI models describing the short-range potentials are both successful in calculating the quadrupolar splittings of 5CB – d_{19} in the mixtures 55 % 1132/EBBA and 70% 5CB/EBBA. In both cases the trans-gauche energy difference is consistent with the upper range of acceptable values, 700 kcal/mol. The model parameters k_z and k_{xy} of the CZ model and k and k_s of the CI model are useful in comparing the short-range potentials

between these two mixtures. The values obtained agree quite well with those obtained from a study of 46 solutes in a zero efg nematic solvent.

Chapter 6

Comparison of short-range interactions using 5CB – d_{19} as a solute

6.1 Introduction

In the preceding chapter the perdeuteriated molecule 4-n-pentyl-4'-cyanobiphenyl, 5-CB, was studied as solute in three zero efg mixtures. The spectra at a given temperature, however, were not the same in the different mixtures. Do the differences imply that the nature of the short-range potential is liquid crystal dependent? In this chapter we shall demonstrate that the short-range potential is the same in all three mixtures — the spectral differences arise from the differing effects of temperature on the different parts of the potential.

A convenient way to understand the spectral differences is to calculate the NMR spectrum using a potential and to analyse the differences in terms of the potential. The quadrupolar splittings observed in the NMR spectrum are calculated using the equations (5.40), (5.41) and (5.42). The probablity, p_i, of each conformer i is rewritten as

$$p_i = \frac{\exp(\frac{-U_{int,i}}{kT}) \int \exp(\frac{-U_{sr,i}(\Omega)}{kT}) d\Omega}{\sum_i \exp(\frac{-U_{int,i}}{kT}) \int \exp(\frac{-U_{sr,i}(\Omega)}{kT}) d\Omega} \tag{6.46}$$

In equation (6.46) we note that all potential terms are divided by T. A simple Maier Saupe mean field theory of nematics [79] would predict a unique value for $U_{sr,i}(\Omega)/T$ at the nematic-isotropic phase transition temperature, T_{NI}. As T_{NI} varies for different liquid crystals, and as $U_{int,i}$ is a constant for a given conformer, the $U_{int,i}/T_{NI}$ part of the potential for the solute 5CB at the nematic-isotropic transition will vary inversely with T_{NI}. The simple Maier Saupe potential predicts the same reduced temperature,

$T_r = T/T_{NI}$, dependence of the order parameter. Thus differences at T_{NI} are expected to propagate throughout the nematic temperature range. Could this variation with T_{NI} of the $U_{int,i}/T$ part of the potential account for the observed spectral differences? To examine this possibility in terms of the intra- and inter-molecular potentials acting on 5CB as solute in the nematic mixtures that we are investigating here, we need to analyze the results in terms of the parameters on which these potentials, and thus the quadrupolar splittings, depend.

6.2 Analysis

In section 5.4.3 of the preceding chapter we saw that fits to the spectrum obtained at each individual temperature using the E_{tg} value 700 cal/mol give very good agreement between the experimental and calculated quadrupolar splittings. In section 5.4.5 we found that the global fit calculation using the E_{tg} value 700 cal/mol gives very good agreement between the fitted model parameters in our study and the parameters found in a study of 46 solutes in the 55% 1132/EBBA zero electric field gradient nematic mixture [40, 41]. Therefore, an appropriate choice of E_{tg} for comparison of the short-range potentials in the zero electric field gradient mixtures is 700 cal/mol. The model parameters k_i are k_z and k_{xy} for the CZ model, and k and k_s for the CI model. Therefore, the quadrupolar splitting of deuteron j, $\Delta\nu_j$, can be written

$$\Delta\nu_j = f(j, \frac{k_z}{T}, \frac{k_{xy}}{T}, \frac{E_{tg}}{T}) \tag{6.47}$$

for the CZ model with a similar equation for the CI model.

To compare the potentials in the various liquid crystals, it is instructive to plot the calculated k_i/T values versus $\Delta\nu_1$. The choice of $\Delta\nu_1$ as a plotting parameter requires some explanation. In the quadrupolar splitting *vs.* temperature plot in Figure 5.29 and the k_i/T *vs.* reduced temperature plots in Figures 5.34 - 5.35 an unusual temperature

dependence was observed for the 70% 5CB/EBBA mixture. Therefore we wish to choose a quantity, other than reduced temperature, for comparison. The first quantity that comes to mind is the order parameter for the sample. However, this quantity is difficult to define, especially for the liquid crystal mixtures used in this work. In addition, a Maier Saupe mean field theory for binary mixtures of axially symmetric nematic liquid crystals gives the anisotropic part of the mean-field intermolecular potential for particle i as [80, 81, 82]

$$U_i(\Omega) = [\rho_i U_{ii} S_i + \rho_j U_{ij} S_j] P_2(\cos\Omega) \tag{6.48}$$

where ρ_i is the number density of component i, U_{ij} is the anisotropic interaction strength between components i and j, and S_i is the order parameter of component i. Note that it is easy to extend equation (6.48) to multicomponent mixtures by adding a U_{ij} term for each component. This potential predicts in general different values for the order parameters of components i and j. In addition the value of $U_i(\Omega)/T$ for a given liquid crystal i will not necessarily be the same at a given reduced temperature in different mixtures; this could explain some of the difference between mixtures observed in Figures 5.34 - 5.35. As we wish to compare the intermolecular potential acting on our solute 5CB in the different liquid crystal mixtures, it would make sense to choose for comparison situations where the order parameter of the solute is the same. In terms of equation (6.48) for an axially symmetric nematic, this would require that $U_i(\Omega)/T$ be the same in both mixtures. In the real case, 5CB is not axially symmetric, and exists in many conformations. Thus the test for similar potentials would be that the various contributions to the potential, i.e. the two terms in equations (1.26) and (1.29) or the terms in equation (6.48), divided by temperature, give equal contributions to the total potential. Fortunately the lack of symmetry in 5CB allows us to fit our spectral results to potentials with more than one parameter: the comparison between mixtures then involves comparison of these

parameters.

As an aside, equation (6.48) has also been used to describe mixtures of a nematic liquid crystal with a solute that does not itself exhibit a liquid crystalline phase [83]. Thus, for all solutes i to experience the same anisotropic potential in different liquid crystal mixtures, in terms of equation (6.48) it is required that $U_{ik} = c_{kj} \times U_{ij}$ with c_{kj} a constant depending only on liquid crystal components j and k, but being independent of solute i. Note that the requirement for a zero field gradient mixture is that for all solutes the anisotropic components of the field gradient cancel when terms for all component liquid crystals are added.

Because of the lack of symmetry and intramolecular motions in 5CB, the choice of its order parameter for comparison purposes presents a problem. A more convenient choice would be the quadrupolar splittings $\Delta\nu_j$ of $5CB - d_{19}$ which are related to this order parameter. But which splitting is the best to use? Note that we are interested in separating the temperature effects of the $U_{int,i}$ and $U_{sr,i}(\Omega)$. In a calculation of the quadrupolar splittings of $5CB - d_{19}$ at two different temperatures having the same k_i/T values, we found that $\Delta\nu_1$ is the least dependent of the quadrupolar splittings on the E_{tg}/T term. Thus it is appropriate to use $\Delta\nu_1$ for comparing the liquid crystal mixtures.

To examine the liquid crystal mixture dependence of the k_i parameters, we plot k_z/T, k_{xy}/T, k_s/T and k/T *vs.*$\Delta\nu_1$ in Figures 6.38 to 6.41. The k_i values in these plots are those that were obtained in the preceding chapter from a separate least squares fitting for each spectrum at each different temperature. The plots in these figures show that for a given $\Delta\nu_1$ the k_i/T values of 55% 1132/EBBA are in excellent agreement with those of 70% 5CB/EBBA. Based on this agreement, we can write for a given $\Delta\nu_1$:

$$(k_i/T)_{55} = (k_i/T)_{70} \tag{6.49}$$

where k_i/T can be k_z/T, k_{xy}/T, k_s/T or k/T. The subscripts 55 and 70 stand for the

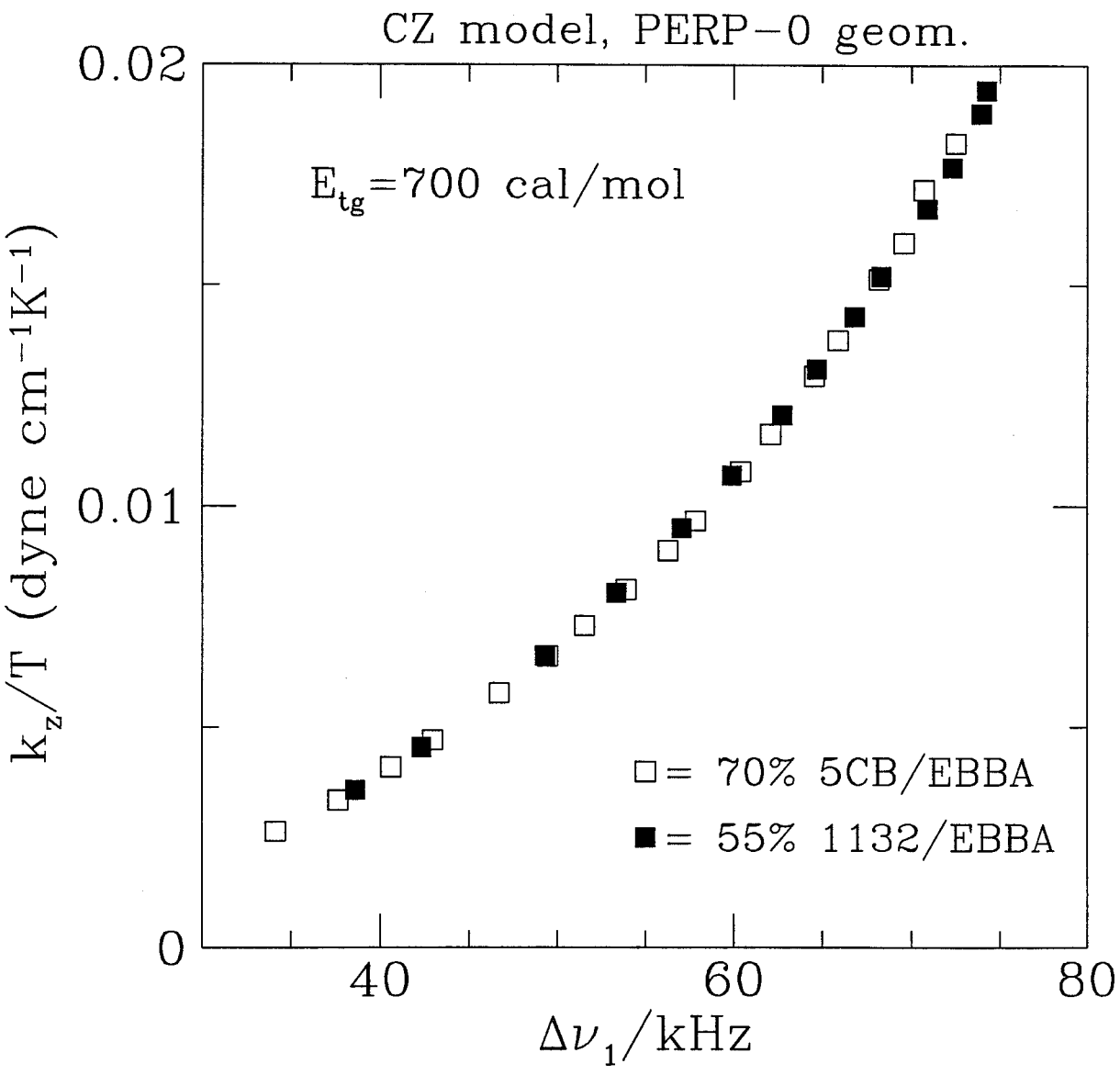

Figure 6.38: Reduced model parameter, k_z/T, against $\Delta\nu_1$ for the E_{tg} = 700 cal/mol.

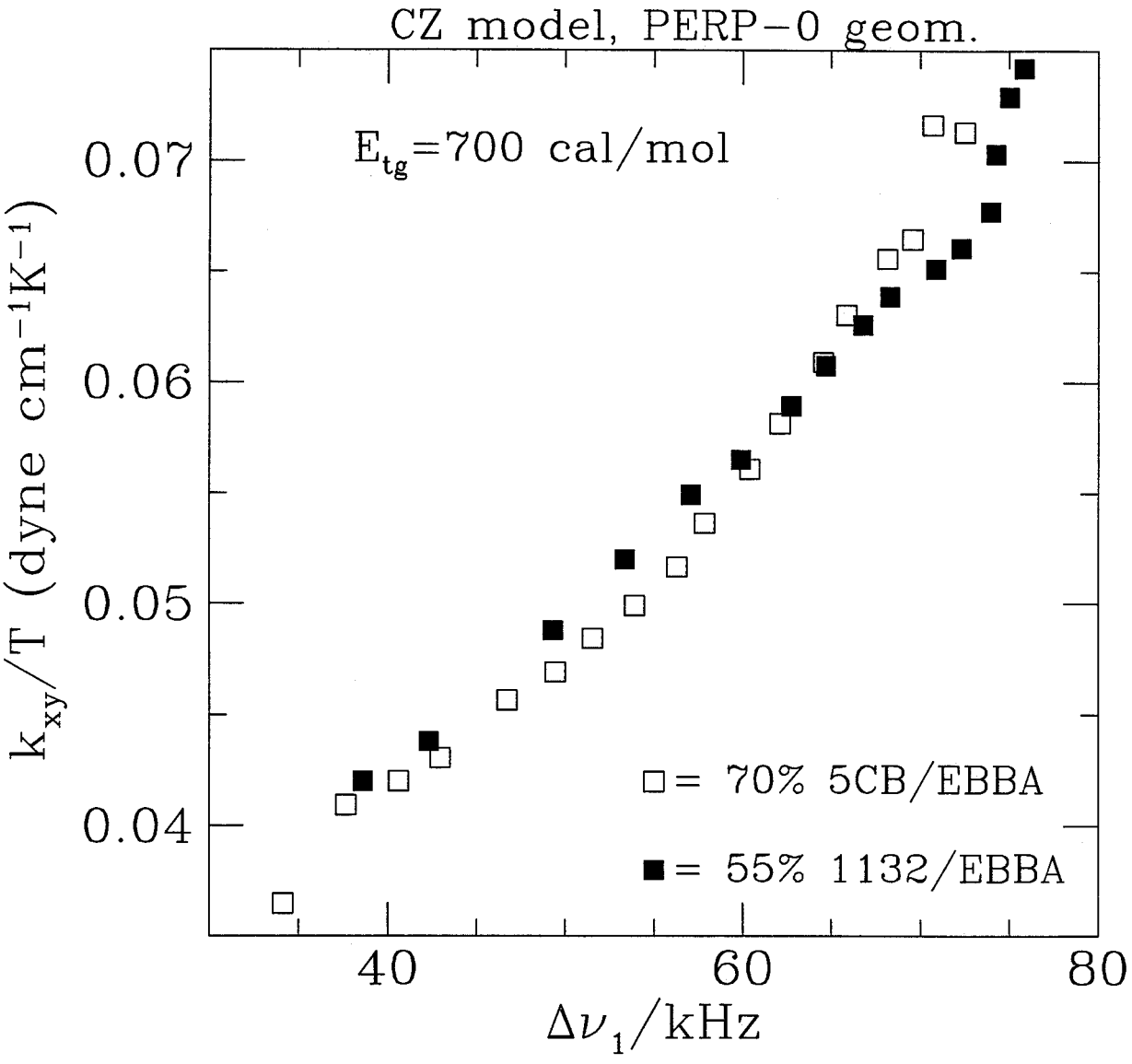

Figure 6.39: Reduced model parameter, k_{xy}/T, against $\Delta\nu_1$ for the E_{tg} = 700 cal/mol.

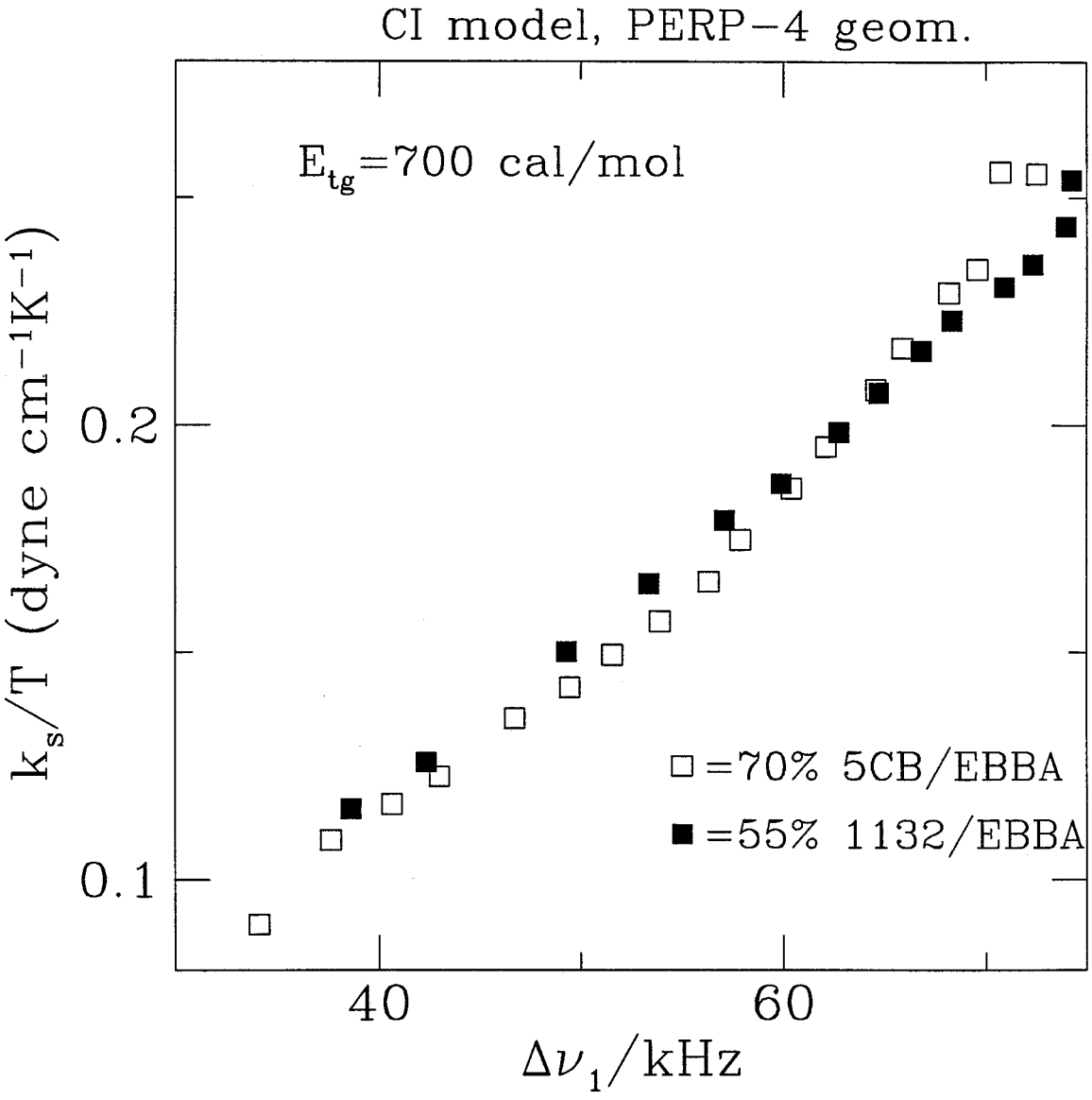

Figure 6.40: Reduced model parameter, k_s/T, against $\Delta\nu_1$ for the E_{tg} = 700 cal/mol.

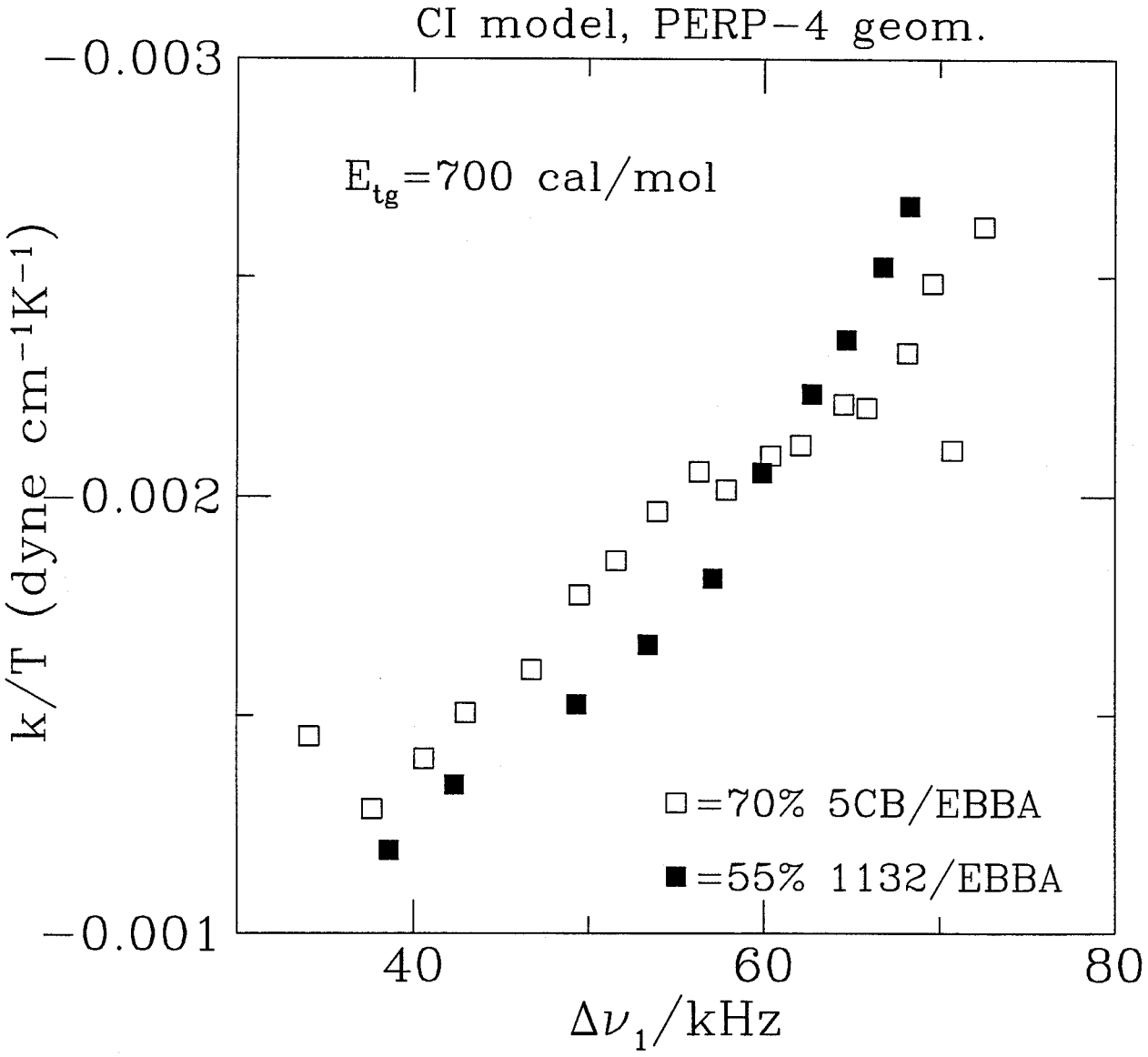

Figure 6.41: Reduced model parameter, k/T, against $\Delta\nu_1$ for the E_{tg} = 700 cal/mol.

liquid crystal mixtures 55% 1132/EBBA and 70% 5CB/EBBA. This demonstrates that the choice of $\Delta\nu_1$ (as a parameter proportional to the 5CB order parameter) for comparison purposes was a good one. Because the two parameters describing the potential scale in the same way, Figures 6.38 to 6.41 demonstrate that the anisotropic short-range potentials in 55% 1132/EBBA and 70% 5CB/EBBA are the same. Substituting eq. (6.49) into eq. (1.26) and eq. (1.29), we obtain for a given $\Delta\nu_1$

$$(U_{sr}/T)_{55} = (U_{sr}/T)_{70}. \tag{6.50}$$

Thus, for a given $\Delta\nu_1$, the experimental results of the preceding chapter are described by the same reduced short-range potentials and reduced model parameters for both zero electric field gradient mixtures. This conclusion is independent of the model chosen for analysis. Note that by a reduced quantity we mean the actual quantity divided by temperature.

As the purpose of this chapter is to examine several zero electric field gradient mixtures and to investigate to what extent the description of the anisotropic short-range potential is similar in the various mixtures, it is worthwhile analyzing equations (6.49) and (6.50) further. As pointed out in the preceding chapter, one way of emphasizing small differences among zero electric field gradient mixtures is to plot ratios of the quadrupolar splittings, such as $\Delta\nu_5/\Delta\nu_1$, against $\Delta\nu_1$. In Figure 5.30 we chose the ratio $\Delta\nu_5/\Delta\nu_1$ for comparison because the quadrupolar splittings at the 5 position are more difficult to fit than the quadrupolar splittings at other positions of the chain. This is because the methyl deuterons are sensitive to all internal chain motions. However, qualitatively similar results are obtained for other chain positions.

6.2.1 Individual Fit Parameters

In Figs 6.42 and 6.43 we compare experimental ratios from Fig. 5.30 (filled symbols) with those recalculated from the best-fit parameters obtained from separate fits to each experimental spectrum in section 5.4.3 of the preceding chapter(dotted symbols). Fig 6.42 presents results for the CZ model, and Fig 6.43 for the CI model. Although there is a deviation between the calculated and experimental quadrupolar splitting ratios, the general experimental trends are observed with both models. More important, the differences between the liquid crystal mixtures are well predicted. The deviation between experiment and theory is mainly due to the inadequacy of the models.

We now turn to the question "If the intermolecular potential is the same, why do the quadrupolar splitting ratios $\Delta\nu_5/\Delta\nu_1$ differ with liquid crystal solvent in the ratio plots of Figures 6.42 and 6.43?" Equation. (6.47) tells us that there is another parameter, E_{tg}/T, on which the quadrupolar splitting $\Delta\nu_j$ depends. The value of E_{tg} is constant, and is set to 700 cal/mol throughout this chapter. However, the temperature at which a given $\Delta\nu_1$ is observed in the 55% 1132/EBBA mixture, T_{55}, is different from that in the 70% 5CB/EBBA mixture, T_{70}. As a result, the E_{tg}/T term is different for the two mixtures. Therefore, the differences in quadrupolar splitting ratios $\Delta\nu_5/\Delta\nu_1$ must be due to the different temperatures (T_{55} and T_{70}) associated with the different liquid crystal mixtures 55% 1132/EBBA and 70% 5CB/EBBA.

Of course the above analysis is based on independent fits of spectra in the different mixtures. Perhaps a better demonstration that the spectral differences are due to the temperature dependence of the conformational averaging would be to predict the spectrum of one mixture from the k_i parameters of the other mixture. We shall call the quadrupolar splittings of these predicted spectra "scaled quadrupolar splittings".

In this study, we shall start from the reduced model parameters of 70% 5CB/EBBA

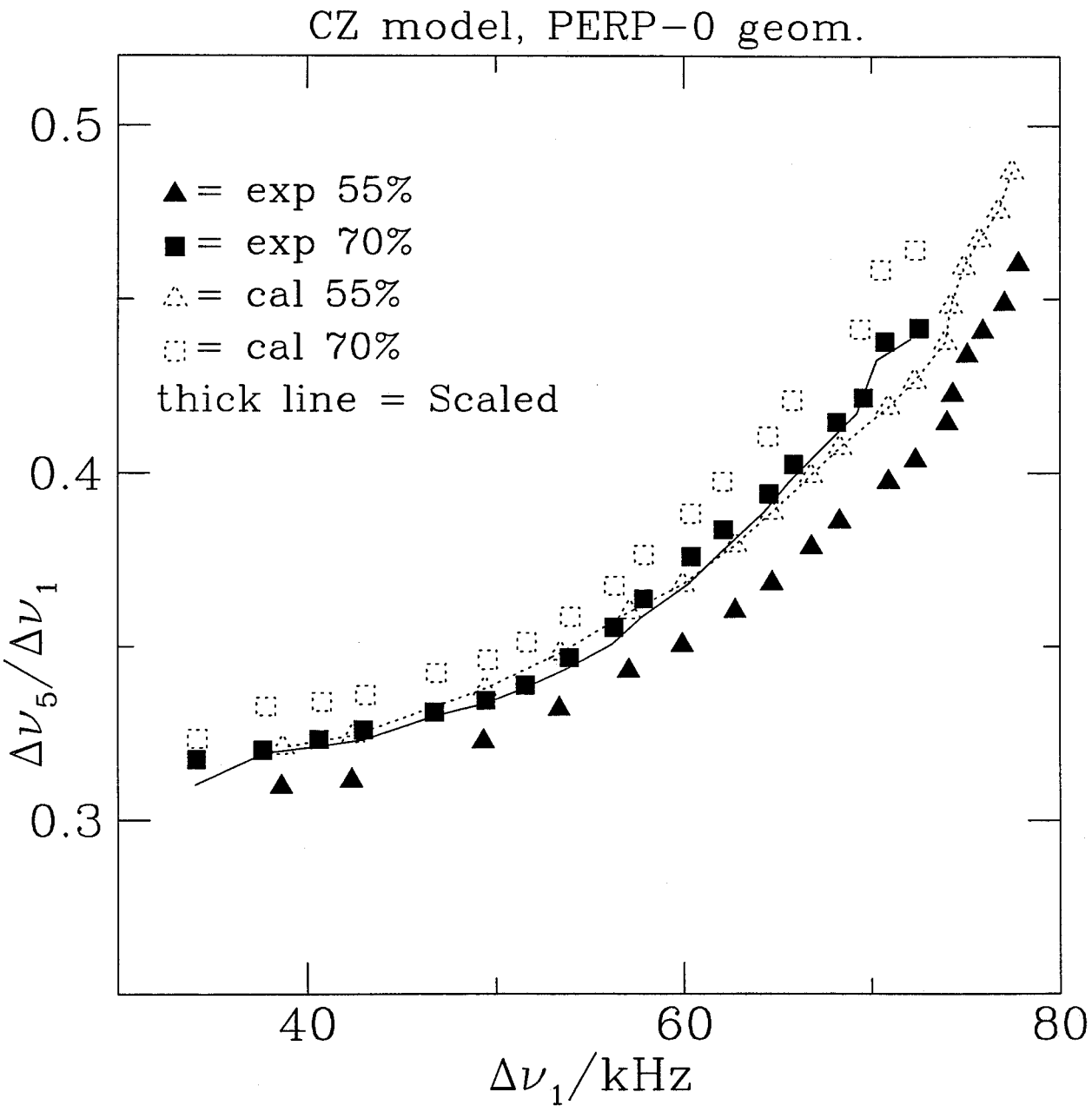

Figure 6.42: Quadrupolar splitting ratios $\Delta\nu_5/\Delta\nu_1$ versus $\Delta\nu_1$ using Individual fit CZ model parameters.

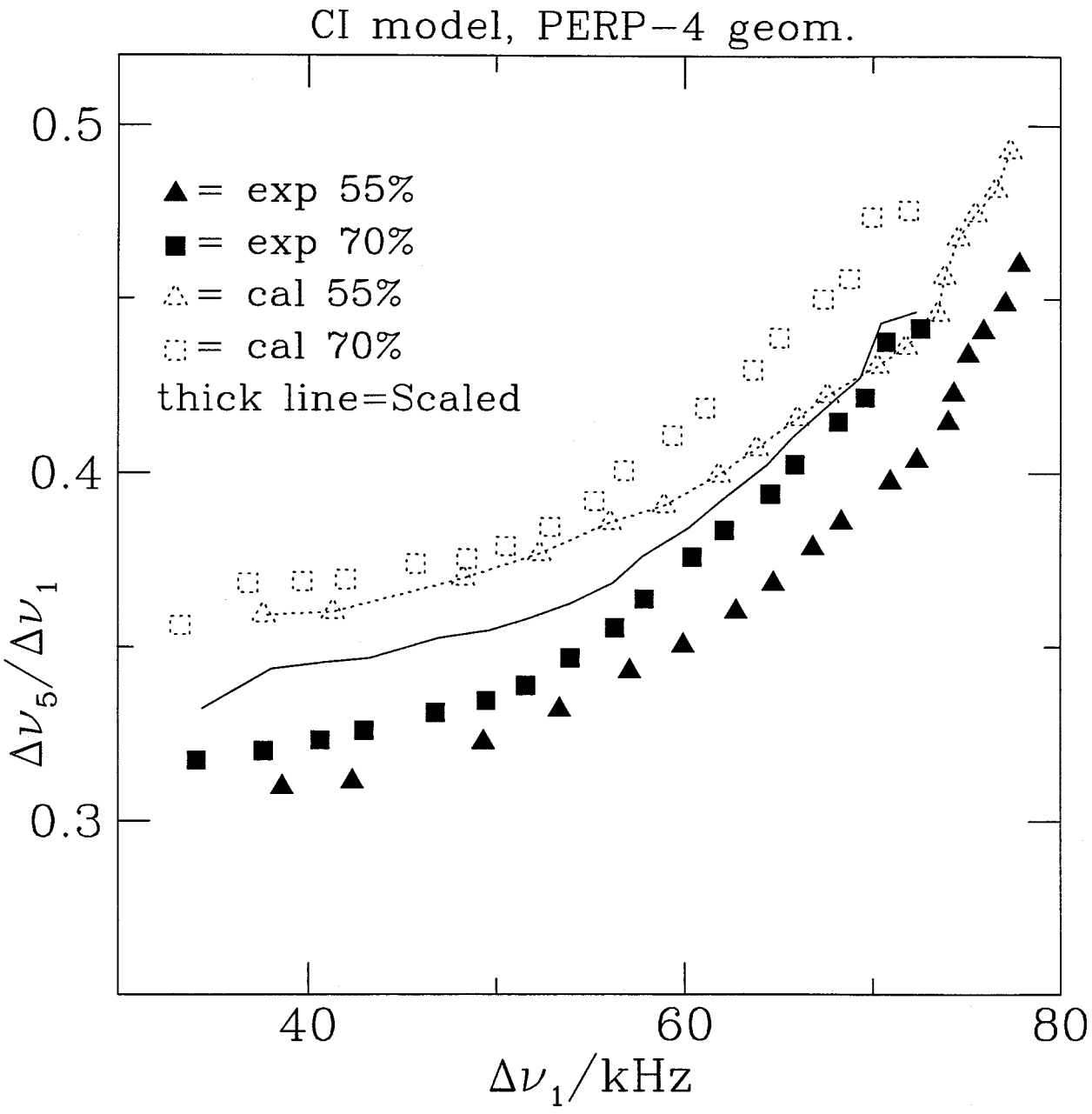

Figure 6.43: Quadrupolar splitting ratios $\Delta\nu_5/\Delta\nu_1$ versus $\Delta\nu_1$ using Individual fit CI model parameters.

and shall predict the quadrupolar splittings of the 55% 1132/EBBA mixture. In order to predict the quadrupolar splittings in 55% 1132/EBBA, it is necessary to use the appropriate temperatures in the E_{tg}/T term; the temperature in the E_{tg}/T term has to be scaled by a factor T_{55}/T_{70}. In order to simplify the notation, we define this factor T_{55}/T_{70} as the Temperature Scaling Factor (TSF). The TSF values are calculated from the results of the preceding chapter for a given $\Delta\nu_1$ and tabulated with the corresponding temperatures of the 70% 5CB/EBBA mixture in Table 6.14. For each entry in Table 6.14, the reduced short-range potentials $U_{sr,i}(\Omega)/T$ along with $U_{int,i}/(T_{70} \times \text{TSF})$ are used to calculate the "scaled quadrupolar splittings". If we are correct that the spectral differences arise from the temperature effect on the conformational averaging, these scaled splittings should equal the recalculated splittings of 5CB – d_{19} in the 55% 1132/EBBA mixture. To demonstrate that this is indeed the case, we plot "scaled" along with experimental and recalculated quadrupolar splitting ratios $\Delta\nu_5/\Delta\nu_1$ in Figures 6.42 (CZ model) and 6.43 (CI model). The agreement between the "scaled" (thick lines, predicted from the results of the 70% 5CB/EBBA experiments) and recalculated (dotted lines, fits to the 55% 1132/EBBA experiments themselves) quadrupolar splitting ratios is excellent for the CZ model. This agreement confirms that the differences in the quadrupolar splitting ratios $\Delta\nu_5/\Delta\nu_1$ come from the different temperatures T_{55} and T_{70} of 55% 1132/EBBA and 70% 5CB/EBBA for a given $\Delta\nu_1$. For a given value of $U_{sr,i}(\Omega)/T$, the different temperatures affect the quadrupolar splittings via the effect of the different $U_{int,i}/T$ on the conformational averaging.

In section 5.4.5 of the preceding chapter the results were analysed by fitting all spectra at all temperatures in a given liquid crystal solvent to a set of global parameters. In these fits the ratio between the k_i values, ξ or ξ', were kept constant for a given solvent. Above we have seen that, for a given experimental $\Delta\nu_1$, the reduced model parameters are transferable from one zero electric field gradient mixture to another and the reduced

Table 6.14: Temperature scaling factors

T_{70}/K of 70% 5CB/EBBA	TSF
251.9	1.114
255.9	1.117
261.2	1.107
265.3	1.108
271.1	1.106
276.1	1.097
281.9	1.094
285.9	1.092
292.1	1.082
296.6	1.077
302.0	1.069
306.8	1.061
308.8	1.058
310.8	1.058
312.7	1.062
313.7	1.061
314.7	1.065
315.7	1.065
$TSF_{average}$	1.083

Temperature scaling factors, TSF (see text).

short-range potentials of the two zero electric field gradient mixtures are equal. The global fit parameters can be tested in a similar analysis.

6.2.2 Global Fit Parameters

First, we shall examine the fitted parameters in Tables 5.12 and 5.13 of the preceding chapter corresponding to E_{tg} of 700 cal/mol. Based on eq. 6.49, we intuitively expect that the ratios $\xi = k_{xy}/k_z$ or $\xi' = k/k_s$ should be the same in all zero electric field gradient mixtures. The ξ values are -4.02 and -4.79 and the ξ' values are -.013 and -.013 for the liquid crystal mixtures 55% 1132/EBBA and 70% 5CB/EBBA. The ξ and ξ' values of these two liquid crystal mixtures are in excellent agreement. Thus, the ratios ξ and ξ'

are transferable from one zero electric field gradient mixture to another.

As was the situation above, a most useful comparison is to check the transferability of reduced model parameters by calculating the "scaled quadrupolar splittings". We start with the reduced model parameters k_0/T_{70}, k_1/T_{70} and k_2/T_{70} of 70% 5CB/EBBA. Then we use $T = T_{70} \times \mathrm{TSF}_{\mathrm{average}}$ (see Table 6.14) in the calculation of U_{int}/T to calculate the "scaled quadrupolar splittings".

The "scaled", experimental and recalculated quadrupolar splitting ratios $\Delta\nu_5/\Delta\nu_1$ are plotted against $\Delta\nu_1$ in Figs 6.44 (CZ model) and 6.45 (CI model). The agreement between the "scaled" (solid line, predicted from the results of the 70% 5CB/EBBA experiments) and recalculated (dotted line, fits to the 55% 1132/EBBA experiments themselves) quadrupolar splitting ratios is excellent for the CI model. In addition, the fits are in reasonable agreement with the experimental results, and the general features of the experimental quadrupolar splittings are predicted. In this case a temperature independent ξ' seems the correct choice. For the CZ model, however, the fits are not as good. This is because the ξ parameter was kept constant with temperature. In the preceding chapter it was shown for this model with $E_{tg} \leq 700$ cal/mol that the best results are obtained with a temperature dependent ξ. This is evident from the deviation between the experimental and recalculated quadrupolar splitting ratios in Fig. 6.44. The "scaled quadrupolar splitting" ratios agree well with the recalculated quadrupolar splitting ratios at high temperatures. However, the deviation is large for low temperatures. This deviation is partly due to the fact that the TSF ratios, T_{55}/T_{70}, at low temperatures are very different from the $\mathrm{TSF}_{\mathrm{average}}$ (1.083), whereas these ratios are very close to the $\mathrm{TSF}_{\mathrm{average}}$ at high temperatures.

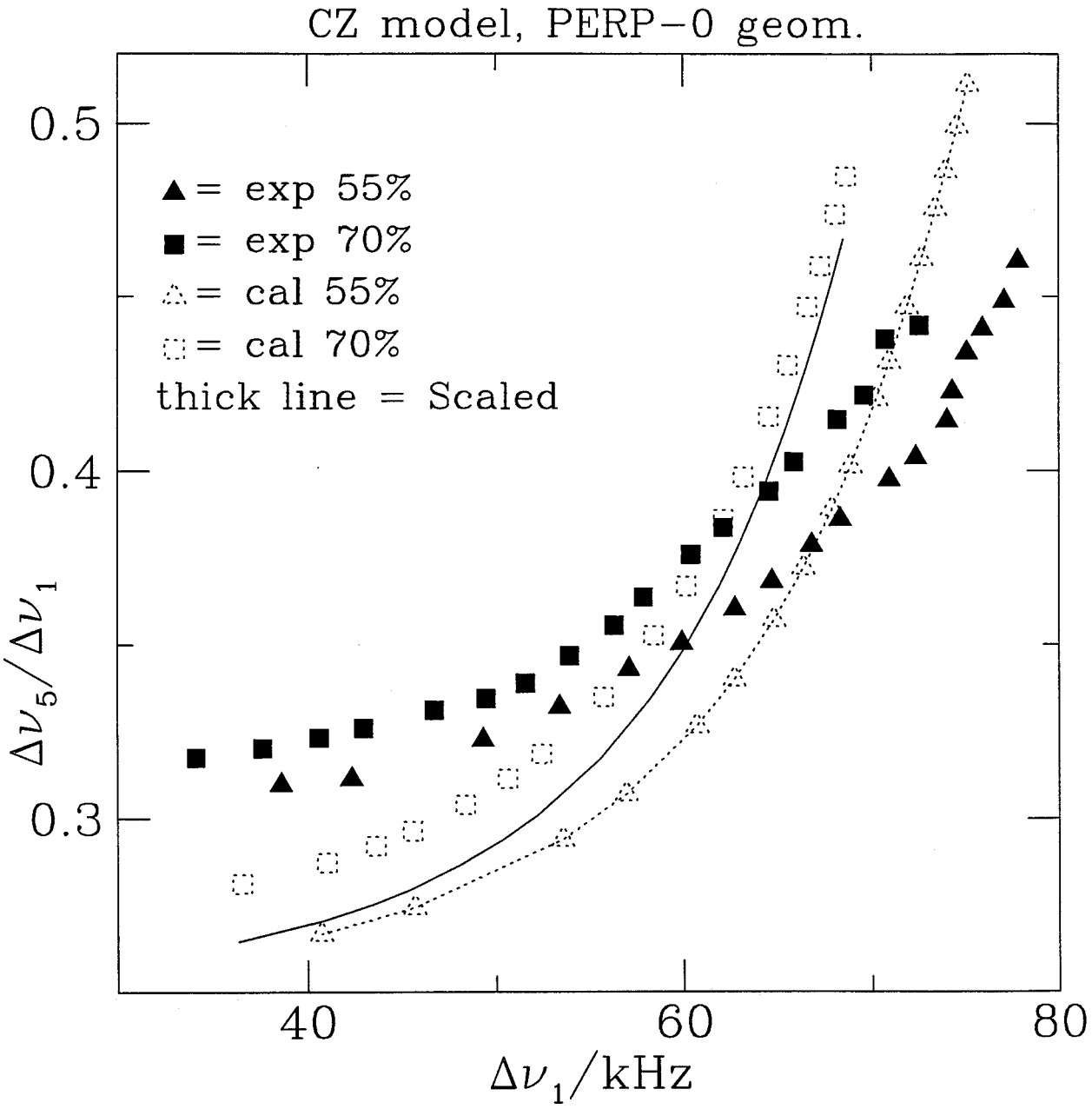

Figure 6.44: Quadrupolar splitting ratios $\Delta\nu_5/\Delta\nu_1$ versus $\Delta\nu_1$ using Global fit CZ model parameters.

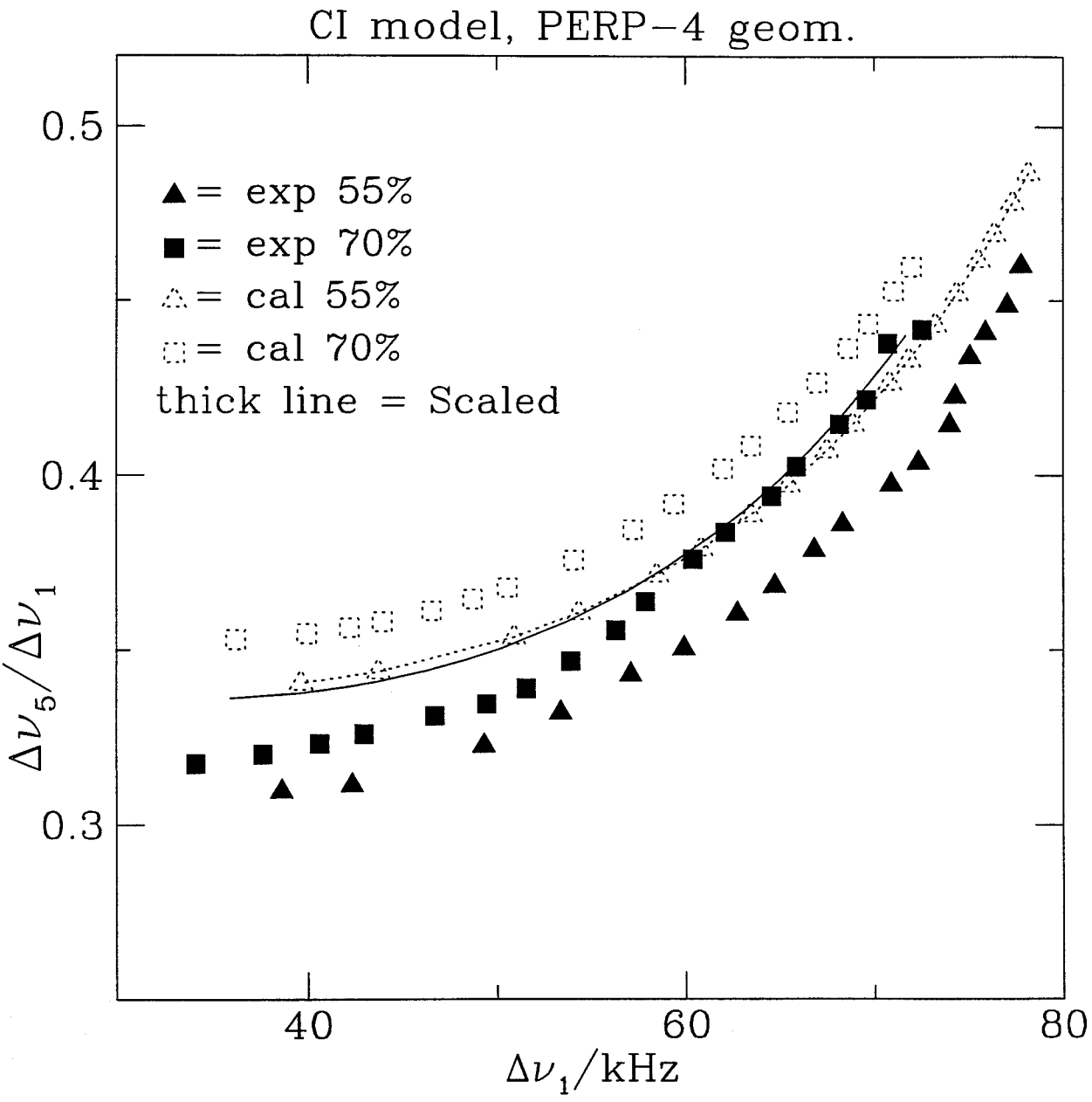

Figure 6.45: Quadrupolar splitting ratios $\Delta\nu_5/\Delta\nu_1$ versus $\Delta\nu_1$ using Global fit CI model parameters.

6.3 Summary

In this chapter we have demonstrated in several different ways that for a given experimental $\Delta\nu_1$ the reduced model parameters k_i/T of 55 % 1132/EBBA are the same as those of 70% 5CB/EBBA. That is, irrespective of the model used for analysis, the reduced short-range potential appears to be the same in all zero electric field gradient nematic mixtures. In other words, the quadrupolar splittings of 5CB – d_{19} in one zero electric field gradient mixture can be predicted knowing the reduced model parameters of another zero electric field gradient mixture. The differences in spectra between mixtures result from the temperature dependence of the internal energy contribution to the conformer probabilities.

Chapter 7

Conclusion

Intermolecular forces play an important role in understanding the orientational nature of liquid crystals. Due to the different strengths of intermolecular potentials, the orientational properties of liquid crystals differ from one liquid crystal to another. The orientational differences among pure liquid crystals such as 1132, EBBA and 5CB can be explained by the presence of long range intermolecular forces. In the absence of the long range forces, such as in the special mixtures 55 wt% 1132/EBBA, 56.5 wt% 1132/EBBA and 70 wt% 5CB/EBBA, one expects that the orientation would be negligibly small. However, the orientational studies of small solutes show that there exists short-range forces which orient the solutes in these special mixtures. In order to understand the role of short-range forces in zero efg mixtures, the orientational studies were undertaken in the zero efg mixtures.

The study of C_{2V} symmetry solutes in mixtures 56.5 wt% 1132/EBBA at 323K and 70 wt% 5CB/EBBA at 316K, using proton NMR, shows that the solutes orient in the same way, upon scaling for the different nematic-isotropic transition temperature values, T_{NI}, of the two mixtures. The experimental order parameters were related to the short-range potential with the aid of a model. It has been found that the short-range potentials experienced by the solutes are similiar in both mixtures.

The temperature dependence of the solutes meta dichlorobenzene, ortho dichlorobenzene, 1,3-bromochlorobenzene, benzene and 2-butyne in the special mixtures 55 wt% 1132/EBBA and 70 wt% 5CB/EBBA shows that the solutes orient in the same way in

both mixtures. The results were analysed to compare the short-range interactions in these two mixtures. It is found that the reduced short-range potentials are the same in both mixtures. The analysis of biaxial order parameters shows that the temperature effect on the electric field gradient is small.

Although the study of small solutes as probes in liquid crystals gives a starting point, the temperature dependence study of a liquid crystal, 5CB-d_{19}, in the zero efg mixtures 55 wt% 1132/EBBA, 56.5 wt% 1132/EBBA and 70 wt% 5CB/EBBA gives a better understanding about the intermolecular forces among constituent liquid crystal molecules. The flexible chain part of the constituent liquid crystal molecule plays an important role in orienting the liquid crystal molecules. The free rotation along the C-C bond leads to several conformations for the constituent liquid crystal molecule. The probability of each conformer depends on the internal energy, $U_{int,i}$, of the constituent liquid crystal molecule.

The temperature dependence study of 5CB – d_{19} as solute in the mixtures 55 wt% 1132/EBBA, 56.5 wt% 1132/EBBA and 70 wt% 5CB/EBBA indicates that the solute 5CB – d_{19} experiences the same reduced potential in all three mixtures. These results have been confirmed using two independent models for the short-range interactions. Since the solute 5CB – d_{19} experiences the same reduced potential in the special mixtures, one would expect that the ^{2}H-NMR spectra of the liquid crystal 5CB – d_{19} in the special mixtures be identical. However, the spectra in the mixtures 55 wt% 1132/EBBA and 70 wt% 5CB/EBBA are different, and the spectral differences are explained in terms of different nematic-isotropic transition temperature, T_{NI}, values. As T_{NI} varies for different special mixtures, the $\frac{U_{int,i}}{T_{NI}}$ part of the potential for the solute 5CB – d_{19} will vary inversely with T_{NI}. Thus differences at T_{NI} propagate throughout the nematic temperature range. This variation with T_{NI} of the $\frac{U_{int,i}}{T_{NI}}$ part of the potential explains the observed spectral differences of 5CB – d_{19} in these special mixtures.

Other useful information which can be obtained from our study is the value of E_{tg} for the flexible chain part of the 5CB – d_{19} molecule. Although the E_{tg} values for the flexible chain molecules in isotropic solvents are available, the E_{tg} value in the nematic phase is not available. We have used the values of 500, 700 and 900 cal/mol for the E_{tg} in Chapter 5 and $E_{tg} = 700$ cal/mol for the analysis in Chapter 6. To obtain an estimate for the E_{tg} value, we shall now compare the temperature dependence study of 5CB – d_{19} with that of small solutes (Chapter 4), where the extra complexity due to E_{tg} does not exist. In figure 7.46, we plot the reduced model parameter, k_s/T, against T_r for both the small solutes and the liquid crystal 5CB – d_{19}. The figure suggests that the k_s/T values for all aromatic solutes are in good agreement with those of 5CB – d_{19} at $E_{tg} = 700$ cal/mol. It should be noted that the k_s values for 5CB – d_{19} are slightly underestimated because the 5CB – d_{19} data were fitted using the two-parameter model (equation 1.29), having k_s and k terms (with k being very small), whereas the order parameters of the small solutes were fitted using the one-parameter model (equation 1.28), only the k_s term.

For the linear molecule, 2-butyne, however the k_s/T values are close to those of 5CB – d_{19} at $E_{tg} = 500$ cal/mol. Although we expected that the k_s/T vs. T_r plots for all the small solutes would behave similiarly, the different behavior for the linear molecule, 2-butyne, from the aromatic solutes is not understood well. It should, however, be noted that k_s/T values for 2-butyne is close to 500 cal/mol, which is the most commonly accepted literature value. Based on agreement between the temperature dependence studies of small solutes and of liquid crystal 5CB – d_{19}, we report the E_{tg} value as 700 cal/mol although an exact estimate can not be predicted from our study.

Having studied the three zero efg mixtures 55 wt% 1132/EBBA, 56.5 wt% 1132/EBBA and 70 wt% 5CB/EBBA, it is interesting to see whether we can extend our results to other possible zero efg mixtures. Some other possible zero efg mixtures are: PCH-7/EBBA, PCH-7/MBBA and 5CB/MBBA, where the measured electric field gradient has been

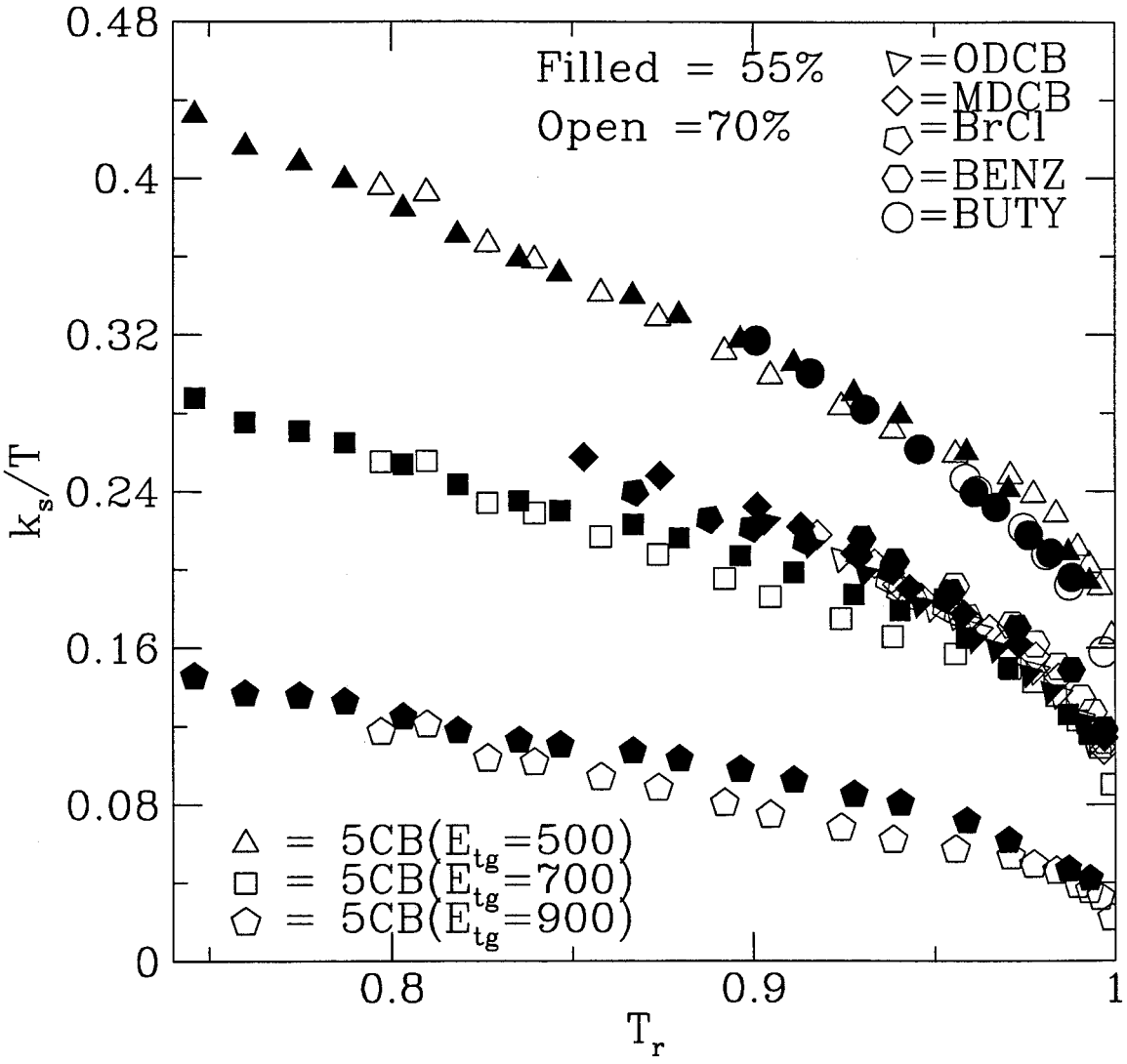

Figure 7.46: Reduced model parameter, k_s/T *vs.* T_r for all the solutes and the liquid crystal 5CB-d_{19}.

found to be opposite in sign in the liquid crystals PCH-7 and MBBA [84]. For example, a study of a solute in the zero efg mixtures 70 wt% 5CB/EBBA and x wt% 5CB/MBBA, where x has to be determined experimentally, may lead to an understanding how that particular solute prefers to orient with a particular liquid crystal site.

Another interesting aspect in the zero efg mixtures is the ability to determine the quadrupole moment of a solute. For example, to determine the quadrupole moment of the solute benzene, the following methods could be used. The orientational study of benzene dissolved in pure 5CB, pure EBBA and 70 wt% 5CB/EBBA could be undertaken, using proton NMR. The short-range potential, which can be be determined in the zero efg mixture 70 wt % 5CB/EBBA, could be transfered to the pure liquid crystals 5CB and EBBA. Having known the short-range potential contribution to the intermolecular potential, the long-range potential can be determined for the pure liquid crystals 5CB and EBBA. Note that the long-range potential is decribed in terms of electric quadrupole moment - electric field gradient interaction. The electric field gradient has already been measured in the pure liquid crystals EBBA and 5CB [32, 50]. Hence, it may be possible to determine the electric quadrupole moment of the benzene.

Bibliography

[1] F. Reinitzer, 1888, *Monatsh. Chem.*, **9**, 421

[2] de Jeu, W.H., *"Physical Properties of Liquid Crystalline Materials"*, 1980, Gordon and Breach, Science Publishers, Inc.

[3] deGennes, P.G., *"The Physics of Liquid Crystals"*, 1974, Cambridge University Press.

[4] Emsley, J.W., and Lindon, J.C., *"NMR Spectrosocopy using Liquid Crystal Solvents"*, 1975, Pergamon Press.

[5] Emsley, J.W., *"Nuclear Magnetic Resonance of Liquid Crystals"*, 1985, Reidel Press.

[6] Diehl, P., and Khetrapal, C.L., *"NMR Basic Principles and Progress"*, 1969, Vol.1.

[7] Dong, R.Y., *" Nuclear Magnetic Resonance of Liquid Crystals"*, 1993, Springer-Verlag Press.

[8] Dong, R.Y., and Richards, G.M., 1992, *J. Chem . Soc. Faraday Trans.*, **88**, 1885.

[9] Dong, R.Y., 1991, *Phys. Rev. A*, **43**, 4310.

[10] Dong, R.Y., and Richards, G.M., 1990, *Chem . Phys. Lett.*, **171**, 389.

[11] Beckmann, P.A., Emsley, J.W., Luckhurst, G.R., and Turner, D.L., 1986, *Mol. Phys.*, **59**, 97.

[12] Beckmann, P.A., Emsley, J.W., Luckhurst, G.R., and Turner, D.L., 1983, *Mol. Phys.*, **50**, 699.

[13] Slichter, C.P., *"Principles of Magnetic Resonance"*, 1989, Springer-Verlag Press.

[14] Saupe, A., *Molecular Crystals.*, 1966, **1**, 527.

[15] Pake, A., *J. Chem. Phys.*, 1948, **16**, 327.

[16] Maier, W., and Saupe, A., *Z. Naturforsch.*, 1958, **A 13**, 564; 1959, **A 14**, 882; 1960, **A 15**, 287;

[17] Luckhurst, G.R., Zannoni, C., Nordio, P.L., and Segre, U., 1975, *Mol. Phys.*, **30**, 1345.

[18] Photinos, D.J., Samulski, E.T., and Toriumi, H., 1991, *Mol. Crst. Liq. Crst.*, **204**, 161.

[19] Photinos, D.J., Samulski, E.T., and Toriumi, H., 1990, *J. Phys. Chem.*, **94**, 4688.

[20] Photinos, D.J., Samulski, E.T., and Toriumi, H., 1990, *J. Phys. Chem.*, **94**, 4694.

[21] Yim, C.T., and Gilson, D.F.R., 1991, *J. Phys. Chem.* , **95**, 980.

[22] Yim, C.T., and Gilson, D.F.R., 1990, *Can. J. Chem.* , **68**, 875.

[23] Yim, C.T., and Gilson, D.F.R., 1989, *Can. J. Chem.* , **67**, 54.

[24] Yim, C.T., and Gilson, D.F.R., 1988, *Can. J. Chem.* , **66**, 1749.

[25] Yim, C.T., and Gilson, D.F.R., 1987, *Can. J. Chem.* , **65**, 2513.

[26] Ferrarini, A., Moro, G.J., and Nordio, P.L., 1992, *Mol. Phys.* , **77**, 1.

[27] Jokisaari, J., Ingman, P., Lounila, J., Pulkkinen, O., Diehl, P., and Muenster, O., 1993, *Mol. Phys.* , **78**, 41.

[28] Ingman, P., Jokisaari, J., Pulkkinen, O., Diehl, P., and Muenster, O., 1991, *Chem. Phys. Lett.*, **182**, 253.

[29] Ingman, P., Jokisaari, J., and Diehl, P., 1991, *J. Magn. Res.*, **92**, 163.

[30] Jokisaari, J., 1994, *Progress in Nuclear Magnetic Resonance Spectroscopy*, **26**, 1.

[31] Burnell, E.E., de Lange, C.A., and Snijders, J.G., 1982, *Phys. Rev. A*, **25**, 2339.

[32] Barker, P.B., van der Est, A.J., Burnell, E.E., Patey, G.N., de Lange, C.A., and Snijders, J.G., 1984, *Chem. Phys. Lett.*, **107**, 426.

[33] Patey, G.N., Burnell, E.E., Snijders, J.G., and de Lange, C.A., 1983, *Chem. Phys. Lett.*, **99**, 271.

[34] Stone, A.J., 1979, *The Molecular Physics of Liquid Crystals*, edited by Luckhurst, G.R., and Gray, G.W., (Academic Press), Chapter 2.

[35] Buckingham, A.D., 1970 *An Advanced Treatise in Physical Chemistry*, **4**, 349.

[36] Code, R.F., and Ramsey, N.F., 1971, *Phys. Rev. A*, **4**, 1945.

[37] van der Est, A.J., Barker, P.B., Burnell, E.E., de Lange, C.A., and Snijders, J.G., 1985, *Mol. Phys.*, **56**, 161.

[38] van der Est, A.J., Kok, M.Y., Burnell, E.E., 1987, *Mol. Phys.*, **60**, 397.

[39] van der Est, A.J., 1987, Ph. D. thesis, University of British Columbia.

[40] Zimmerman, D.S., and Burnell, E.E., 1990, *Mol. Phys.*, **69**, 1059.

[41] Zimmerman, D.S., and Burnell, E.E., 1993, *Mol. Phys.*, **78**, 687.

[42] Barnhoorn, J.B.S., de Lange, C.A., and Burnell, E.E., 1993, *Liq. Crystals.*, **13**, 319.

[43] Photinos, D.J., Samulski, E.T., and Toriumi, H., 1991, *J. Chem. Phys.*, **94**, 2758.

[44] Samulski, E.T., and Dong, R.Y., 1982, *J. Chem. Phys.*, **77**, 5090.

[45] Sinton, S.W., Zax, D.B., Murdoch, J.B., and Pines, A., 1984, *Mol. Phys.*, **53**, 333.

[46] Emsley, J.W., Luckhurst, G.R., Gray, G.W., and Mosley, A., 1978, *Mol. Phys.*, **35**, 1499.

[47] Emsley, J.W., Lindon, J.C., and Luckhurst, G.R., 1975, *Mol. Phys.*, **30**, 1913.

[48] Sinton, S.W., and Pines, A., 1980, *Chem. Phys. Lett.*, **76**, 263.

[49] Emsley, J.W., Luckhurst, G.R., and Stockley, C.P., 1982, *Proc. R. Soc. A*, **381**, 117.

[50] Weaver, A., van der Est, A.J., Rendell, J.C.T., Hoatson, G.L., Bates, G.S., and Burnell, E.E., 1987, *Liq. Crystals.*, **2**, 633.

[51] Keller, P., and Liebert, L., 1978, *Solid State Phys. Suppl.*, **14**, 19.

[52] Hoatson, G.L., Bailey, A.L., van der Est, A.J., Bates, G.S., and Burnell, E.E., 1988, *Liq. Crystals.*, **3**, 683.

[53] Davis, J.H., Jeffrey, K.R., Bloom, M., Valic, M.I. and Higgs, T.P., 1976, *Chem. Phys. Lett.*, **42**, 390.

[54] Lounila, J., and Jokisaari, J., 1982, *Progress in Nuclear Magnetic Resonance Spectroscopy*, **15**, 249.

[55] Diehl, P., Kellarhals, H., and Lusting, E., *"NMR Basic Principles and Progress"*, 1972, **6**, 1.

[56] Kok, M.Y., 1986, M. Sc. thesis, University of British Columbia.

[57] Harmony, M.D., Laurie, V.M., Kuczkowski, R.L., Schwendeman, R.H., Ramsay, D.A., Lovas, F.J., Lafferty, W.J., and Maki, A.G., 1979, *J. Phys. Chem. Ref. Data*, **8**, 619.

[58] Diehl, P., Henrichs, P.M., and Niederberger, W., 1971, *Mol. Phys.*, **20**, 139.

[59] Bondi, A., 1964, *J. Phys. Chem.*, **68**, 441.

[60] Tanimoto, M., Kuchitsu, K., and Morino, Y., 1969, *Bull. Chem. Soc. Japan*, **42**, 2519.

[61] Buckingham, A.D., Burnell, E.E., and de Lange, C.A., 1968, *Mol. Phys.*, **15**, 285.

[62] Bos, P.J., Pirs, J., Ukleja, P., and Doane, J.W., 1977, *Mol. Cryst. Liq. Cryst.*, **40**, 59.

[63] Emsley, J.W., Hashim, R., Luckhurst, G.R., Rumbles, G.N., and Viloria, F.R., 1983, *Mol. Phys.*, **49**, 1321.

[64] Flory, P.J., 1969, *"Statistical Mechanics of Chain Molecules "*.

[65] Emsley, J.W., and Luckhurst, G.R., 1980, *Mol. Phys.*, **41**, 19.

[66] Burnell, E.E., de Lange, C.A., and Mouritsen, O.G., 1982, *J. Magn. Reson.*, **50**, 188.

[67] Diehl, P., and Reinhold, M., 1978, *Mol. Phys.*, **36**, 143.

[68] Davis, J.H., and Jeffrey, K.R., 1977, *Chemistry and Physics of Lipids*, **20**, 87.

[69] Marcelja, 1974, *J. Chem. Phys.*, **60**, 3599.

[70] Emsley, J.W., Luckhurst, G.R., and Stockley, C.P., 1981, *Mol. Phys.*, **44**, 565.

[71] van der Est, A.J., Burnell, E.E., and Lounila, 1988, *J. Chem. Soc., Faraday Trans. 2*, **84**, 1095.

[72] Sheppard, N., and Szasz, G.J., 1949, *J. Chem. Phys.*, **17**, 86.

[73] Verma, A.L., Murphy, W.F., and Bernstein, H.J., 1974, *J. Chem. Phys.*, **60**, 1540.

[74] Bradford, W.F., Fitzwater, S., and Bartell, L.S., 1977, *J. Mol. Struct.*, **38**, 185.

[75] Colombo, L.,and Zerbi, G., 1980, *J. Chem. Phys.*, **73**, 2013.

[76] Kint, S., Scherer, J.R., and Snyder, R. G., 1980, *J. Chem. Phys.*, **73**, 2599.

[77] Rosenthal, L., Rabolt, J.F., and Hummel, J., 1982, *J. Chem. Phys.*, **76**, 817.

[78] Wiberg, K.B., and Murcko, M.A., 1988, *J. Am. Chem. Soc.*, **110**, 8029.

[79] Maier, W., and Saupe, A., 1959, Z. Naturf. (a), **14**, 882.

[80] Humphries, R.L., James, P.G., and Luckhurst, G.R., 1971, *Symp. Faraday Soc.*, **5**, 107.

[81] Palffy-Muhoray, P., de Bruyn, J.R., and Dunmur, D.A., 1985, *Mol. Cryst. Liquid Cryst.*, **127**, 301.

[82] Bates, G.S., Beckmann, P.A., Burnell, E.E., Hoatson, G.L., Palffy-Muhoray, P., 1986, *Mol. Phys.*, **57**, 351.

[83] Bates, G.S., Burnell, E.E., Hoatson, G.L., Palffy-Muhoray, P., Weaver, A., 1987, *Chem. Phys. Letts.*, **134**, 161.

[84] Ter Beek, L.C., Private communication.

Appendix A

Transformation

The order parameter $S_{\alpha\beta}$ is related to the intermolecular potential by:

$$S_{\alpha\beta} = \frac{\int(3\cos\theta_\alpha \cos\theta_\beta - \delta_{\alpha\beta})exp(-U(\Omega)/kT)d\Omega}{2\int exp(-U(\Omega)/kT)d\Omega} \tag{A.51}$$

where α, β = x,y,z, molecule fixed axes and the angle Ω denotes the Eulerian angle (ϕ,θ,ψ) that transform from the molecule-fixed axis system to director-fixed axis system. Since the nematic phase is an uniaxial phase, the transformation needs only two angles θ and ϕ. The angle θ is the angle between the director axis and the molecule-fixed z axis (see Figure A.47), and the angle ϕ is the angle between the projection of the director, $\underline{n}$, on the xy plane and the molecule-fixed axis x.

The order parameters S_{zz}, S_{xx} and S_{yy} for a solute molecule dissolved in a uniaxial nematic phase can be expressed in terms of θ and ϕ as:

$$S_{zz} = \frac{\int\int(3\cos^2\theta - 1)exp(-U(\theta,\phi)/kT)\sin\theta d\theta d\phi}{2\int\int exp(-U(\theta,\phi)/kT)\sin\theta d\theta d\phi} \tag{A.52}$$

$$S_{xx} = \frac{\int\int(3\sin^2\theta\cos^2\phi - 1)exp(-U(\theta,\phi)/kT)\sin\theta d\theta d\phi}{2\int\int exp(-U(\theta,\phi)/kT)\sin\theta d\theta d\phi} \tag{A.53}$$

$$S_{yy} = \frac{\int\int(3\sin^2\theta\sin^2\phi - 1)exp(-U(\theta,\phi)/kT)\sin\theta d\theta d\phi}{2\int\int exp(-U(\theta,\phi)/kT)\sin\theta d\theta d\phi} \tag{A.54}$$

Simliarly, the off-diagonal matrix elements S_{xy}, S_{xz} and S_{yz} can be described in terms of θ and ϕ. If the molecule-fixed axis system (x,y,z) is the principal axis system, then the orientation of the solute in the nematic phase can be described by two independent

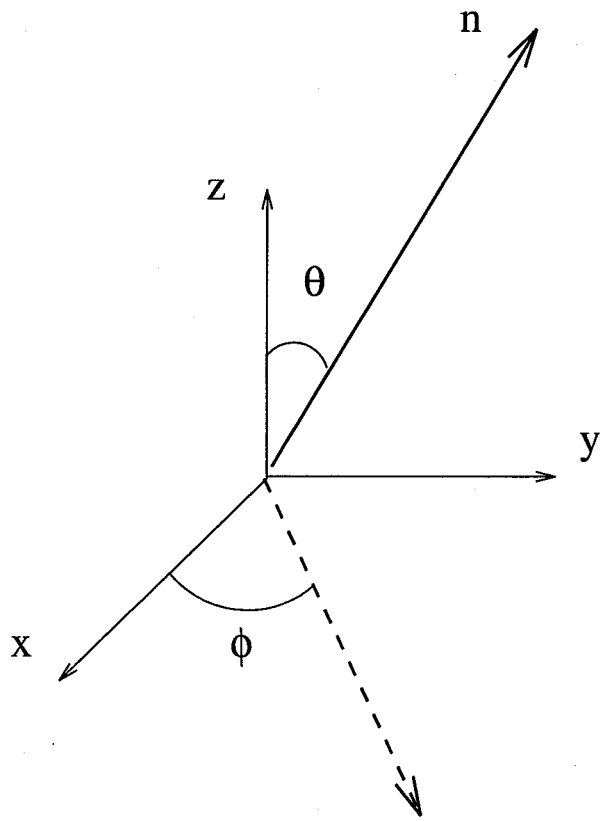

Figure A.47: The angles θ and ϕ represent the transformation between the molecule-fixed axis system (x,y,z) and the director-fixed axis system of the nematic liquid crystal.

order parameters since the order matrix is a traceless tensor. If two or more order parameters are needed to describe the orientation of a solute molecule in the nematic phase, then the solute is referred to have biaxiality. If a solute molecule has a 3-fold or higher symmetry, the $U(\phi, \theta)$ is invariant of the angle ϕ. Therefore, it can be shown that the order parameters S_{xx} and S_{yy} become equal for these higher symmetry solutes. The orientations of a 3-fold or higher symmetry solute in the nematic phase can be described by a single order parameter.

Appendix B

Dipolar Couplings

Temp / K	$D_{12} = D_{34}$	$D_{13} = D_{24}$	D_{14}	D_{23}
301	-1036.32 ±0.04	-132.30 ±0.01	-64.49 ±0.02	-494.85 ±0.05
305	-996.55 ±0.05	-128.31 ±0.02	-63.11 ±0.02	-484.58 ±0.06
310	-945.08 ±0.03	-122.93 ±0.08	-61.05 ±0.09	-469.47 ±0.04
315	-886.20 ±0.10	-116.50 ±0.29	-58.46 ±0.22	-450.11 ±0.13
320	-817.69 ±0.16	-108.92 ±0.39	-55.20 ±0.44	-424.28 ±0.19
322	-799.08 ±1.11	-106.65 ±0.33	-54.79 ±0.46	-417.20 ±1.28
325	-747.60 ±0.46	-99.74 ±1.01	-51.64 ±1.48	-394.86 ±0.66
327	-710.45 ±0.70	-95.73 ±0.21	-49.01 ±0.29	-379.39 ±0.80
330	-643.93 ±1.02	-87.12 ±0.32	-43.87 ±0.43	-349.43 ±1.17
	$J_{12} = J_{34} = 8.00$	$J_{13} = J_{24} = 1.50$	$J_{14} = 0.30$	$J_{23} = 7.40$

Table B.15: Dipolar couplings obtained from the ^{1}H-NMR spectra for the solute orthodichlorobenzene dissolved in 55% 1132/EBBA.

Temp / K	$D_{12} = D_{34}$	$D_{13} = D_{24}$	D_{14}	D_{23}
294	-987.28 ±0.15	-119.75 ±0.38	-55.50 ±0.54	-422.13 ±0.19
302	-895.03 ±0.02	-110.30 ±0.09	-51.77 ±0.02	-396.67 ±0.07
304	-879.09 ±0.04	-108.66 ±0.10	-51.13 ±0.03	-392.03 ±0.08
305	-865.92 ±0.09	-107.26 ±0.02	-50.69 ±0.03	-387.92 ±0.11
306	-848.48 ±0.12	-105.47 ±0.03	-49.97 ±0.05	-382.62 ±0.14
311	-766.75 ±0.28	-96.28 ±0.68	-46.57 ±0.87	-354.58 ±0.35
313	-715.33 ±0.36	-90.26 ±1.03	-43.47 ±0.94	-335.75 ±0.42
315	-661.30 ±0.18	-84.37 ±0.44	-40.69 ±0.56	-314.04 ±0.23
316	-606.30 ±0.64	-77.70 ±1.77	-37.00 ±1.40	-293.59 ±0.75
	$J_{12} = J_{34} = 8.00$	$J_{13} = J_{24} = 1.50$	$J_{14} = 0.30$	$J_{23} = 7.40$

Table B.16: Dipolar couplings obtained from the ^{1}H-NMR spectra for the solute orthodichlorobenzene dissolved in 70% 5CB/EBBA.

Temp / K	$D_{12} = D_{14}$	D_{13}	$D_{23} = D_{34}$	D_{24}
285	-114.72 ±0.20	-30.71 ±0.30	-1280.81 ±0.15	-314.09 ±0.34
292	-110.92 ±0.03	-29.68 ±0.04	-1244.09 ±0.02	-305.45 ±0.04
301	-105.26 ±0.09	-27.72 ±0.14	-1184.33 ±0.07	-290.71 ±0.15
305	-101.47 ±0.03	-26.69 ±0.04	-1143.91 ±0.02	-281.08 ±0.05
310	-96.69 ±0.02	-25.54 ±0.03	-1089.42 ±0.01	-267.52 ±0.03
315	-90.48 ±0.02	-24.17 ±0.05	-1015.79 ±0.02	-249.21 ±0.05
320	-85.83 ±0.16	-23.12 ±0.25	-961.63 ±0.11	-235.87 ±0.26
325	-80.40 ±0.14	-21.94 ±0.26	-893.69 ±0.16	-218.90 ±0.25
333	-61.68 ±0.33	-16.90 ±0.72	-665.52 ±0.35	-161.67 ±0.52
	$J_{12} = J_{14} = 1.97$	$J_{13} = 0.36$	$J_{23} = J_{34} = 8.10$	$J_{24} = 0.89$

Table B.17: Dipolar couplings obtained from the ^{1}H-NMR spectra for the solute metadichlorobenzene dissolved in 55% 1132/EBBA.

Temp / K	$D_{12} = D_{14}$	D_{13}	$D_{23} = D_{34}$	D_{24}
290	-106.31±0.28	-31.04 ±0.50	-1122.60 ±0.27	-272.06 ±0.59
295	-99.77±0.24	-29.85 ±0.39	-1063.15 ±0.17	-258.17 ±0.48
297	-95.52±0.01	-28.91 ±0.02	-1018.82 ±0.01	-247.81 ±0.03
299	-92.82±0.03	-28.00 ±0.05	-991.35 ±0.02	-241.22 ±0.06
303	-88.39±0.04	-26.54 ±0.06	-945.86 ±0.03	-230.10 ±0.09
305	-85.92±0.06	-25.70 ±0.08	-922.39 ±0.05	-224.44 ±0.15
309	-80.19±0.06	-23.86 ±0.10	-860.27 ±0.05	-209.50 ±0.13
311	-75.49±0.05	-22.51 ±0.07	-810.48 ±0.04	-197.29 ±0.09
315	-60.42±0.34	-15.28 ±0.65	-631.39 ±0.36	-151.58 ±0.66
	$J_{12} = J_{14} = 1.97$	$J_{13} = 0.36$	$J_{23} = J_{34} = 8.10$	$J_{24} = 0.89$

Table B.18: Dipolar couplings obtained from the ^{1}H-NMR spectra for the solute metadichlorobenzene dissolved in 70% 5CB/EBBA.

Temp / K	D_{12}	D_{13}	D_{14}	D_{23}	D_{24}	D_{34}
294	-124.24 ±1.12	-25.04 ±0.28	-90.25 ±1.25	-1175.89 ±5.31	-313.29 ±0.82	-1357.82 ±4.37
301	-118.24 ±0.97	-24.03 ±0.19	-86.92 ±1.08	-1133.45 ±4.19	-298.57 ±0.59	-1287.84 ±3.56
305	-114.99 ±0.70	-23.50 ±0.13	-86.69 ±0.78	-1111.64 ±3.24	-293.89 ±0.47	-1266.44 ±2.74
310	-111.18 ±0.99	-23.05 ±0.20	-85.81 ±1.11	-1085.06 ±4.83	-286.90 ±0.70	-1235.71 ±4.05
315	-105.03 ±1.68	-22.75 ±0.42	-86.80 ±1.96	-1045.72 ±10.32	-280.03 ±1.74	-1208.34 ±8.50
318	-103.69 ±2.27	-22.39 ±0.44	-83.20 ±2.53	-1026.77 ±11.72	-269.52 ±1.70	-1163.15 ±9.98
323	-95.41 ±2.50	-21.22 ±0.55	-81.70 ±2.94	-954.00 ±16.28	-254.79 ±2.73	-1095.39 ±13.53
	$J_{12} = 2.00$	$J_{13} = 0.20$	$J_{14} = 1.90$	$J_{23} = 8.00$	$J_{24} = 0.90$	$J_{34} = 8.00$

Table B.19: Dipolar couplings obtained from the ^{1}H-NMR spectra for the solute 1,3-Bromochlorobenzene dissolved in 55% 1132/EBBA.

Temp / K	D_{12}	D_{13}	D_{14}	D_{23}	D_{24}	D_{34}
300	-109.46 ±0.77	-25.61 ±0.17	-81.68 ±0.88	-985.12 ±3.91	-263.45 ±0.70	-1156.86 ±3.17
301	-109.02 ±1.56	-25.33 ±0.26	-77.35 ±1.71	-978.18 ±6.47	-256.68 ±0.94	-1123.12 ±5.44
302	-106.89 ±1.68	-24.73 ±0.29	-78.15 ±1.87	-963.61 ±7.57	-253.84 ±1.19	-1113.89 ±6.29
305	-104.66 ±2.36	-24.35 ±0.38	-75.03 ±2.60	-944.14 ±9.70	-246.76 ±1.36	-1077.95 ±8.23
306	-101.51 ±0.93	-23.87 ±0.16	-75.87 ±1.04	-928.19 ±4.21	-243.34 ±0.63	-1067.15 ±3.54
307	-100.45 ±1.75	-23.53 ±0.31	-74.98 ±1.95	-919.89 ±7.78	-241.32 ±1.14	-1051.19 ±6.55
	$J_{12} = 2.00$	$J_{13} = 0.20$	$J_{14} = 1.90$	$J_{23} = 8.00$	$J_{24} = 0.90$	$J_{34} = 8.00$

Table B.20: Dipolar couplings obtained from the ^{1}H-NMR spectra for the solute 1,3-Bromochlorobenzene dissolved in 70% 5CB/EBBA.

Temp / K	$D_{12} = D_{16} = D_{23}$ $= D_{34} = D_{45} = D_{56}$	$D_{13} = D_{15} = D_{24}$ $= D_{26} = D_{35} = D_{46}$	$D_{14} = D_{25} = D_{36}$
306	-624.04 ±0.01	-120.77 ±0.01	-78.65 ±0.01
309	-596.57 ±0.00	-115.44 ±0.00	-75.17 ±0.01
314	-558.20 ±0.02	-107.98 ±0.02	-70.32 ±0.02
320	-512.80 ±0.03	-99.18 ±0.03	-64.58 ±0.04
325	-457.03 ±0.03	-88.45 ±0.04	-57.58 ±0.04
328	-373.43 ±0.22	-72.56 ±0.13	-46.99 ±0.17
	$J_{12} = J_{16} = J_{23}$ $= J_{34} = J_{45} = J_{56} = 7.55$	$J_{13} = J_{15} = J_{24}$ $= J_{26} = J_{35} = J_{46} = 1.38$	$J_{14} = J_{25} = J_{36} = 0.65$

Table B.21: Dipolar couplings obtained from the ^{1}H-NMR spectra for the solute Benzene dissolved in 55% 1132/EBBA.

Temp / K	$D_{12} = D_{16} = D_{23}$ $= D_{34} = D_{45} = D_{56}$	$D_{13} = D_{15} = D_{24}$ $= D_{26} = D_{35} = D_{46}$	$D_{14} = D_{25} = D_{36}$
300	-565.83 ±0.02	-109.51 ±0.03	-71.35 ±0.04
305	-516.40 ±0.01	-99.99 ±0.01	-65.13 ±0.01
307	-491.57 ±0.02	-95.11 ±0.03	-61.95 ±0.04
309	-461.94 ±0.01	-89.43 ±0.02	-58.24 ±0.02
311	-417.48 ±0.03	-80.78 ±0.04	-52.59 ±0.05
312	-398.03 ±0.06	-76.72 ±0.08	-50.08 ±0.09
313	-357.22 ±0.12	-68.87 ±0.14	-44.79 ±0.15
	$J_{12} = J_{16} = J_{23}$ $= J_{34} = J_{45} = J_{56} = 7.55$	$J_{13} = J_{15} = J_{24}$ $= J_{26} = J_{35} = J_{46} = 1.38$	$J_{14} = J_{25} = J_{36} = 0.65$

Table B.22: Dipolar couplings obtained from the ^{1}H-NMR spectra for the solute Benzene dissolved in 70% 5CB/EBBA.

Temp / K	$D_{11} = D_{22}$	D_{12}
300	2066.07 ±0.04	-163.94 ±0.04
305	1958.81 ±0.02	-155.51 ±0.02
310	1838.25 ±0.04	-146.05 ±0.04
315	1705.11 ±0.04	-135.55 ±0.03
320	1560.53 ±0.10	-124.26 ±0.07
322	1559.38 ±24.85	-119.94 ±0.04
325	1352.55 ±40.46	-112.37 ±0.08
327	1315.09 ±37.91	-107.64 ±0.08
329	1398.75 ±51.04	-101.17 ±0.09
	$J_{12} = 2.70$	

Table B.23: Dipolar couplings obtained from the ^{1}H-NMR spectra for the solute 2-Butyne dissolved in 55% 1132/EBBA.

Temp / K	$D_{11} = D_{22}$	D_{12}
300	1606.40 ±0.02	-127.37 ±0.02
301	1564.18 ±0.01	-124.05 ±0.01
305	1439.99 ±0.03	-114.16 ±0.03
307	1350.21 ±0.07	-107.20 ±0.07
309	1247.35 ±0.04	-98.95 ±0.03
312	992.09 ±34.09	-81.22 ±0.06
	$J_{12} = 2.70$	

Table B.24: Dipolar couplings obtained from the ^{1}H-NMR spectra for the solute 2-Butyne dissolved in 70% 5CB/EBBA.

Appendix C

Order Parameters

Temp / K	$D_{HH}(TCB)$	S_{zz}	S_{xx}	k_s
301	-172.970	-0.21801	0.06337	67.53812
305	-167.165	-0.21037	0.06202	64.82430
310	-159.503	-0.20034	0.06007	61.37217
315	-150.443	-0.18868	0.05757	57.28411
320	-139.527	-0.17489	0.05430	52.47647
322	-136.508	-0.17111	0.05338	51.33454
325	-128.217	-0.16042	0.05044	47.64440
327	-122.103	-0.15282	0.04849	45.04757
330	-111.752	-0.13894	0.04459	40.37634

Table C.25: Experimental order parameters S_{zz} and S_{xx} for the solute orthodichlorobenzene dissolved in 55% 1132/EBBA as a function of temperature.

Temp / K	$D_{HH}(TCB)$	S_{zz}	S_{xx}	k_s
294	-160.958	-0.20354	0.05414	60.46520
302	-147.713	-0.18569	0.05084	54.43857
304	-145.327	-0.18259	0.05024	53.53156
305	-143.330	-0.18001	0.04971	52.69720
306	-140.632	-0.17660	0.04903	51.47000
311	-128.517	-0.16031	0.04540	46.04045
313	-120.278	-0.14995	0.04294	42.52127
315	-111.610	-0.13898	0.04023	38.90255
316	-102.083	-0.12783	0.03750	35.24450

Table C.26: Experimental order parameters S_{zz} and S_{xx} for the solute orthodichlorobenzene dissolved in 70% 5CB/EBBA as a function of temperature.

Temp / K	$D_{HH}(TCB)$	S_{zz}	S_{xx}	k_s
285	-188.590	-0.23853	0.03197	73.47398
292	-183.035	-0.23137	0.03057	72.40457
301	-174.340	-0.22006	0.02881	69.91814
305	-168.393	-0.21242	0.02763	67.70210
310	-160.598	-0.20234	0.02637	64.56969
315	-150.162	-0.18890	0.02494	59.93653
320	-142.450	-0.17895	0.02379	56.80786
325	-132.707	-0.16673	0.02274	52.69603
333	-99.620	-0.12530	0.01864	37.97432

Table C.27: Experimental order parameters S_{zz} and S_{xx} for the solute metadichlorobenzene dissolved in 55% 1132/EBBA as a function of temperature.

Temp / K	$D_{HH}(TCB)$	S_{zz}	S_{xx}	k_s
290	-168.690	-0.21281	0.03363	63.15729
295	-159.695	-0.20104	0.03110	59.84965
297	-153.107	-0.19260	0.02973	57.08479
299	-149.018	-0.18732	0.02879	55.48940
303	-142.245	-0.17864	0.02735	52.99610
305	-138.642	-0.17404	0.02641	51.67089
309	-129.542	-0.16233	0.02464	48.02930
311	-122.123	-0.15290	0.02317	44.95268
315	-95.548	-0.11994	0.01929	33.95981

Table C.28: Experimental order parameters S_{zz} and S_{xx} for the solute meta dichlorobenzene dissolved in 70% 5CB/EBBA as a function of temperature.

Temp / K	$D_{HH}(TCB)$	S_{zz}	S_{xx}	S_{xy}	k_s
294	-182.595	-0.23221	0.02546	-0.01318	70.43817
301	-174.883	-0.22172	0.02447	-0.01154	67.96272
305	-171.878	-0.21795	0.02392	-0.01113	67.41445
310	-167.900	-0.21284	0.02345	-0.01049	66.47770
315	-163.525	-0.20751	0.02306	-0.00939	65.37035
318	-159.245	-0.20097	0.02279	-0.00907	63.29045
323	-149.897	-0.18936	0.02158	-0.00763	59.65535

Table C.29: Experimental order parameters S_{zz}, S_{xx} and S_{xy} for the solute 1,3- bromochlorobenzene dissolved in 55% 1132/EBBA as a function of temperature.

Temp / K	$D_{HH}(TCB)$	S_{zz}	S_{xx}	S_{xy}	k_s
300	-157.755	-0.19965	0.02605	-0.01175	58.40745
301	-154.538	-0.19534	0.02576	-0.01111	56.96485
302	-152.912	-0.19299	0.02519	-0.01102	56.38040
305	-149.010	-0.18789	0.02478	-0.01031	55.03480
306	-147.177	-0.18528	0.02431	-0.01007	54.30561
307	-145.388	-0.18331	0.02395	-0.00966	53.79278

Table C.30: Experimental order parameters S_{zz}, S_{xx} and S_{xy} for the solute 1,3- bromochlorobenzene dissolved in 70% 5CB/EBBA as a function of temperature.

Temp / K	$D_{HH}(TCB)$	S_{zz}	k_s
306	-160.738	-0.15838	66.05761
309	-154.227	-0.15141	63.06516
314	-145.058	-0.14167	59.10931
320	-133.790	-0.13015	54.43838
325	-119.867	-0.11600	48.30814
328	-98.610	-0.09486	38.82091

Table C.31: Experimental order parameters $S_{zz}$for the solute benzene dissolved in 55% 1132/EBBA as a function of temperature.

Temp / K	$D_{HH}(TCB)$	S_{zz}	k_s
300	-144.465	-0.14361	57.39262
305	-132.525	-0.13107	52.31176
307	-126.790	-0.12476	49.68468
309	-119.402	-0.11724	46.47961
311	-108.560	-0.10596	41.69242
312	-103.712	-0.10101	39.60073
313	-93.460	-0.09066	35.22472

Table C.32: Experimental order parameters $S_{zz}$for the solute benzene dissolved in 70% 5CB/EBBA as a function of temperature.

Temp / K	$D_{HH}(TCB)$	S_{zz}	k_s
300	-175.418	0.20608	95.12899
305	-169.237	0.19538	91.64436
310	-161.773	0.18336	87.40088
315	-153.080	0.17008	82.37475
320	-143.097	0.15566	76.63711
322	-139.210	0.15070	74.66101
325	-132.395	0.14118	70.65552
327	-127.438	0.13524	68.10666
329	-120.798	0.12711	64.47373

Table C.33: Experimental order parameters $S_{zz}$for the solute 2-Butyne dissolved in 55% 1132/EBBA as a function of temperature.

Temp / K	$D_{HH}(TCB)$	S_{zz}	k_s
300	-145.760	0.16023	73.90833
301	-142.678	0.15602	72.22457
305	-133.440	0.14363	67.42133
307	-126.613	0.13468	63.70778
309	-118.320	0.12442	59.28707
312	-99.097	0.10204	49.24637

Table C.34: Experimental order parameters $S_{zz}$for the solute 2-Butyne dissolved in 70% 5CB/EBBA as a function of temperature.